

BROWN DWARFS IN YOUNG MOVING GROUPS FROM PAN-STARRS1. I. AB DORADUS

KIMBERLY M. ALLER^{1,4}, MICHAEL C. LIU¹, EUGENE A. MAGNIER¹, WILLIAM M. J. BEST¹, MICHAEL C. KOTSON^{1,2}, WILLIAM S. BURGETT¹, KENNETH C. CHAMBERS¹, KLAUS W. HODAPP¹, HEATHER FLEWELLING¹, NICK KAISER¹, NIGEL METCALF³, JOHN L. TONRY¹, RICHARD J. WAINSCOT¹, CHRISTOPHER WATERS¹

¹ University of Hawaii, Institute of Astronomy, 2860 Woodlawn Drive, Honolulu, HI 96822

² Lincoln Laboratory, Massachusetts Institute of Technology and

³ Department of Physics, Durham University, South Road, Durham DH1 3LE, UK

To appear in ApJ.

ABSTRACT

Substellar members of young ($\lesssim 150$ Myr) moving groups are valuable benchmarks to empirically define brown dwarf evolution with age and to study the low-mass end of the initial mass function. We have combined Pan-STARRS1 (PS1) proper motions with optical–IR photometry from PS1, 2MASS and *WISE* to search for substellar members of the AB Dor Moving Group within ≈ 50 pc and with spectral types of late-M to early-L, corresponding to masses down to $\approx 30 M_{Jup}$ at the age of the group (≈ 125 Myr). Including both photometry and proper motions allows us to better select candidates by excluding field dwarfs whose colors are similar to young AB Dor Moving Group members. Our near-IR spectroscopy has identified six ultracool dwarfs (M6–L4; ≈ 30 – $100 M_{Jup}$) with intermediate surface gravities (INT-G) as candidate members of the AB Dor Moving Group. We find another two candidate members with spectra showing hints of youth but consistent with field gravities. We also find four field brown dwarfs unassociated with the AB Dor Moving Group, three of which have INT-G gravity classification. While signatures of youth are present in the spectra of our ≈ 125 Myr objects, neither their J – K nor $W1$ – $W2$ colors are significantly redder than field dwarfs with the same spectral types, unlike younger ultracool dwarfs. We also determined PS1 parallaxes for eight of our candidates and one previously identified AB Dor Moving Group candidate. Although radial velocities (and parallaxes, for some) are still needed to fully assess membership, these new objects provide valuable insight into the spectral characteristics and evolution of young brown dwarfs.

Subject headings: brown dwarfs – stars:low-mass

1. INTRODUCTION

Young moving groups (YMGs) are coeval associations of stars with similar space motions and with ages ranging from ~ 10 – 100 Myr. It is believed that these groups have left their natal molecular cloud after formation and dispersed into the field (Zuckerman & Song 2004). As such, YMGs link stars in molecular clouds (~ 1 Myr) to field stars ($\gtrsim 1$ Gyr) no longer affiliated with their birth sites. Thus YMGs are valuable laboratories for studying recent star formation in the solar neighborhood. Because of the proximity of the known YMGs ($\lesssim 100$ pc), they are ideal candidates for characterizing the initial mass function (IMF) down to substellar masses. Although substellar objects are generally very faint, younger brown dwarfs are more luminous (Chabrier et al. 2000) thus more readily detected.

Characterization of young brown dwarfs and directly imaged planets have revealed that their spectral properties differ from those of their old field counterparts (e.g. Chauvin et al. 2005; Marois et al. 2008; Bowler et al. 2010, 2013; Patience et al. 2010). Young brown dwarfs have redder NIR colors and have spectra distinct from field objects. Studies of brown dwarfs in young clusters and moving groups have begun to delineate the brown dwarf spectral evolution, due to the lower surface gravity of younger objects (e.g. Allers et al. 2007; Allers & Liu 2013). In order to further characterize this evolution, we need to identify a larger sample of substellar

objects at various young ages (~ 10 – 100 Myr). Determining the substellar spectral sequence in YMGs with different ages would be a key step towards better understanding substellar evolution and benchmarking spectral indicators of youth.

The AB Doradus (AB Dor) Moving Group was first recognized as a sparse, comoving group of stars in the Local Association by Zuckerman et al. (2004). The age estimates for the AB Dor Moving Group vary substantially depending on the method, ranging from 50 to 150 Myr. Initially, Zuckerman et al. (2004) estimated an age of ~ 50 Myr from color-magnitude diagrams. Analysis using evolutionary tracks and dynamical masses to study AB Dor C, a member of a quadruple system in the AB Dor Moving Group, yielded an age for the system of ~ 75 Myr (Close et al. 2007). However, color-magnitude diagram comparisons of the lower-mass AB Dor Moving Group members with the Pleiades (≈ 125 Myr; e.g. Basri et al. 1996; Martín et al. 1998) and IC 2391 (~ 35 – 50 Myr; e.g. Barrado y Navascués et al. 1999, 2004) suggested that the AB Dor Moving Group is roughly coeval with the Pleiades and older than IC 2391 (Luhman et al. 2005). Traceback of the AB Dor Moving Group kinematics have also concluded that the group and the Pleiades likely formed from the same large-scale star formation event, and thus should be nearly same age (Luhman et al. 2005; Ortega et al. 2007). By combining chemical and kinematic analysis of the AB Dor Moving Group members, Barenfeld et al. (2013) have also constrained the group to be approximately the age of the Pleiades with a lower age limit of 110 Myr.

Currently, the AB Dor Moving Group has one of the largest number of stellar members of the known YMGs, with ≈ 50 confirmed members with parallaxes (Zuckerman & Song

⁴ Visiting Astronomer at the Infrared Telescope Facility, which is operated by the University of Hawaii under Cooperative Agreement no. NNX-08AE38A with the National Aeronautics and Space Administration, Science Mission Directorate, Planetary Astronomy Program.

2004; Torres et al. 2008; Zuckerman et al. 2011). However, the lack of low-mass stars ($\lesssim 0.5 M_{\odot}$) in the known membership has prompted several recent surveys aimed at discovering these missing members. By using photometry and/or kinematics, several additional low mass stellar candidate members (late-K–mid-M dwarfs; $\sim 0.1\text{--}0.5 M_{\odot}$) have emerged (e.g. Shkolnik et al. 2009; Schlieder et al. 2012; Malo et al. 2013). However, these surveys were less sensitive to the cooler, fainter substellar members. Currently, only CD-35 2722 B (L3; Wahhaj et al. 2011), 2MASS J1425–3650 (L4; Gagné et al. 2015b), 2MASS J0355+1133 (L5; Liu et al. 2013a; Faherty et al. 2013), WISEP J0047+6803 (L7; Gizis et al. 2015) and SDSS J1110+0116 (T5.5; Gagné et al. 2015a) have been confirmed as bona fide substellar members of the AB Dor Moving Group. Gagné et al. (2014, 2015b) have begun a systematic search to identify lower mass stellar and substellar candidate members using Bayesian inference to calculate their YMG membership probabilities from proper motion, photometry, and, if available, radial velocities and distances.

In order to further the search for substellar YMG members, we are conducting a deep, wide-field search based on optical imaging data from Pan-STARRS1. Pan-STARRS1 (PS1) is a multi-wavelength, multi-epoch, optical imaging survey which covers $\approx 75\%$ of the sky. PS1 goes ~ 1 mag fainter than SDSS in the z band (York et al. 2000). Also, PS1 has a novel y_{P1} ($0.918\text{--}1.001 \mu\text{m}$) filter, which extends the wavelength coverage further into the near-infrared than past optical surveys, such as SDSS. Compared to previous optical surveys, the PS1 red optical filters, z_{P1} and y_{P1} , allow for more sensitivity and better characterization at redder wavelengths, both of which are advantageous for identifying substellar objects. We also combine PS1 and 2MASS astrometry to compute proper motions for our search (the addition of 2MASS astrometry increases our time baseline by a factor of ~ 3). Precise proper motions significantly increases our ability to distinguish faint, substellar candidate AB Dor Moving Group members from field interlopers.

We use 2MASS, PS1, and *WISE* to select substellar AB Dor Moving Group candidates. In Section 2 we discuss the PS1 photometry and proper motion precision as well as the addition of 2MASS and *WISE* data. In Section 3 we describe our search method, which uses photometrically determined spectral types and proper motion analysis to select candidates. In Section 4 we describe our spectroscopic followup and reduction. In Section 5 we determine spectral types, determine parallactic and photometric distances, assess the youth of our candidates, consider their membership in the AB Dor Moving Group, and estimate their physical properties. Our discussion is in Section 6, and our conclusions are in Section 7.

2. SURVEY DATA

PS1 is a 1.8 m, wide-field telescope located on Haleakalā on the island of Maui. The PS1 3π Survey covers the sky north of -30° decl., $\approx 75\%$ of the sky. The survey’s five optical filters, g_{P1} , r_{P1} , i_{P1} , z_{P1} , and y_{P1} , are described in Stubbs et al. (2010) and Tonry et al. (2012). At each epoch a single field is exposed for 60 s in g_{P1} , 38 s in r_{P1} , and 30 s in i_{P1} , z_{P1} , and y_{P1} . The photometry and astrometry from each epoch have been combined to obtain average magnitudes and proper motions.

We used data from the PS1 3π survey (which began in 2010) to construct spectral energy distributions (SEDs) and determine proper motions of our candidates. We chose good quality data according to the photometric quality flags set in

the PS1 Desktop Virtual Observatory (DVO) database (Magnier 2006). Specifically, we select objects characterized by all of the following attributes: fits a point-spread function (PSF) model (not extended), is not saturated, has good sky measurement, is not likely a cosmic ray, a diffraction spike, a ghost or a glint, and does not lie between the image chips (i.e. to choose y_{P1} data we require $(y_{P1}:\text{flags} \ \& \ 0x0000.0300) \neq 0$ and $(y_{P1}:\text{flags} \ \& \ 0x0000.1000) \neq 0$); and has the quality flag $\text{psf_qf} \geq 0.9$ to ensure that at least 90% of the object is unmasked. Furthermore, we require objects to be detected at least twice in a single night in at least one of the five filters (g_{P1} , r_{P1} , i_{P1} , z_{P1} , y_{P1}) to remove potential spurious sources that would only appear as single detections. Finally, we require that a single bandpass measurement error be ≤ 0.1 mag in order to use that bandpass.

We then matched PS1 objects with their 2MASS counterparts using the 2MASS Point Source Catalog (Skrutskie et al. 2006). We chose good J , H , and K photometry based on the following requirements: measurement error ≤ 0.2 mag and $\text{cc_flg} = 0$ (i.e. no confusion). We also matched PS1 objects with their *WISE* counterparts from the *WISE* Point Source Catalog (Wright et al. 2010), which was available when we began our search. We chose objects with good photometry in $W1$ and $W2$ with measurement errors ≤ 0.2 mag and $\text{cc_flg} = 0$ (i.e. no confusion). The final *WISE* photometry for our objects presented here is from the updated AllWISE Catalog (Kirkpatrick et al. 2014), which was released after our initial search.

We also used astrometric data from PS1 and 2MASS. The PS1 proper motions have a 2–3 year time baseline. To increase the time baseline from 2–3 years to ~ 10 years, we combined astrometry from PS1 and 2MASS. For our dataset, the typical 2MASS astrometric uncertainties are ≈ 70 mas, far larger than our typical PS1 uncertainties of ≈ 15 mas. By extending our time-baseline, we improved our typical proper motion precision from $\approx 7 \text{ mas yr}^{-1}$ to $\approx 5 \text{ mas yr}^{-1}$.

When calculating the proper motion for our objects, we used an outlier-resistant fitting method which calculates bisquare weights (Tukey’s biweight) and iteratively fits the data to minimize the residuals. This method reduces the effects that potentially spurious data points have on our final proper motion fit. We determined our proper motion uncertainties by using bootstrap resampling of our data. We discuss the quality of our PS1+2MASS proper motions in the Appendix.

Finally, we constructed an initial catalog of objects with good quality PS1+2MASS+*WISE* photometry and PS1+2MASS proper motions signal-to-noise ratio (S/N) ≥ 10 , corresponding to a typical proper motion of $\geq 140 \text{ mas yr}^{-1}$. Although by requiring the proper motions to have a high S/N we will miss slower-moving candidate members, only $\approx 13\%$ of the confirmed AB Dor Moving Group members tabulated in Malo et al. (2013) have proper motions below 140 mas yr^{-1} and are within 50 pc (the approximate photometric distance limit of our search).

3. CANDIDATE SELECTION

After combining PS1, 2MASS, and *WISE* photometry to create an initial catalog of objects with good quality proper motions and photometry (Section 2), we screened our initial catalog for probable late-M and L dwarfs using the following color cuts: $y - J \geq 1.4$, $z - y \geq 0.5$, and $W1 - W2 \geq 0$. In addition, we selected for objects with $i_{P1} - z_{P1} \geq 0.9$ if the i_{P1} photometry met our quality requirements (Section 2). In

order to remove potential galaxies from our sample we chose objects with $W2 - W3 \leq 3$ (Wright et al. 2010).

Next, we constructed SEDs and estimated spectral types and photometric distances using the template-fitting method of Aller et al. (2013). We first created template SEDs from known ultracool dwarfs with spectral types of M and L based on the compilations by Kraus & Hillenbrand (2007), Faherty et al. (2009), Leggett et al. (2010), and DwarfArchives.org. Then we estimated the spectral type of our candidates by determining the best-matched template SED using a chi-squared fit. Our estimated photometric distances (d_{phot}) were based on the Dupuy & Liu (2012) average J_{2MASS} absolute magnitudes as a function of spectral type (Section 5.2). We required our candidates to have estimated spectral types from our SED fit later than M5, which corresponds to the stellar/substellar boundary at the age of the AB Dor Moving Group.

In addition, we limited our search to candidates with proper motions between 40 and 1000 mas yr⁻¹. The lower proper motion limit is set because we only chose candidates with proper motion S/N ≥ 10 and our minimum proper motion uncertainty was ≈ 4 mas yr⁻¹. Also, because we only matched PS1 sources with 2MASS counterparts within a 10'' radius, our proper motion upper limit was approximately 1000 mas yr⁻¹.

Because moving group members have space motions with a common characteristic direction and amplitude, we further refined our candidate selection using proper motion and sky position. Following Schlieder et al. (2012), we screened for candidates with space motions consistent with the AB Dor Moving Group. Specifically, we used proper motions to calculate the angle (θ) projected onto the plane of the sky between our candidates' proper motions and the average space motion vector of the known members of the AB Dor Moving Group (Torres et al. 2008). We also determined the kinematic distance (d_{kin}), namely a candidate's distance if it were a member of the AB Dor Moving Group with the same absolute proper motion velocity (i.e. velocity in km s⁻¹) as the average of the known members. In order to determine our selection criteria, we calculated θ and d_{kin} for the known members of the AB Dor Moving Group with parallaxes from Torres et al. (2008) and determined that these members mainly have $\theta \lesssim 40^\circ$ (Figure 1). In addition, the 1σ distance range for known AB Dor Moving Group members is within 50 pc (Gagné et al. 2014). Therefore, we required our candidate AB Dor Moving Group members to have $\theta - \sigma_{\theta} \leq 40^\circ$ and $d_{kin} - \sigma_{d_{kin}} \leq 50$ pc. Finally, we also chose objects with d_{phot} less than 50 pc ($d_{phot} - \sigma_{d_{phot}} \leq 50$ pc) and consistent with their d_{kin} within the uncertainties in both d_{kin} and d_{phot} . We allowed the d_{phot} to vary within 50% to allow for uncertainties in determining photometric distance and in the absolute magnitudes of our candidates based on estimated spectral type.

In addition to photometric and kinematic information, we limited our search for AB Dor Moving Group members by sky positions. Based on the positions of known members, all candidates were selected to have Galactic latitude below 60° and declinations below 70°. We also ignored objects within 3° of the Galactic plane because of crowding.

Given the photometric distance limit of our search, we could detect objects with spectral types of \approx L4 at 50 pc, which corresponds to a mass of $\approx 30 M_{Jup}$ given the age of the AB Dor Moving Group. Thus our search is sensitive to candidate substellar AB Dor Moving Group members with masses from the substellar-stellar boundary down to $\approx 30 M_{Jup}$ out to 50 pc. We tabulate the photometry, proper

motions, d_{phot} , d_{kin} , and θ for our new candidate AB Dor Moving Group members in Table 1.

4. OBSERVATIONS

Field M and L dwarfs have similar colors and are more numerous than M and L dwarf members of the AB Dor Moving Group. Therefore we require spectroscopy to determine whether our candidates are young brown dwarfs, and thus potential members of this young (≈ 125 Myr old) moving group. Young brown dwarfs are spectroscopically distinguishable from field ultracool dwarfs because their lower surface gravity affects the depths of absorption lines and the overall continuum shape in the NIR (e.g. Allers et al. 2007; Allers & Liu 2013).

We obtained spectroscopic followup using SpeX (Rayner et al. 2003), the near-IR (0.8–2.5 μ m) spectrograph on the 3 m NASA Infrared Telescope Facility (IRTF) on Maunakea. We used the low-resolution (LowRes15) prism mode with a 0.5'' slit width ($R \sim 130$) for dwarfs with estimated spectral types from SED fitting later than M8. For earlier M dwarfs, we used the moderate-resolution cross-dispersed (SXD) mode ($R \sim 750$). These resolutions are sufficient to determine spectral type and assess youth using the Allers & Liu (2013) classification methods. Note that all spectra taken after 2014 August were observed using the upgraded version of SpeX (uSpeX), which has slightly larger wavelength coverage, 0.7–2.5 μ m.

We also obtained spectroscopic followup using GNIRS, the near-IR (0.8–2.5 μ m) spectrograph on the 8 m *Gemini* telescope on Maunakea. We used the moderate-resolution ($R \sim 1700$) cross-dispersed (SXD) mode with the 32 l mm⁻¹ grating with the 0.15''/pix camera and the 0.3'' slit.

Our observations were obtained using a standard ABBA nod pattern for sky subtraction. We observed an A0V standard star following each candidate and then took wavelength and flatfield calibrations immediately afterward. All SpeX spectra were reduced using version 3.4 (version 4.0 for uSpeX data) of the SpeXtool package (Vacca et al. 2003; Cushing et al. 2004). We reduced the GNIRS spectra using a custom version of SpeXtool (Liu et al. 2013b). Table 2 summarizes the observation details.

5. RESULTS

5.1. Spectral Analysis

We determined the NIR spectral type of our objects using both the index-based and visual methods of Allers & Liu (2013). First, the quantitative method combines the spectral-type sensitive indices from Allers et al. (2007), Slesnick et al. (2004), and McLean et al. (2003) to calculate the average spectral type. All of these spectral type indices are valid across the spectral type range of our candidates except the McLean et al. (2003) H₂O–D index, which is only valid for L dwarfs. We also performed a Monte Carlo simulation to propagate measurement errors of our reduced spectra into the index calculations in order to determine the spectral type uncertainties derived from each index.

Second, in addition to measuring indices to determine spectral type, we also visually compared our objects to M and L dwarf spectroscopic standards defined in Kirkpatrick et al. (2010). We used standard spectra taken from the IRTF Spectral Library (Cushing et al. 2005) and the SpeX Prism Library². Following the visual classification methods for young

² <http://pono.ucsd.edu/~adam/browndwarfs/spexprism>

and intermediate age objects of Allers & Liu (2013), we normalize both our candidates and the standard template in each NIR band separately (see Figure 2 for an example). However, because the H band of young/intermediate-aged brown dwarfs often have a distinctly different shape from old objects, the H band is not used for visual spectral type classification. Because selecting a standard with 1 subtype difference compared to our best-fitting standard produced a noticeably poorer fit, we assumed an uncertainty of 1 subtype for our visual classification (consistent with Allers & Liu 2013).

Our final spectral type is the weighted mean of the index-based and visual spectral types as in Allers & Liu (2013). As we use the Allers & Liu (2013) method, we also adopt a conservative spectral type uncertainty of 1 subtype. The spectral types for our candidates are tabulated in Table 3. In Figure 3 we show the spectra of our candidates in addition to the four known brown dwarf members, CD-35 2722 B (Wahhaj et al. 2011), 2MASS J0355+1133 (Liu et al. 2013a; Faherty et al. 2013), WISEP J0047+6803 (Gizis et al. 2015) and SDSS J1101+0116 (Gagné et al. 2015a).

We then assessed the gravity classification of our objects using spectral indices defined in Allers & Liu (2013). Under their classification scheme, several indices are measured in the J and H bands and then are each assigned a score (0, 1, or 2) according to the index value and the spectral type of the object, with higher numbers indicating lower gravity. These scores are combined into a final 4-number gravity score that represent the FeH, VO, alkali lines, and H -band continuum indices (e.g. 0110, 2110, etc.). Finally, this gravity score is used to determine the overall gravity classification for the object: field gravity (FLD-G), intermediate gravity (INT-G), or very low gravity (VL-G). We describe the method in more detail below and also describe some modifications we have made to account for the modest S/N of some of our spectra.

5.1.1. Gravity Index Calculations and Uncertainties

Depending on the spectral resolution, there is a specific set of gravity indices used to assess the overall gravity classification of an object. The FeH_z , VO_z and KI_J indices from Allers & Liu (2013) are tailored to assess gravity in low resolution ($R \sim 130$) spectra. In order to measure these indices from our moderate-resolution SXD spectra ($R \sim 750$), we smoothed those spectra to $R=130$. The H -cont index from Allers & Liu (2013), is used to assess gravity in either low or moderate-resolution spectra by measuring the shape of the H -band, specifically how close the blue end of the H -band continuum is to a straight line. For our moderate resolution spectra, following Allers & Liu (2013), we also used the FeH_J index and the alkali line indices in the J band (NaI [1.138 μm], KI [1.169 μm], KI [1.177 μm], and KI [1.253 μm]) to assess gravity with the continuum used to compute pseudo-equivalent widths defined by a linear fit.

For each of these gravity indices, Allers & Liu (2013) estimate the flux uncertainties from the rms scatter about a linear fit to the continuum window around each index. In the case of high S/N spectra this uncertainty in fitting the continuum is the dominant source of error to measure pseudo-equivalent widths. However, this approach underestimates the uncertainties for our lower S/N spectra with $S/N \sim 40$ –100. Therefore, in our method, we determined the uncertainty in each index (σ) using a Monte Carlo simulation to propagate the spectrum measurement errors.

In order to examine the effects of low S/N in calculating the uncertainties for the gravity indices, we simulated spec-

tra with a range of S/N and determined the alkali line gravity index values and uncertainties. We degraded the S/N of Gl 752B, an M8 from the IRTF Spectral Library (Rayner et al. 2009), from S/N of 500 down to 10. Then we calculated the measurement errors for the alkali line gravity indices (NaI [1.138 μm], KI [1.169 μm], KI [1.177 μm], and KI [1.253 μm]) using both a Monte Carlo simulation to propagate the measurement errors and the original method of Allers & Liu (2013). Our simulation shows that although both methods are consistent within uncertainties for these indices (Figure 4), the measurement errors are the main source of error for spectra with modest S/N ($\lesssim 200$).

5.1.2. Gravity Index Scores

After computing the index values and their uncertainties, we determine gravity scores for each of these indices, namely 0, 1 or 2. Following Allers & Liu (2013), indices that are undefined for an object, because of spectral type and/or resolution, are given a score of "n". The Allers & Liu (2013) method also gives indices with values that are within 1σ (the index uncertainty) from the field sequence values a score of "?". We handle such objects slightly differently and instead do not give indices a score of "?" in order to better identify borderline objects between the INT-G and FLD-G values.

For objects with low-resolution spectra ($R \sim 130$), only the FeH_z , VO_z , KI_J and H -cont indices are used. As an example, for PSO J039.6–21, the FeH_z , VO_z , KI_J and H -cont scores are: 1021. But strictly following Allers & Liu (2013), the final scores would instead be 102? because the H -cont index value is within 1σ of the FLD-G value.

For objects with moderate-resolution spectra ($R \sim 750$), the Allers & Liu (2013) method uses a similar set of four measurements to assess gravity: one based on FeH , VO_z , the alkali lines, and H -cont. The index scores for VO_z and H -cont are computed in the same manner as for the low-resolution spectra. However, unlike for the low-resolution spectra, the final FeH and alkali line scores are determined by combining the scores from multiple indices. The final alkali line score is the mean (rounded up to the nearest integer) of the individual scores from the NaI [1.138 μm], KI [1.169 μm], KI [1.177 μm], and KI [1.253 μm] indices. As an example, for PSO J035.8–15, the scores for NaI [1.138 μm], KI [1.169 μm], KI [1.177 μm], and KI [1.253 μm] are 0101, thus the final alkali line index score is 1. The final FeH index score is the larger of the FeH_z and FeH_J scores. For 2MASS J0233–15, the scores for FeH_z and FeH_J are 11, and thus the final FeH score is 1. After amalgamating the indices used to compute the final FeH and alkali line scores, the four scores (FeH , VO_z , alkali lines, and H -cont) of our example object, PSO J035.8–15, are 1n12. In this example, the scores are the same when strictly following the Allers & Liu (2013) method, since none of the index scores are "?".

5.1.3. Gravity Classification

Following Allers & Liu (2013), after determining the scores for the FeH , VO_z , alkali lines (KI_J for the low-resolution spectra or a combination of four pseudo-equivalent widths for moderate-resolution spectra), and H -band continuum indices, we reduce these four scores into a single value to represent the overall gravity classification. This overall gravity classification value is the median of these final four scores. If there was an even number of defined indices, we take the average of the two scores straddling the median. Objects with an overall gravity classification value ≤ 0.5 are classified as FLD-G.

Those objects with $0.5 < \text{gravity classification value} < 1.5$ are classified as INT-G, and those with a gravity classification value ≥ 1.5 are classified as VL-G.

Because our method uses a Monte Carlo simulation to propagate measurement uncertainties into the index values, our overall gravity classification also has uncertainties. Each Monte Carlo realization of an object's spectrum produces an overall gravity classification value, and we report the median value from all the realizations as the final result and the 68% confidence limits as the uncertainty. For instance, 2MASS J0223–15 has an overall gravity classification value of $1.0^{+1.0}_{-0.0}$, which corresponds to INT-G. For comparison, using the original Allers & Liu (2013) method, 2MASS J0223–15 has gravity scores of 1n12, so the overall gravity classification value would be 1, which also corresponds to INT-G but without any uncertainties.

As mentioned in Section 5.1.2, unlike Allers & Liu (2013), we do not ignore indices with values straddling the intermediate gravity and field gravity values. As a result, we may be able to identify borderline objects that have index values that hint at intermediate gravities but are not clearly separated from the field values. Therefore, we choose to classify objects with overall gravity classification values within 1σ of INT-G as borderline intermediate gravity (INT-G?). For example, an object with an overall gravity classification value of $0.5^{+0.5}_{-0.5}$ would be classified as INT-G?

Figures 5 and 6 compare the index values for each of our objects with the FLD-G, INT-G, and VL-G regions. In addition, as a visual check on the overall gravity classification, we compare our spectra to known old field dwarfs (FLD-G) and young dwarfs (VL-G) in Figures 7–14. Table 4 tabulates the gravity indices and classification for our objects.

5.2. PS1 Parallaxes, Photometric Distances and Absolute Magnitudes

PS1 has observed the field of each target repeatedly over several years, allowing us to measure the parallax and proper motions of our targets using relative astrometry techniques. We use the image calibrations calculated by the standard Pan-STARRS analysis, but we re-fit the parallax and proper motions for each object with our own re-analysis of these calibrated coordinates (Magnier et al. 2016, in preparation).

The standard astrometric analysis of the PS1 images uses a set of low-order polynomial transformations to correct for the distortion introduced by the optical system and the atmosphere, along with individual corrections for each of the 60 CCDs. The camera-level polynomials are of the form $\sum a_{i,j} x^i y^j$ with $i+j \leq 3$. The individual chip corrections consist of a linear transformation (to account for the chip location and rotation) plus a grid of fine corrections across the chip, with up to 6×6 correction cells per chip. The astrometric transformations are determined by an iterative calculation to minimize the scatter of the adopted reference stars in the database. Mean per-epoch residuals for moderately bright stars range from 10 to 25 mas depending on the Galactic latitude: regions of higher stellar density allow for a better correction.

The standard astrometry analysis also fits each star for proper motion and parallax, but it does not currently use a sufficiently robust outlier rejection scheme. We have specifically re-fitted the proper motion and parallax for our targets with a more stringent rejection of outliers. We first reject any detection with flags indicating failures in the photometry

analysis as well as any detections with insufficient coverage of unmasked pixels ($psf_qf < 0.85$). We use 100 bootstrap resamples of the dataset to measure the parallax and proper motion of the object. For each of these samples we then measure the distance of each point from the fitted path on the sky, scaled by the position errors. Detections which are more than 5σ from the path in more than 50% of the samples are marked as outliers and excluded from the final fit. We also use 1000 bootstrap resample tests of the remaining points to determine the errors on the fitted parameters.

Using our custom astrometry analysis, we have determined parallaxes for eight of our objects and one of the previously known substellar candidate AB Dor members, 2MASS J0058425–0651239 (Gagné et al. 2015c). We show the final fits in Figures 15 and 16. In Figure 17 we plot the fitted parallax motion with the data and the residuals. Our parallaxes are tabulated in Table 1 (for our new candidate members only) and in Table 5.

We also calculated photometric distances for all of our objects (Table 1). We used the average 2MASS *J*-band absolute magnitudes as a function of spectral type tabulated by Dupuy & Liu (2012) to determine photometric distances from our NIR spectral types and *J* apparent magnitude. While Dupuy & Liu (2012) also provide polynomial relations between spectral type and absolute magnitude, these relations have a larger dispersion compared to their tabulated averages because the spectral type range (M6–T9) spanned by the polynomials is much larger than the range for our objects (M6–L4). Therefore, using the average absolute magnitudes as a function of spectral type is more accurate than using the polynomial relation for our purposes. We assume that the photometric distance uncertainty is 20%, in accord with Dupuy & Liu (2012).

Because young late-M dwarfs can be overluminous compared with their older counterparts (e.g. Liu et al. 2013a), we allow their absolute magnitudes to be up to 1.5 mag brighter than the field value since we do not know the ages of our objects. For our late-M dwarfs, we calculate two values for the photometric distance, one using the field absolute magnitudes and one brighter by 1.5 mag. However, young early L dwarfs have absolute magnitudes consistent with those of their older counterparts (e.g. Liu et al. 2013a). Therefore, for our L dwarfs we use the field value when converting from spectral type to absolute magnitude. Thus the uncertainty in the photometric distance for our M dwarfs is significantly larger than for our L dwarfs.

Figure 18 shows the resulting color-magnitude diagram for our objects compared to previously known young and field objects. For our objects, we synthesized *MKO* magnitudes in order to compare with field dwarfs because of the larger amount of *MKO* photometry available for young companions and the Pleiades objects. When synthesizing photometry we used the 2MASS (Skrutskie et al. 2006)³ and *MKO* (Tokunaga et al. 2002) filter profiles and used the 2MASS photometry for flux calibration. We then compared our candidates (Table 6) against known Pleiades members (e.g. Lodieu et al. 2007; Bihain et al. 2010), whose age (125 Myr; e.g. Basri et al. 1996; Martín et al. 1998), is similar to that of the AB Dor Moving Group. In addition, we compared our objects to field dwarfs and young substellar companions based on the compilation by Dupuy & Liu (2012). Our candidate AB Dor Moving Group members have NIR absolute magnitudes and colors consis-

³ http://www.ipac.caltech.edu/2mass/releases/second/doc/sec3_1b1.html

tent with the Pleiades sequence, as expected given the similar ages of the two stellar associations. (Although by construction the NIR absolute magnitudes, for objects without parallaxes, should be consistent with their ages, the NIR colors would not necessarily be the same for our candidates as for other objects with the same age and absolute magnitude.)

5.3. AB Dor Moving Group Membership

We assessed our candidates' membership in the AB Dor Moving Group using the BANYAN II webtool (Malo et al. 2013; Gagné et al. 2014), which calculates membership probabilities for objects using Bayesian inference and the proper motion, sky coordinates and parallactic (or photometric) distance (Section 5.2). In addition, because our objects have spectral signatures of youth, we could improve the accuracy of the BANYAN-II membership probabilities by only using a young (< 1 Gyr) field population to determine the field membership probability. Although the BANYAN II webtool analysis (which uses kinematics only) is different from the full BANYAN II analysis (Gagné et al. 2014, incorporates kinematics and photometry), we have used their field contamination rate curves to approximate the membership quality of our candidates. These field contamination curves suggest that objects (with distances but no radial velocities) with BANYAN II membership probabilities of $\gtrsim 15\%$, $\approx 15\text{--}75\%$, and $\gtrsim 75\%$ would have field contamination rates of $\gtrsim 50\%$, $\approx 50\text{--}10\%$, and $\gtrsim 10\%$, respectively. Also, we note that bona fide members (i.e. members with signatures of youth, proper motions, RVs and parallaxes) can have BANYAN II membership probabilities from 10% to 95% (Gagné et al. 2015b). Therefore, we have roughly divided our sample into three bins based on their BANYAN II webtool memberships, with a few exceptions (Section 5.6): strong candidates ($\geq 75\%$), possible candidates (15–75%), and probable young field interlopers ($< 15\%$).

The BANYAN II webtool also computes statistical distances, i.e. the most probable distance if an object were a member of a given moving group (in this case, the AB Dor Moving Group). We tabulate these distances in Table 1. We compared both the statistical distance and the d_{kin} with the parallactic (or photometric for objects without parallaxes) distances for all of our objects. The statistical distances are consistent within 2σ with the parallactic (or photometric) distances for all of our objects except PSO J035.8–15 where the large difference (3σ) between the statistical and parallactic distances suggests it is a probable young field interloper. For all of our objects, except PSO J236.8–16, the d_{kin} is consistent within the 2σ with the parallactic (or photometric) distance (Figure 19). The discrepancy between the parallactic distance and d_{kin} for PSO J236.8–16 is consistent with it having a low AB Dor Moving Group membership probability and being a probable young field interloper. We also note that the statistical distances are consistent within 2σ of the d_{kin} for all objects.

As another way of assessing membership, we compared the θ for our objects with the θ for the known members (see Section 3, Figure 1). All of our objects have θ under 15° which is consistent with the known members.

We also compared the heliocentric kinematics (UVW) and space positions (XYZ) of our AB Dor Moving Group candidates in Figures 20–31 with the YMG members from Torres et al. (2008) with membership probabilities of at least 75%. For the plotted YMG members, we used radial velocities and parallaxes with values from the literature. For

our candidates, we assumed an probable RV range of -20 to $+20$ km/s, consistent with the range of the bona fide YMG members from Torres et al. (2008) plotted. Eight of our candidates' positions are consistent within 2σ of the average positions of the known AB Dor members within their uncertainties. Note that 3 km/s is the uncertainty in the mean UVW position for the group given the uncertainties in the each coordinate ($\approx 1\text{--}2$ km/s) and that the spatial positions (XYZ) of the known members are more spread out in comparison to the UVW positions (10–50 pc encompasses the 1σ distance range). However, PSO J004.7+41, PSO J035.8–15, PSO J167.1+68, and PSO J236.8–16 have UVW positions inconsistent with AB Dor membership. We tabulate the distance between the mean group UVW and XYZ positions and the closest possible positions of our candidates (within the assumed RV range) in Table 1.

In total, we have three strong candidates, five possible candidates, and four probable young field interlopers. We summarize the final BANYAN II webtool membership probabilities in Table 1, and the BANYAN II webtool and Gagné et al. (2015b,c) membership probabilities, when available, in Table 5. However, these probabilities are likely a lower limit on the actual membership probabilities because our candidates are ≈ 125 Myr, the age of the AB Dor Moving Group, much younger than the 1 Gyr old field population used in the BANYAN II web tool.

5.4. Physical Properties

We calculated the bolometric magnitudes, effective temperatures and masses for our AB Dor Moving Group candidate members, the previously known bona fide substellar members, and candidate substellar members with spectroscopically confirmed youth (Table 7). For all of these properties, we used a Monte Carlo simulation to propagate measurement errors (in distance, spectral type, and age) and determine the 68% confidence limits for each calculated parameter.

We use the Liu et al. (2010) H -band bolometric corrections to determine the absolute bolometric magnitude because the H -band corrections have the lowest dispersion and the bolometric correction changes slowly with spectral type. To use these corrections, we used our synthesized MKO H -band magnitudes.

For our objects, we determined T_{eff} and mass from our estimated bolometric luminosities using the Chabrier et al. (2000) evolutionary models. For our analysis, we assume the age of the AB Dor Moving Group is 125 ± 20 Myr (Luhman et al. 2005; Ortega et al. 2007; Barenfeld et al. 2013) and propagate the uncertainties in age using a Monte Carlo simulation. For our young field interlopers we adopt a more conservative age of 150 ± 100 Myr. Our late-M dwarfs PSO J035.8–15, PSO J236.8–16, and PSO J351.3–11 have masses of 50–100 M_{Jup} . Our L dwarfs, PSO J004.7+41, PSO J039.6–21, PSO J167.1+68, PSO J318.4+35, and PSO J358.5+22 have masses of $\sim 35\text{--}45 M_{Jup}$.

5.5. Comparison with BASS

Eight of our new young brown dwarfs are in the very large ($\sim 10^4$ objects) input catalog of color-selected brown dwarfs from the Gagné et al. (2015b) BASS program, an all-sky survey constructed by combining 2MASS and WISE. Three of our new young brown dwarf candidate members, PSO J292.9–06, PSO J306.0+16 and PSO J318.4+35, are missing from the BASS input catalog because their low

Galactic latitudes ($b = -11^\circ.9$, $-11^\circ.7$ and $-9^\circ.3$, respectively) excluded them from the BASS search ($|b| \geq 15^\circ$). PSO J334.2+28 is also missing from the BASS input catalog, possibly due to its faint 2MASS magnitudes.

However, none of these eight candidate AB Dor Moving Group members included in the BASS input catalog, are in the final Gagné et al. (2015b) catalog of ~ 300 high priority candidate YMG members. In creating this high priority catalog, Gagné et al. (2015b) used 2MASS+WISE proper motions and a color-magnitude diagram to select candidates that are redder than the field sequence. However, based on our parallactic (or photometric) distances to calculate absolute magnitudes, three of our INT-G and one of our FLD-G objects in the BASS input catalog (PSO J035.8–15, PSO J039.6–21, PSO J236.8–16, and PSO J004.7+41) are slightly blue compared to other known young objects and are consistent with the field given their spectral type (Figures 32 and 33) and thus could have been rejected from the high priority catalog.

Although our remaining four objects present in the BASS input catalog, PSO J167.1+68, PSO J236.8–16, PSO J232.2+63, and PSO J358.5+22, may have a red enough $J-K$ color compared with the model used in the BASS survey, our absolute magnitudes may differ from theirs because we calculate absolute magnitudes from photometric distance (from spectral type) whereas they use the statistical distance from their Bayesian analysis. Thus, the BASS survey may have placed these objects in different location on a color-magnitude diagram and rejected them as likely young objects in their analysis. Although the 2MASS+WISE proper motion from Gagné et al. (2015b) could also have removed these objects from their high priority catalog, our PS1+2MASS proper motions are consistent within the uncertainties (Table 1).

Three of our objects present in the BASS input catalog, PSO J167.1+68 (2MASS J11083081+6830169), PSO J232.2+63 (2MASS J15291017+6312539) and PSO J236.8–16 (2MASS J15470557–1626303A), were independently found as candidate moving group members in Gagné et al. (2015c) as part of their less-restricted initial search (see Section 5.6 for details). Determining RVs for PSO J236.8–16 and PSO J232.2+63 would be needed for any further membership assessment. We conclude that PSO J167.1+68 is a young field interloper using the literature RV (Blake et al. 2010) and our PS1 parallax (Section 5.6).

5.6. Summary of Properties of Individual Objects

We have determined properties (i.e. spectral type and mass) and assessed the group membership for our 12 objects. We summarize the results in the following paragraphs (see Section 5.1, Section 5.3, Section 5.4, Section 5.5, and Table 5 for details).

PSO J004.7+41 is a FLD-G, L0.1 dwarf ($40^{+11}_{-13} M_{Jup}$), with a spectrum that shows hints of youth. However, the UVWXYZ positions are inconsistent with AB Dor Moving Group membership and the BANYAN II membership is low, thus we consider it to be a probable young field interloper.

PSO J035.8–15 is an INT-G M7.1 dwarf ($80^{+40}_{-30} M_{Jup}$). Although the UVWXYZ positions for PSO J035–15 are inconsistent with AB Dor Moving Group membership it has a moderate BANYAN II webtool membership probability (49%). We speculate that the membership probability may be optimistic due to the large distance uncertainty. Thus we consider this object to be a probable young field interloper.

PSO J039.6–21 is an INT-G L2 dwarf ($37 \pm 5 M_{Jup}$) with a high membership probability. Its UVWXYZ positions are

also consistent with AB Dor Moving Group membership (except U, which is consistent within 2.5σ). However, it appears to be spectroscopically peculiar. When comparing to known field dwarfs, its spectrum matches very well with the blue L2 dwarf 2MASS J1431+14 (Sheppard & Cushing 2009), a candidate subdwarf. We also note that the overall continuum is more blue than both the FLD-G and VL-G standards, also indicating spectral peculiarity. Thus, as the Allers & Liu (2013) gravity indices were not intended for use on subdwarfs, the INT-G classification may be invalid. However, the kinematics and position appear to be consistent with possible membership with the AB Dor Moving Group. Therefore we conclude that although membership in the group is possible, it could also be a field L-type subdwarf. Thus a radial velocity is still needed to conclude its group membership, or lack thereof.

PSO J167.1+68 is an INT-G L1.8 dwarf ($52^{+14}_{-16} M_{Jup}$) with H α emission which was first discovered in Gizis et al. (2000) as an L1 dwarf (optical spectral type). It was also independently identified as a low probability candidate Carina member in Gagné et al. (2015c). After combining the space positions+kinematics (UVWXYZ; Figure 23), the literature RV (Blake et al. 2010) and our PS1 parallax, we suggest that it is actually unlikely to be a Carina member (BANYAN II webtool probability of zero). As we can completely determine the UVWXYZ positions for this object we conclude that this object is a young field member.

PSO J232.2+63 is an INT-G, M7.8 dwarf ($130^{+20}_{-40} M_{Jup}$) with a membership probability of 37% and UVWXYZ consistent with AB Dor Moving Group membership. It was also independently discovered as a candidate member by Gagné et al. (2015c). Although they note that it has a high young field contamination probability, they did not have a parallactic distance. Thus, because we have a parallactic distance and the RV is still unknown, we still consider it a possible member. We note that the parallactic distance is significantly closer than the photometric distance, even if we assume that young M dwarfs are more luminous by 1.5 mag than their field counterparts. The high estimated mass, suggesting a stellar rather than substellar object, is likely due to the overluminosity of this object.

PSO J236.7–16 is an INT-G M9.4 dwarf ($44^{+12}_{-15} M_{Jup}$) with a very low membership probability and UVWXYZ positions inconsistent with AB Dor Moving Group membership. It was also independently discovered in Gagné et al. (2015c) as a low probability member with a high field contamination probability. With the addition of our PS1 parallax to the membership analysis, we conclude that PSO J236.7–16 is a likely young field interloper. We note that Gagné et al. (2015c) also propose that the nearby object, 2MASS J15470557–1626303B is a low-gravity stellar companion with a spectral type of $M5 \pm 2$.

PSO J292.9–06 is an INT-G M7.6 dwarf ($\approx 55\text{--}110 M_{Jup}$). Although it has a low membership probability, the UVWXYZ positions are consistent with AB Dor Moving Group membership. Thus we consider it to be a possible member.

PSO J306.0+16 is an INT-G? L2.3 dwarf ($34^{+5}_{-6} M_{Jup}$) with a membership probability of 36% and UVWXYZ consistent with AB Dor Moving Group membership. The spectrum shows hints of youth but may still be an older field object. We consider this object as a possible candidate member, requiring parallax and RV to further assess membership.

PSO J334.2+28 is an INT-G L3.5 dwarf ($31^{+6}_{-5} M_{Jup}$) with a low BANYAN II webtool membership probability (0.63%) but with heliocentric kinematics (UVW) and space positions

(XYZ) which are consistent with AB Dor Moving Group membership. One possible reason for the low BANYAN II membership probability is that the distance is 59 ± 12 pc, further than the 1σ distance range of the bona fide members which were used to develop the BANYAN II model. Thus we still consider this object to be a possible candidate.

PSO J351.3–11 is an INT-G M6.5 dwarf ($70^{+50}_{-30} M_{Jup}$) with a membership probability of 50%. As the UVWXYZ positions are also consistent with AB Dor Moving Group membership, we consider it as a possible member.

PSO J358.5+22 is an INT-G? L1.9 dwarf ($36^{+5}_{-6} M_{Jup}$) with a high membership probability (79%), UVWXYZ positions consistent with group membership. Thus, we consider it to be a strong candidate member.

6. DISCUSSION

Low gravity (i.e. young) and dusty field L dwarfs are known to have redder *WISE* colors ($W1-W2$) and NIR colors ($J-K$) compared with their old field counterparts of the same spectral type (e.g. Gizis et al. 2012). Our work sheds light on the colors of these objects at intermediate ages (≈ 125 Myr) and intermediate gravities (INT-G). We compared the $W1-W2$ and $J-K$ colors of our candidate AB Dor Moving Group members with the mean $W1-W2$ and mean $J-K$ colors both young (VL-G and INT-G) and old (FLD-G) dwarfs (Figures 32 and 33).

The average $W1-W2$ colors for VL-G dwarfs tend to be redder than both the FLD-G and the INT-G dwarfs from Allers & Liu (2013), while the INT-G dwarfs have colors more consistent with the FLD-G dwarfs. Three of our candidates appear slightly redder than the mean $W1-W2$ color of old field objects, given their spectral type. But the other nine candidates have $W1-W2$ colors consistent with the field values. Interestingly, there is also no obvious segregation in the $W1-W2$ colors between our objects classified as INT-G and those classified as INT-G? or FLD-G.

The average $J-K$ colors for M6–M9 dwarfs with gravity classifications of VL-G, INT-G and FLD-G are consistent within the uncertainties. However, the $J-K$ colors appear to have a stronger dependency with gravity for dwarfs with spectral types of L0 and later. The average $J-K$ colors of VL-G L0–L3 dwarfs are redder than for the FLD-G L0–L3 dwarfs, with the INT-G L0–L3 dwarf average colors intermediate between VL-G and FLD-G. Yet, there is significant scatter about these trends. Two of our objects, PSO J004.7+41 (FLD-G) and PSO J039.6–21 (INT-G) have slightly blue $J-K$ colors compared with the field values. Another four objects, PSO J167.1+68, PSO J306.0+16, PSO J318.4+35 and PSO J334.2+28, (all INT-G) have $J-K$ colors slightly redder than the field sequence. The remaining objects have $J-K$ colors consistent within the uncertainties in the average field values.

One possible reason that our candidate AB Dor moving group members do not have such distinct IR colors from field ultracool dwarfs is that they have older (≈ 125 Myr) than the young brown dwarf members of the TW Hydrae or β Pic moving groups (~ 10 – 20 Myr), which are classified as VL-G in Allers & Liu (2013) as compared to the FLD-G, INT-G?, and INT-G classifications of our objects. Our AB Dor Moving Group candidates have gravity classifications of INT-G or FLD-G, which suggests that at ≈ 125 Myr, ultracool dwarfs tend to have higher gravities than their younger (i.e. ~ 10 – 50 Myr) counterparts. With these intermediate gravities, our ≈ 125 Myr-old dwarfs also have less extreme IR colors com-

pared with the lower gravity, younger, dwarfs.

Table 5 summarizes the full list of AB Dor Moving Group substellar members from our work and the literature. It includes the properties (kinematics, spectral type, gravity classification, parallax, d_{phot} and RV) of the bona fide substellar members, the previously published substellar candidate AB Dor Moving Group members, and our new candidates. We also include our new parallax for 2MASS J0058–06 from PS1 data. We have calculated the BANYAN II webtool membership probabilities for the candidate members using our proper motions when available, or otherwise those from Gagné et al. (2015b), in addition to our (parallactic or photometric) distances. Our PS1 proper motions agree with the Gagné et al. (2015b) proper motions within the uncertainties so do not likely contribute significantly to any membership probability differences. For objects also in Gagné et al. (2015b,c), we include their tabulated BANYAN II probabilities, which also use SEDs to determine membership probabilities and thus will not agree with the webtool probabilities. Our probabilities may also disagree due to differences in the adopted distances.

7. CONCLUSIONS

We have used PS1, 2MASS and *WISE* photometry coupled with proper motions from PS1 + 2MASS to search for AB Dor Moving Group substellar candidates. Our search method combines color selection with SED fitting and proper motion analysis, thereby significantly decreasing the number of field ultracool dwarf interlopers compared with a solely color-selected sample. We have obtained low and moderate-resolution NIR spectroscopy of our candidates and confirmed the youth of nine objects, six of which we conclude are likely AB Dor Moving Group members. We have also determined the Allers & Liu (2013) gravity classification of our objects and assessed their AB Dor Moving Group membership with the BANYAN II web tool probabilities (Malo et al. 2013; Gagné et al. 2014) and their UVWXYZ positions.

We report the discovery of eight AB Dor Moving Group candidate members with spectral types of M6–L4 and masses down to $\approx 30 M_{Jup}$. Six of these have INT-G gravity classifications (thought one of these INT-G objects is spectroscopically peculiar and may be an ultracool subdwarf). The remaining two objects have uncertain gravity classifications of INT-G? but have kinematics and spatial positions consistent with group membership. In order to distinguish any of our candidate members from being either an AB Dor Moving Group member or unassociated with any known YMG (e.g. Shkolnik et al. 2009, 2012), we still need to determine parallaxes (for three more objects) and radial velocities, which are currently underway.

Finally, we find four objects that we conclude to be probable field interlopers. Three objects are INT-G ultracool dwarfs and one object is a FLD-G ultracool dwarf with a spectrum showing possible hints of youth.

Although many known low gravity (i.e. young) substellar objects have redder IR colors than their old field analogs, our intermediate gravity (≈ 125 Myr) brown dwarfs do not seem to follow this trend. The $W1-W2$ color for the majority of our objects are consistent with FLD-G dwarfs (i.e. older dwarfs) with the same spectral type. Also, the average $J-K$ colors for mid-late M dwarfs with both VL-G and INT-G gravities are consistent with those of their FLD-G counterparts. However, the average $J-K$ colors for early L dwarfs are redder for lower gravity objects compared to those of the FLD-G objects, such

that VL-G dwarfs are very red and INT-G dwarfs are slightly red. This suggests that some young brown dwarfs with ages $\gtrsim 100$ Myr may have IR colors consistent with field objects, unlike the case for younger brown dwarfs ($\lesssim 100$ Myr).

Our updated census of the AB Dor Moving Group brown dwarfs provides a snapshot of brown dwarf evolution. In this era of ample large-area surveys which are sensitive to red, faint substellar objects, refined methods such as ours and those of others (e.g. Gagné et al. 2014) will be able to efficiently uncover the substellar members of the known YMGs. An ensemble of young brown dwarfs age benchmarks will allow us to characterize the brown dwarf spectral evolution. Because young brown dwarfs can be analogs of directly imaged planets (e.g. Liu et al. 2013b), this evolutionary sequence will also be valuable to compare with future spectra of young exoplanets.

KMA's research was supported by the National Science Foundation Graduate Research Fellowship under Grant No. DGE-1329626. KMA's research was also supported by NSF grant AST-1518339. Any opinion, findings, and conclusions or recommendations expressed in this material are those of the authors' and do not necessarily reflect the views of the National Science Foundation. The Pan-STARRS1 Surveys (PS1) have been made possible through contributions of the Institute for Astronomy, the University of Hawaii, the Pan-STARRS Project Office, the Max-Planck Society and its participating institutes, the Max Planck Institute for Astronomy, Heidelberg and the Max Planck Institute for Extraterrestrial Physics, Garching, The Johns Hopkins University, Durham University, the University of Edinburgh, Queen's University Belfast, the Harvard-Smithsonian Center for Astrophysics, the Las Cumbres Observatory Global Telescope Network Incorporated, the National Central University of Taiwan, the Space Telescope

Science Institute, the National Aeronautics and Space Administration under Grant No. NNX08AR22G issued through the Planetary Science Division of the NASA Science Mission Directorate, the National Science Foundation under Grant No. AST-1238877, the University of Maryland, and Eotvos Lorand University (ELTE). We also use data products from the Two Micron All Sky Survey, which is a joint project of the University of Massachusetts and the Infrared Processing and Analysis Center/California Institute of Technology, funded by the National Aeronautics and Space Administration and the National Science Foundation. In addition, we use of data products from the *Wide-field Infrared Survey Explorer*, which is a joint project of the University of California, Los Angeles, and the Jet Propulsion Laboratory/California Institute of Technology, funded by the National Aeronautics and Space Administration. This research has also benefited from the M, L, and T dwarf compendium housed at DwarfArchives.org and maintained by Chris Gelino, Davy Kirkpatrick, and Adam Burgasser. We also use the IRTF Spectral Library housed at http://irtfweb.ifa.hawaii.edu/spex/IRTF_Spectral_Library/index.html and maintained by Michael Cushing. We have also made use of TOPCAT (Taylor 2005), an interactive tool for manipulating and merging tabular data. We would like to thank Katelyn Allers for providing us with her custom version of SpeXtool for reducing *Gemini*/GNIRS data. Finally, mahalo nui loa to the kama'āina of Hawai'i for allowing us to operate telescopes on Mauna Kea. We wish to acknowledge the very significant cultural role Mauna Kea has within the indigenous Hawaiian community and that we are very fortunate to be able to conduct observations.

Facilities: IRTF (SpeX), Gemini:North (GNIRS), Pan-STARRS1, 2MASS, *WISE*.

APPENDIX

COMPARISON OF PS1 AND SDSS PROPER MOTIONS IN STRIPE 82

In order to evaluate our proper motion quality, we compared the proper motions of stars in the SDSS Stripe 82 with those measured by our methods using PS1+2MASS data. Stripe 82 (Bramich et al. 2008) has a total sky area of ≈ 250 deg² and spans 99° in R.A. ($\alpha = 20.7^h - 3.3^h$) and 2.52° in decl. ($\delta = -1.26^\circ$ to $+1.26^\circ$). The 7 year time baseline of SDSS yielded proper motions to an accuracy of ≈ 5 mas yr⁻¹. We matched the SDSS Stripe 82 stars with their counterparts in the PS1 catalog using a $2''$ search radius. We then chose the subset of matches which had at least 20 epochs of PS1+2MASS data and had proper motions below $1''$ yr⁻¹. Also, since the PS1 and SDSS z -band filters are similar ($\Delta z \leq 0.2$ mag for stellar objects; Tonry et al. 2012), we excluded stars with significantly deviant PS1 and SDSS z magnitudes ($|\Delta z| \geq 0.2$ mag) in order to remove potential mismatches. Finally, we also required all PS1 objects to have good quality z -band photometry as defined in the same fashion as for our search (Section 2).

The total matched sample consisted of 216,902 stars with PS1 proper motion uncertainties below 20 mas yr⁻¹ in both proper motion in R.A. (μ_α) and in decl. (μ_δ). We separated our analysis into three PS1 proper motion error bins: ≤ 10 mas yr⁻¹, $10-20$ mas yr⁻¹, and ≤ 20 mas yr⁻¹. The median and the 68.5% range of the differences between the PS1 and SDSS proper motions was 3 ± 8 mas yr⁻¹ in μ_α and -7 ± 7 mas yr⁻¹ in μ_δ for objects with PS1 proper motion uncertainties below 10 mas yr⁻¹. For objects with PS1 proper motion uncertainties between 10 and 20 mas yr⁻¹, the differences were 3 ± 18 mas yr⁻¹ in μ_α and -8 ± 21 mas yr⁻¹ in μ_δ . For all the objects with PS1 proper motion uncertainties below 20 mas yr⁻¹, differences were 3 ± 11 mas yr⁻¹ in μ_α and -7 ± 10 mas yr⁻¹ in μ_δ (Figures 34 and 35). Thus, we conclude that the PS1 and SDSS proper motions are consistent within the uncertainties and that the PS1 proper motions are reliable.

REFERENCES

- Aller, K. M., et al. 2013, ApJ, 773, 63
 Allers, K. N., & Liu, M. C. 2013, ApJ, 772, 79
 Allers, K. N., et al. 2007, ApJ, 657, 511
 Barenfeld, S. A., Bubar, E. J., Mamajek, E. E., & Young, P. A. 2013, ApJ, 766, 6

- Barrado y Navascués, D., Stauffer, J. R., & Jayawardhana, R. 2004, *ApJ*, 614, 386
- Barrado y Navascués, D., Stauffer, J. R., & Patten, B. M. 1999, *ApJ*, 522, L53
- Basri, G., Marcy, G. W., & Graham, J. R. 1996, *ApJ*, 458, 600
- Bihain, G., Rebolo, R., Zapatero Osorio, M. R., Béjar, V. J. S., & Caballero, J. A. 2010, *A&A*, 519, A93
- Billér, B. A., et al. 2013, *ApJ*, 777, 160
- Blake, C. H., Charbonneau, D., & White, R. J. 2010, *ApJ*, 723, 684
- Bonnefoy, M., et al. 2013, *A&A*, 555, A107
- . 2014, *A&A*, 562, A111
- Bowler, B. P., Liu, M. C., Dupuy, T. J., & Cushing, M. C. 2010, *ApJ*, 723, 850
- Bowler, B. P., Liu, M. C., Shkolnik, E. L., & Dupuy, T. J. 2013, *ApJ*, 774, 55
- Bramich, D. M., et al. 2008, *MNRAS*, 386, 887
- Burningham, B., et al. 2011, *MNRAS*, 414, 3590
- Carson, J., et al. 2013, *ApJ*, 763, L32
- Chabrier, G., Baraffe, I., Allard, F., & Hauschildt, P. 2000, *ApJ*, 542, 464
- Chauvin, G., Lagrange, A.-M., Dumas, C., Zuckerman, B., Mouillet, D., Song, I., Beuzit, J.-L., & Lowrance, P. 2005, *A&A*, 438, L25
- Close, L. M., Thatte, N., Nielsen, E. L., Abuter, R., Clarke, F., & Tecza, M. 2007, *ApJ*, 665, 736
- Cushing, M. C., Rayner, J. T., & Vacca, W. D. 2005, *ApJ*, 623, 1115
- Cushing, M. C., Vacca, W. D., & Rayner, J. T. 2004, *PASP*, 116, 362
- Delorme, P., et al. 2013, *A&A*, 553, L5
- Dupuy, T. J., & Liu, M. C. 2012, *ApJS*, 201, 19
- Faherty, J. K., Burgasser, A. J., Cruz, K. L., Shara, M. M., Walter, F. M., & Gelino, C. R. 2009, *AJ*, 137, 1
- Faherty, J. K., Rice, E. L., Cruz, K. L., Mamajek, E. E., & Núñez, A. 2013, *AJ*, 145, 2
- Gagné, J., Burgasser, A. J., Faherty, J. K., Lafrenière, D., Doyon, R., Filippazzo, J. C., Bowsher, E., & Nicholls, C. P. 2015a, *ApJ*, 808, L20
- Gagné, J., Lafrenière, D., Doyon, R., Malo, L., & Artigau, É. 2014, *ApJ*, 783, 121
- . 2015b, *ApJ*, 798, 73
- Gagné, J., et al. 2015c, *ApJS*, 219, 33
- Gauza, B., Béjar, V. J. S., Pérez-Garrido, A., Rosa Zapatero Osorio, M., Lodieu, N., Rebolo, R., Pallé, E., & Nowak, G. 2015, *ApJ*, 804, 96
- Gizis, J. E., Allers, K. N., Liu, M. C., Harris, H. C., Faherty, J. K., Burgasser, A. J., & Kirkpatrick, J. D. 2015, *ApJ*, 799, 203
- Gizis, J. E., Monet, D. G., Reid, I. N., Kirkpatrick, J. D., Liebert, J., & Williams, R. J. 2000, *AJ*, 120, 1085
- Gizis, J. E., et al. 2012, *AJ*, 144, 94
- Kirkpatrick, J. D., et al. 2010, *ApJS*, 190, 100
- . 2014, *ApJ*, 783, 122
- Kraus, A. L., & Hillenbrand, L. A. 2007, *AJ*, 134, 2340
- Leggett, S. K., et al. 2010, *ApJ*, 710, 1627
- Liu, M. C., Dupuy, T. J., & Allers, K. N. 2013a, *Astronomische Nachrichten*, 334, 85
- Liu, M. C., Dupuy, T. J., & Leggett, S. K. 2010, *ApJ*, 722, 311
- Liu, M. C., et al. 2013b, *ApJ*, 777, L20
- Lodieu, N., Dobbie, P. D., Deacon, N. R., Hodgkin, S. T., Hambly, N. C., & Jameson, R. F. 2007, *MNRAS*, 380, 712
- Luhman, K. L., Stauffer, J. R., & Mamajek, E. E. 2005, *ApJ*, 628, L69
- Luhman, K. L., et al. 2007, *ApJ*, 654, 570
- Magnier, E. 2006, in *The Advanced Maui Optical and Space Surveillance Technologies Conference*
- Malo, L., Doyon, R., Lafrenière, D., Artigau, É., Gagné, J., Baron, F., & Riedel, A. 2013, *ApJ*, 762, 88
- Marois, C., Macintosh, B., Barman, T., Zuckerman, B., Song, I., Patience, J., Lafrenière, D., & Doyon, R. 2008, *Science*, 322, 1348
- Martín, E. L., Basri, G., Gallegos, J. E., Rebolo, R., Zapatero-Osorio, M. R., & Béjar, V. J. S. 1998, *ApJ*, 499, L61
- McLean, I. S., McGovern, M. R., Burgasser, A. J., Kirkpatrick, J. D., Prato, L., & Kim, S. S. 2003, *ApJ*, 596, 561
- Naud, M.-E., et al. 2014, *ApJ*, 787, 5
- Nielsen, E. L., et al. 2012, *ApJ*, 750, 53
- . 2013, *ApJ*, 776, 4
- Ortega, V. G., Jilinski, E., de La Reza, R., & Bazzanella, B. 2007, *MNRAS*, 377, 441
- Patience, J., King, R. R., de Rosa, R. J., & Marois, C. 2010, *A&A*, 517, A76
- Rayner, J. T., Cushing, M. C., & Vacca, W. D. 2009, *ApJS*, 185, 289
- Rayner, J. T., Toomey, D. W., Onaka, P. M., Denault, A. J., Stahlberger, W. E., Vacca, W. D., Cushing, M. C., & Wang, S. 2003, *PASP*, 115, 362
- Reid, I. N., & Walkowicz, L. M. 2006, *PASP*, 118, 671
- Schlieder, J. E., Lépine, S., & Simon, M. 2012, *AJ*, 143, 80
- Sheppard, S. S., & Cushing, M. C. 2009, *AJ*, 137, 304
- Shkolnik, E., Liu, M. C., & Reid, I. N. 2009, *ApJ*, 699, 649
- Shkolnik, E. L., Anglada-Escudé, G., Liu, M. C., Bowler, B. P., Weinberger, A. J., Boss, A. P., Reid, I. N., & Tama, M. 2012, *ApJ*, 758, 56
- Skrutskie, M. F., et al. 2006, *AJ*, 131, 1163
- Slesnick, C. L., Hillenbrand, L. A., & Carpenter, J. M. 2004, *ApJ*, 610, 1045
- Stubbs, C. W., Doherty, P., Cramer, C., Narayan, G., Brown, Y. J., Lykke, K. R., Woodward, J. T., & Tonry, J. L. 2010, *ApJS*, 191, 376
- Taylor, M. B. 2005, in *Astronomical Society of the Pacific Conference Series*, Vol. 347, *Astronomical Data Analysis Software and Systems XIV*, ed. P. Shopbell, M. Britton, & R. Ebert, 29
- Tokunaga, A. T., Simons, D. A., & Vacca, W. D. 2002, *PASP*, 114, 180
- Tonry, J. L., et al. 2012, *ApJ*, 750, 99
- Torres, C. A. O., Quast, G. R., Melo, C. H. F., & Sterzik, M. F. 2008, *Young Nearby Loose Associations*, 757
- Vacca, W. D., Cushing, M. C., & Rayner, J. T. 2003, *PASP*, 115, 389
- Wahhaj, Z., et al. 2011, *ApJ*, 729, 139
- Weinberger, A. J., Anglada-Escudé, G., & Boss, A. P. 2013, *ApJ*, 762, 118
- Wright, E. L., et al. 2010, *AJ*, 140, 1868
- York, D. G., et al. 2000, *AJ*, 120, 1579
- Zuckerman, B., Rhee, J. H., Song, I., & Bessell, M. S. 2011, *ApJ*, 732, 61
- Zuckerman, B., & Song, I. 2004, *ARA&A*, 42, 685
- Zuckerman, B., Song, I., & Bessell, M. S. 2004, *ApJ*, 613, L65

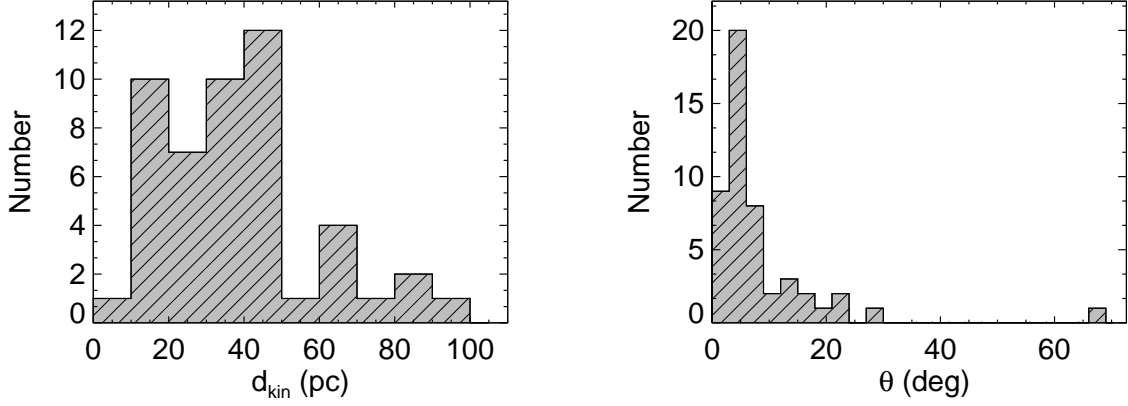


FIG. 1.— The kinematic distance (d_{kin}) and θ for the known AB Dor Moving Group members with membership probability greater than 90% and parallaxes (Torres et al. 2008). We required our candidate AB Dor Moving Group members to have $\theta \leq 40^\circ$ because the majority of the known members also satisfy this requirement.

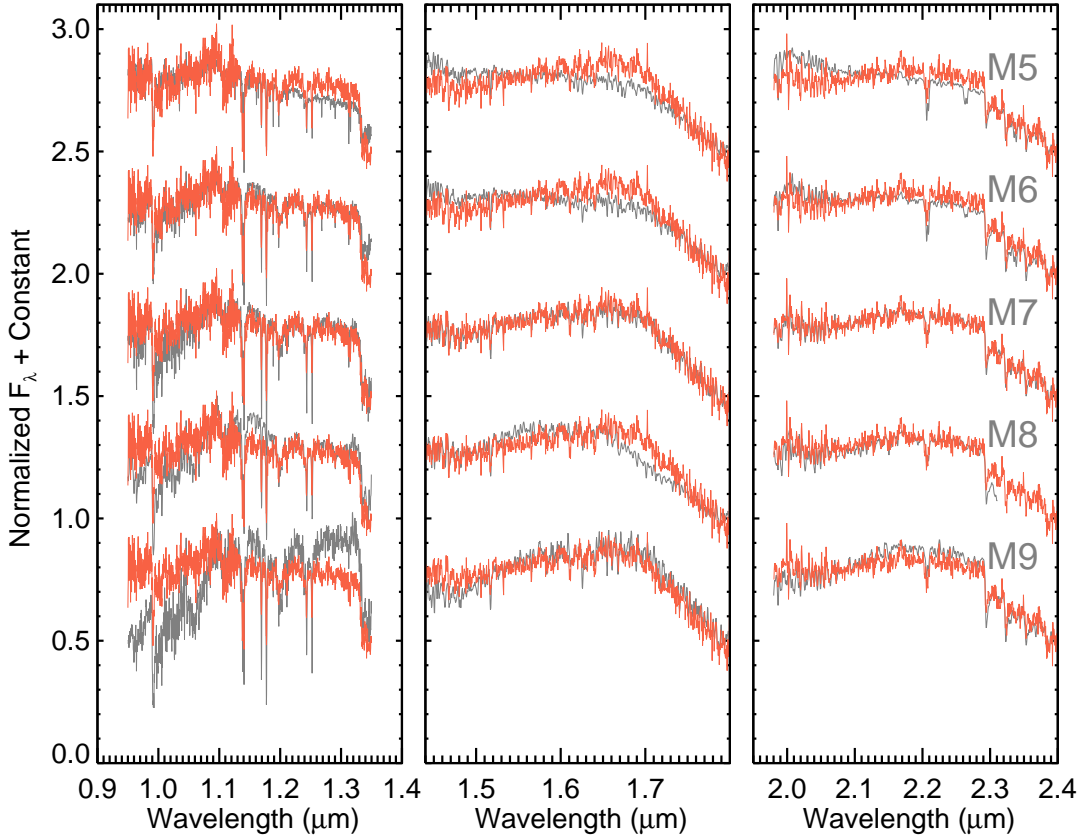


FIG. 2.— An example of visual classification of one of our candidate AB Dor Moving Group members, PSO J035.8-15 (dark orange), by comparing to the Kirkpatrick et al. (2010) spectral standard M dwarfs (gray). The standards were taken from the IRTF Spectral Library (Cushing et al. 2005) and smoothed to the resolution of our candidate spectrum (in this case, $R \sim 750$). The standards are, from top to bottom: Gl 51 (M5), Gl 406 (M6), Gl 644C (M7), VB 10 (M8), and LHS 2924 (M9). The spectral type determined from visual classification for this object is $M7 \pm 1$ in both the J and K band.

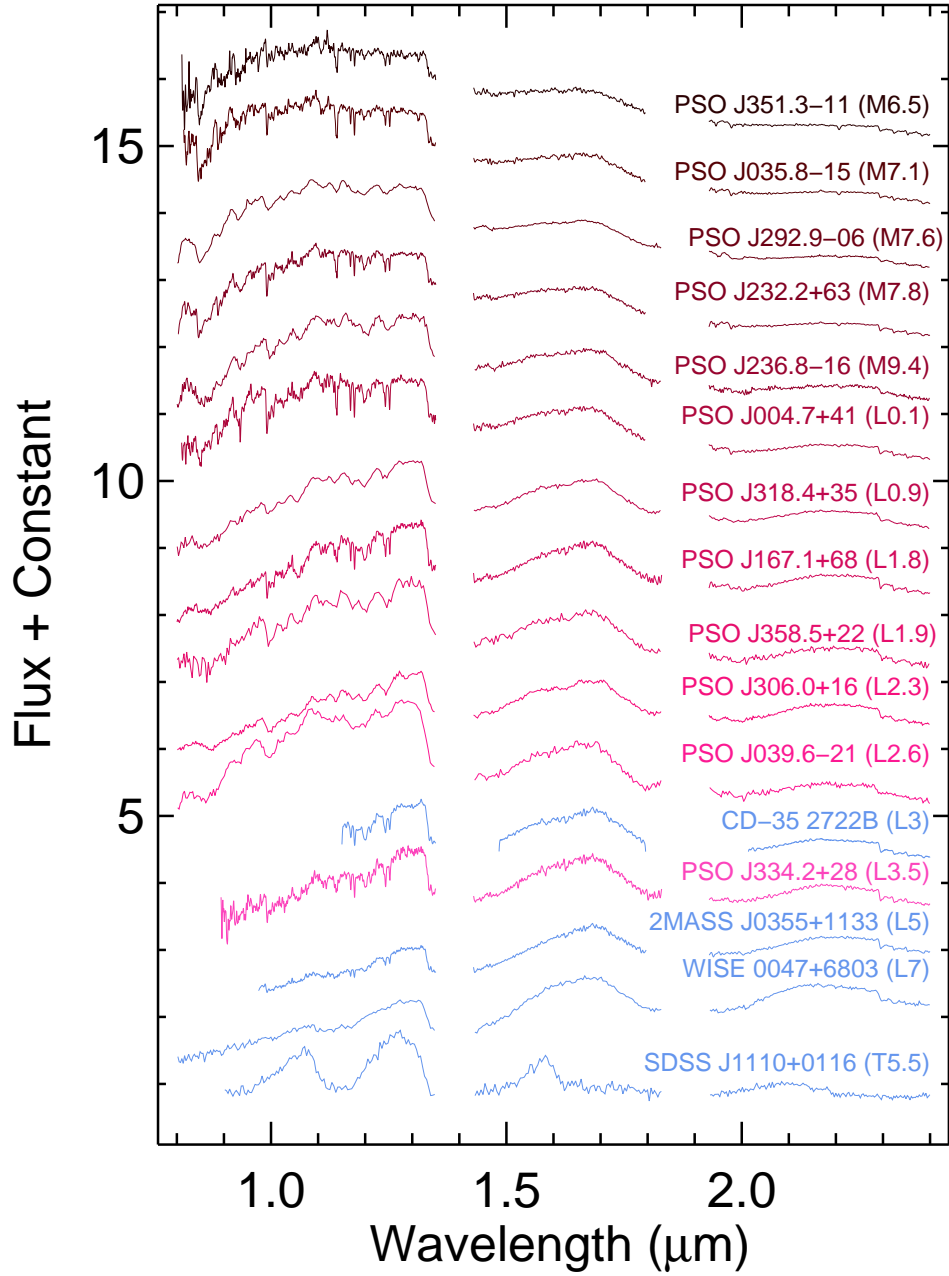


FIG. 3.— NIR spectra of our confirmed-young brown dwarf AB Dor Moving Group candidates (*shades of red*) in addition to the four known brown dwarf members (*blue*) with publicly available spectra: CD-35 2722 B (Wahhaj et al. 2011), 2MASS J0355+1133 (Liu et al. 2013a; Faherty et al. 2013), WISEP J0047+6803 (Gizis et al. 2012, 2015) and SDSS J1110+0116 (Gagné et al. 2015a). The spectra are ordered from earliest spectral type (highest mass) to latest spectral type (lowest mass).

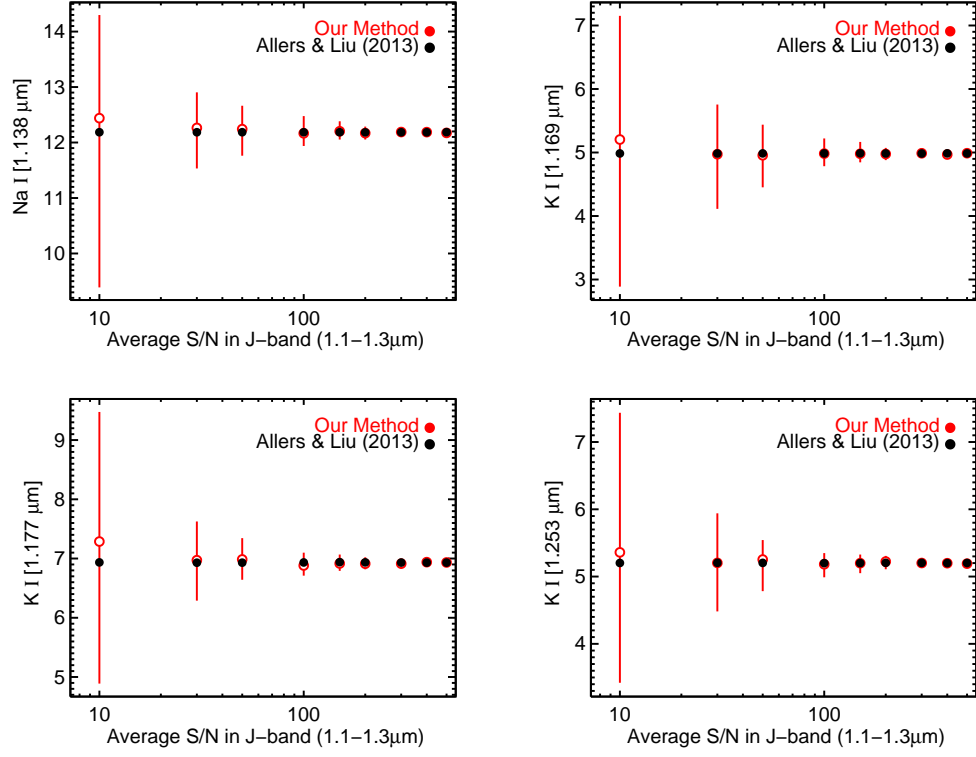


FIG. 4.— Comparison of the pseudo-equivalent width measurement uncertainties using our method (*red open circles*) and the Allers & Liu (2013) method (*black circles*). We include measurement uncertainties, whereas Allers & Liu (2013) only consider uncertainties in measuring continuum, which would dominate for high S/N spectra ($S/N \gtrsim 200$). For our relatively lower S/N objects ($S/N \approx 40$ – 100), we need to also include measurement errors when computing the uncertainties in the pseudo-equivalent widths. Although our measurement uncertainties are larger, our pseudo-equivalent widths are consistent with Allers & Liu (2013).

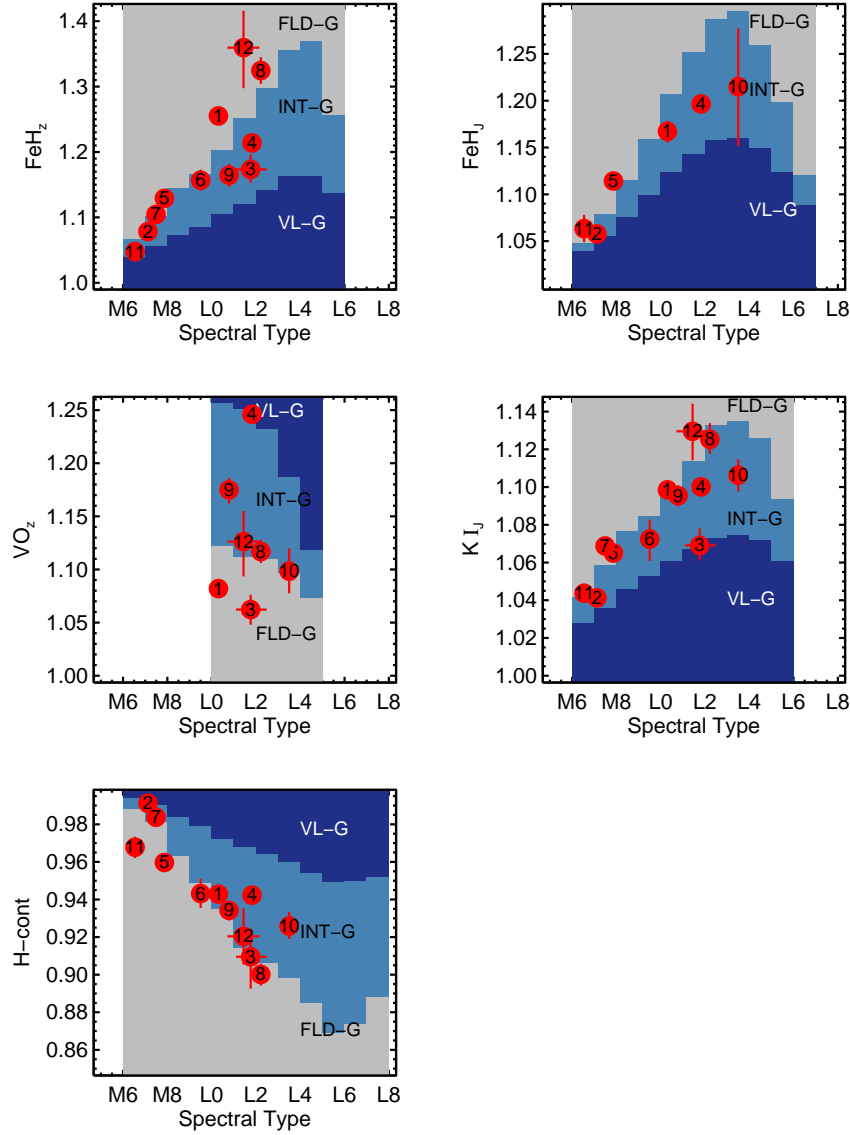


FIG. 5.— NIR spectral indices from all of our candidate AB Dor Moving Group members. For the FeH_z , VO_z and KI_J indices, we smoothed the spectra to prism resolution ($R \sim 130$) because the indices are tailored for prism-resolution spectra. We compare the indices of our numbered candidates (*red circles*) with the defining values for very low gravity (VL-G), intermediate gravity (INT-G) and field gravity (FLD-G) taken from Allers & Liu (2013). Our objects are numbered as follows: (1) PSO J004.7+41, (2) PSO J035.8–15, (3) PSO J039.6–21, (4) PSO J167.1+68, (5) PSO J232.2+63, (6) PSO J236.8–16, (7) PSO J292.9–06, (8) PSO J306.0+16, (9) PSO J318.4+35, (10) PSO J334.2+28, (11) PSO J351.3–11, (12) PSO J358.5+22. The shaded regions define the gravity classification of FLD-G (*gray*), INT-G (*gray blue*) and VL-G (*dark blue*) for each index. Note that some indices only can be used for overall gravity classification within a range of spectral types or resolution (i.e. FeH_J is only for $R \gtrsim 500$). In these cases, we do not use the index value to determine the object's gravity score. We expect our AB Dor Moving Group candidates to have INT-G given the age of the group (≈ 125 Myr).

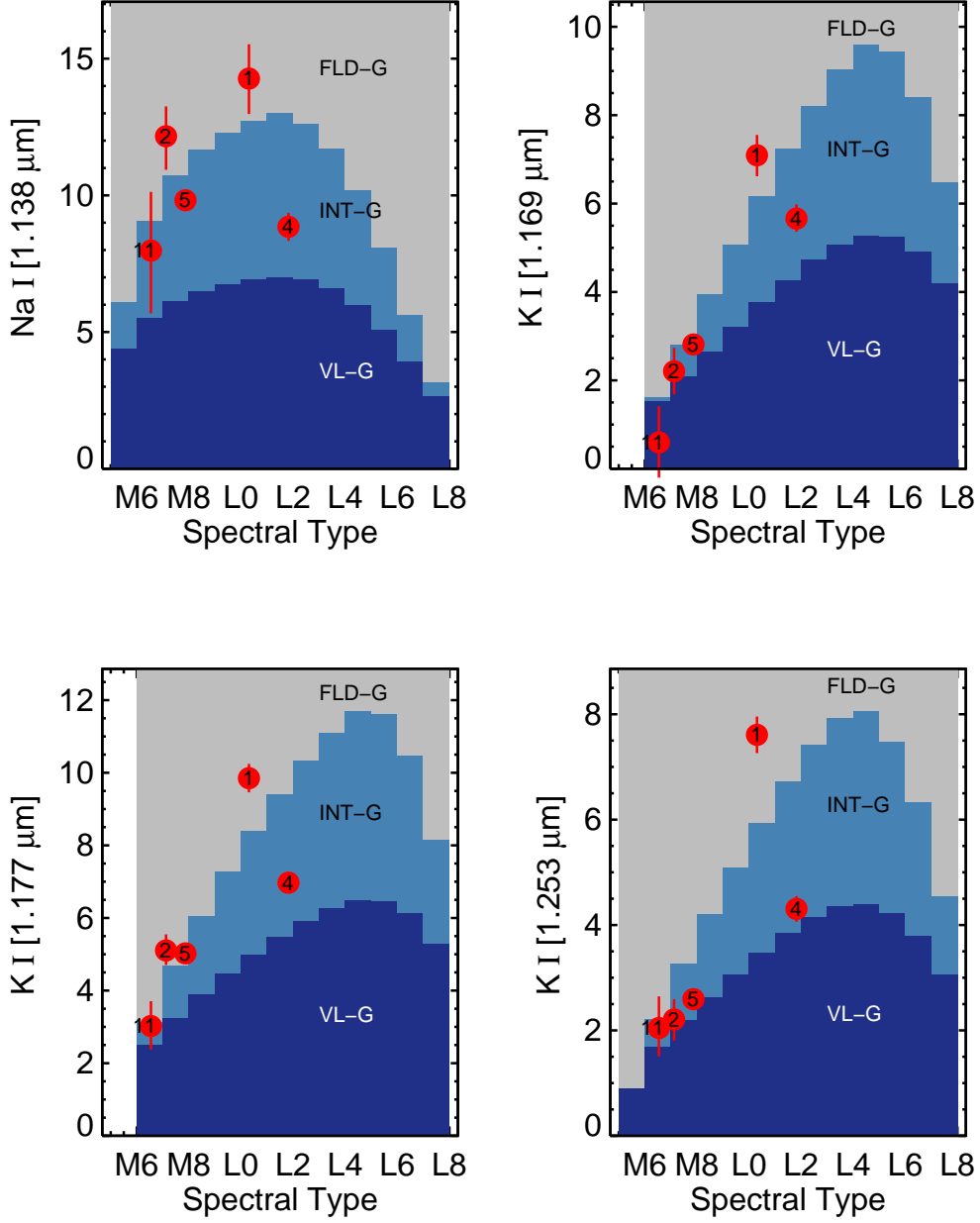


FIG. 6.— NIR spectral indices of our candidate AB Dor Moving Group members taken in the cross-dispersed mode in IRTF/SpEX. We compare the indices of our candidates with the defining values for very low gravity (VL-G), intermediate gravity (INT-G), and field gravity (FLD-G) taken from Allers & Liu (2013). The shaded regions define the gravity classification of FLD-G (gray), INT-G (gray blue) and VL-G (dark blue) for each index. We expect our AB Dor Moving Group candidates to have intermediate gravities. Our objects have the same number labels as Figure 5.

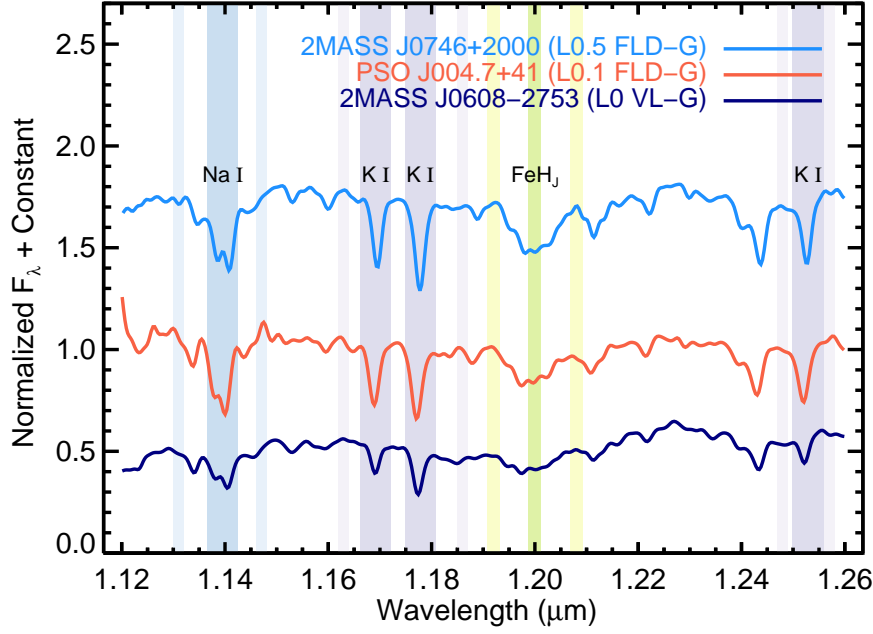


FIG. 7.— NIR moderate-resolution ($R \sim 750$) J -band spectra from IRTF/SpeX of our AB Dor Moving Group candidate, PSO J004.7+41 (red), compared with a field gravity (FLD-G, light blue) and young, very low gravity (VL-G, dark blue) dwarf of similar spectral type (within half a spectral type). For our comparison spectra, we used the field spectral type standard objects from Kirkpatrick et al. (2010) if there was available SXD spectra in the SpeX Library. If not, we used the non-standard field object taken in SXD mode with the closest spectral type to our object. Young dwarfs were taken from the list of standard young objects in Allers & Liu (2013) if there was available moderate-resolution spectra. If not, we used a non-standard VL-G object from Allers & Liu (2013) with a spectral type within a half a spectral type of our object. Gravity-sensitive features in the J band from Allers & Liu (2013) are labeled and the wavelength ranges used to calculate gravity indices are highlighted for Na I (blue), K I (purple), and FeH_J (yellow-green). Members of the AB Dor Moving Group have an age of ≈ 125 Myr, thus are expected to have intermediate gravities lying between the field dwarfs (FLD-G) and young dwarfs (VL-G). Although this object, PSO J004.7+41 has a gravity classification of FLD-G, the gravity indices show minor hints of intermediate gravity.

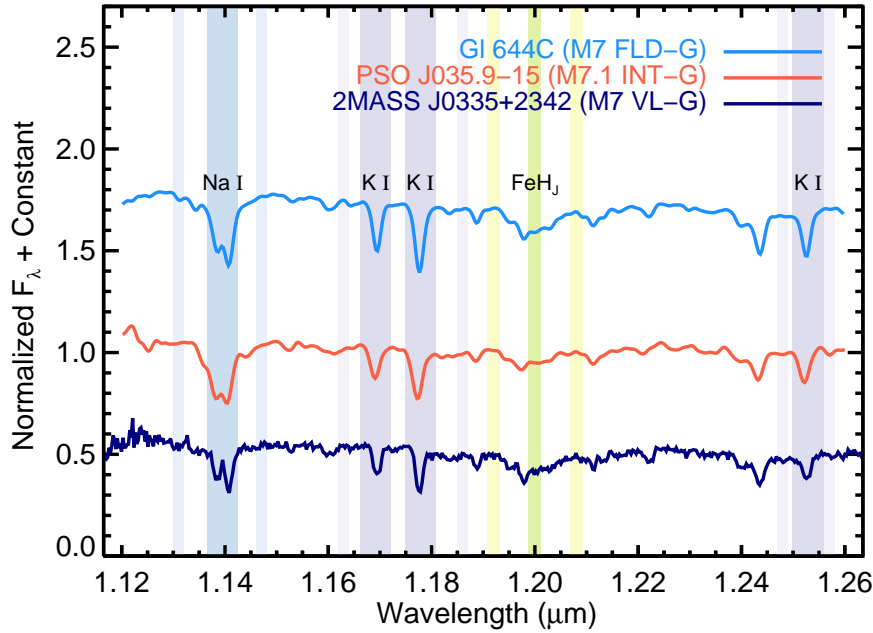


FIG. 8.— NIR moderate-resolution ($R \sim 750$) spectra from IRTF/SpeX of our AB Dor Moving Group candidate, PSO J035.8-15 (red), compared with a FLD-G (light blue) and VL-G (dark blue) dwarf of similar spectral type (within half a spectral type). We choose the comparison spectra as described in Figure 7.

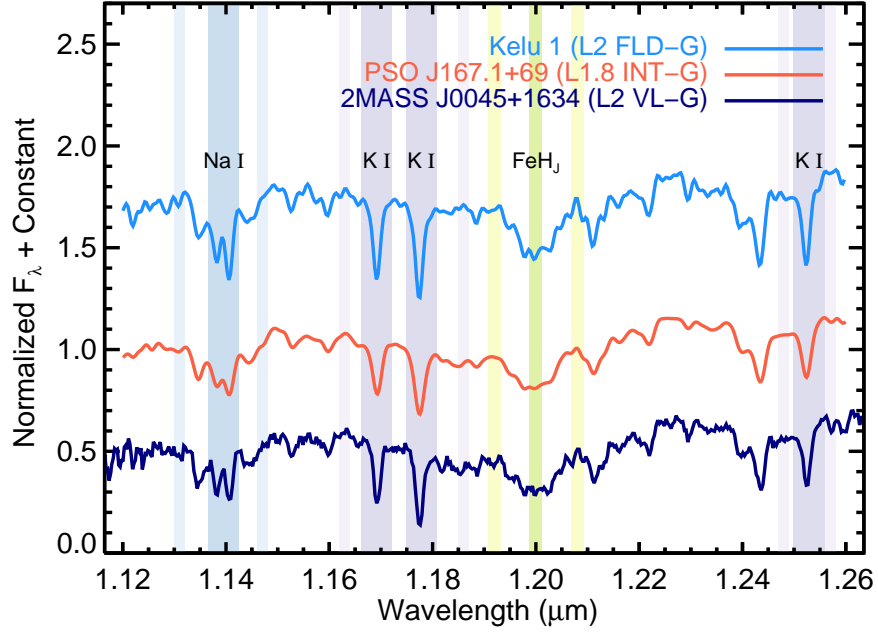


FIG. 9.— NIR moderate-resolution ($R \sim 750$) spectra from IRTF/SpeX of one of our AB Dor Moving Group candidates, PSO J167.1+68 (*red*), compared with a FLD-G (*light blue*) and VL-G (*dark blue*) dwarf of similar spectral type (within half a spectral type). We choose the comparison spectra as described in Figure 7.

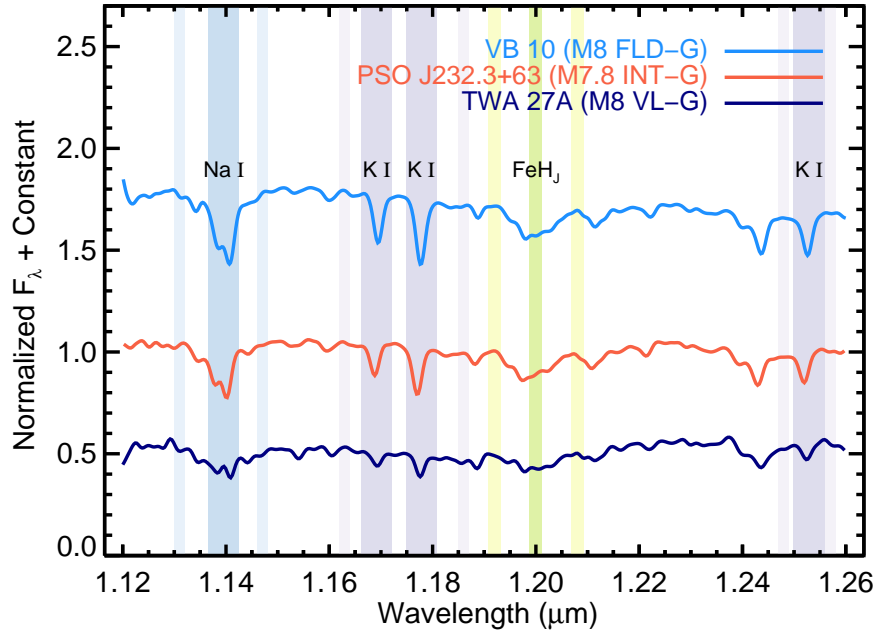


FIG. 10.— NIR moderate-resolution ($R \sim 750$) spectra from IRTF/SpeX of one of our AB Dor Moving Group candidates, PSO J232.2+63 (*red*), compared with a FLD-G (*light blue*) and VL-G (*dark blue*) dwarf of similar spectral type (within half a spectral type). We choose the comparison spectra as described in Figure 7.

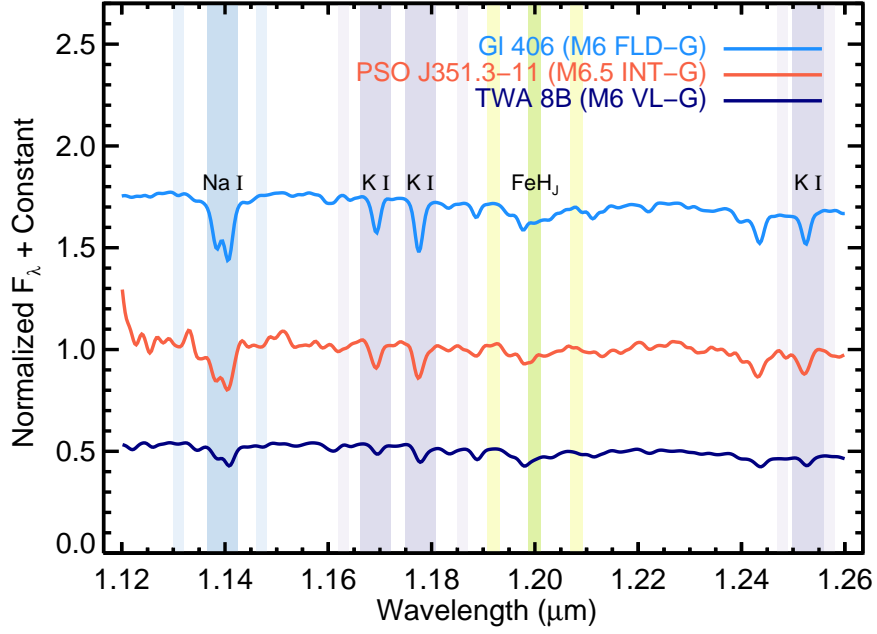


FIG. 11.— NIR moderate-resolution ($R \sim 750$) spectra from IRTF/Spex of one of our AB Dor Moving Group candidates, PSO J351.3–11 (*red*), compared with a FLD-G (*light blue*) and VL-G (*dark blue*) dwarf of similar spectral type (within half a spectral type). We choose the comparison spectra as described in Figure 7.

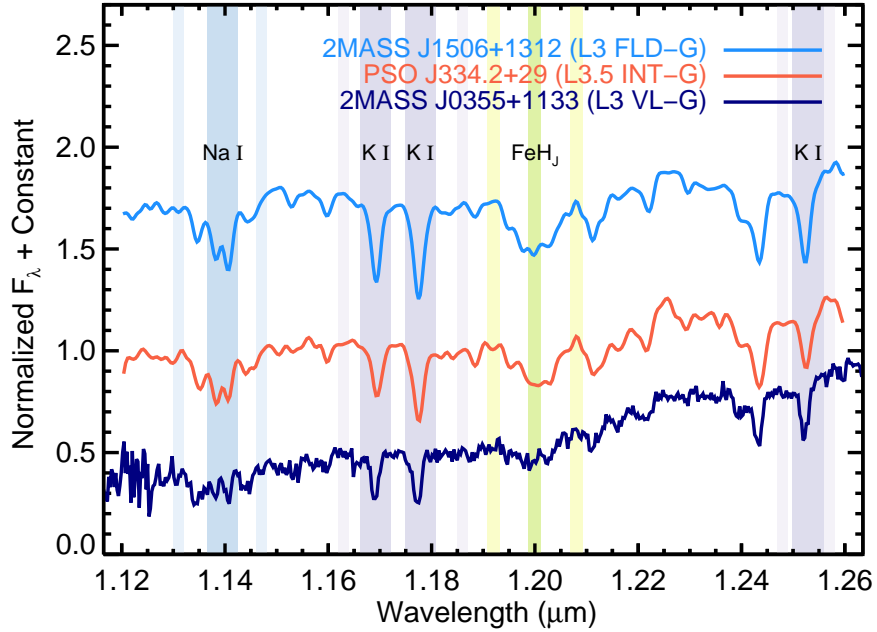


FIG. 12.— NIR moderate-resolution ($R \sim 1700$) spectra from *Gemini*/GNIRS of one of our AB Dor Moving Group candidates, PSO J334.2+28 (*red*), compared with a FLD-G (*light blue*) and VL-G (*dark blue*) dwarf of similar spectral type (within half a spectral type). We choose the comparison spectra as described in Figure 7.

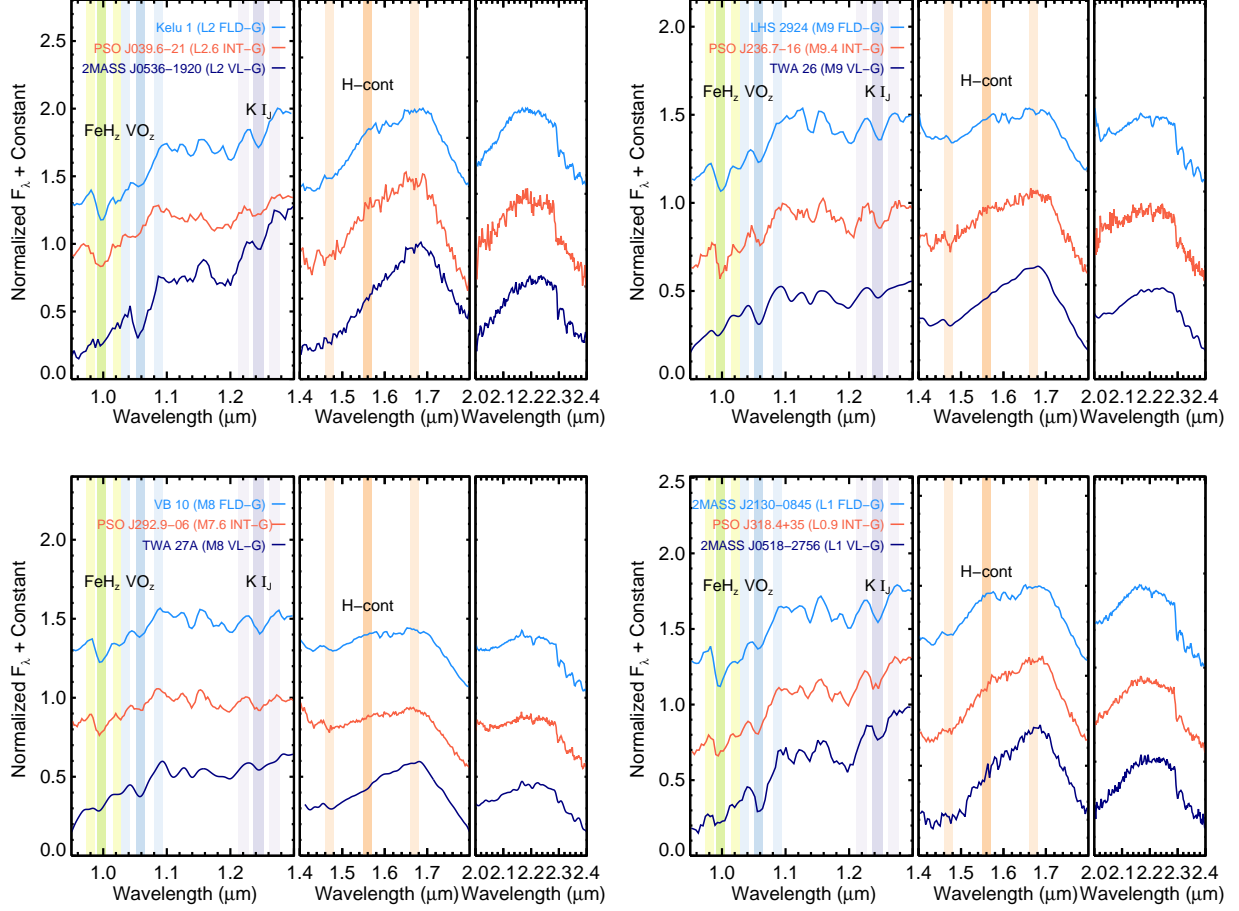


FIG. 13.— NIR low-resolution ($R \sim 130$) spectra from IRTF/SpeX of our candidates with overall gravity classifications of INT-G compared with a FLD-G (*light blue*) and a young, very low gravity (*dark blue*) dwarf of similar spectral type (within half a spectral type). We used field spectral standards from Kirkpatrick et al. (2010) if there was available low-resolution or moderate-resolution spectra. Young dwarfs were taken from the list of standard VL-G objects in Allers & Liu (2013) with publicly available spectra. All comparison spectra have been smoothed to $R \sim 130$. Gravity-sensitive features from Allers & Liu (2013) are labeled and the wavelength ranges used to calculate the gravity indices are highlighted for FeH_2 (yellow-green), VO_2 (blue), KI_J (purple), and H-cont (orange).

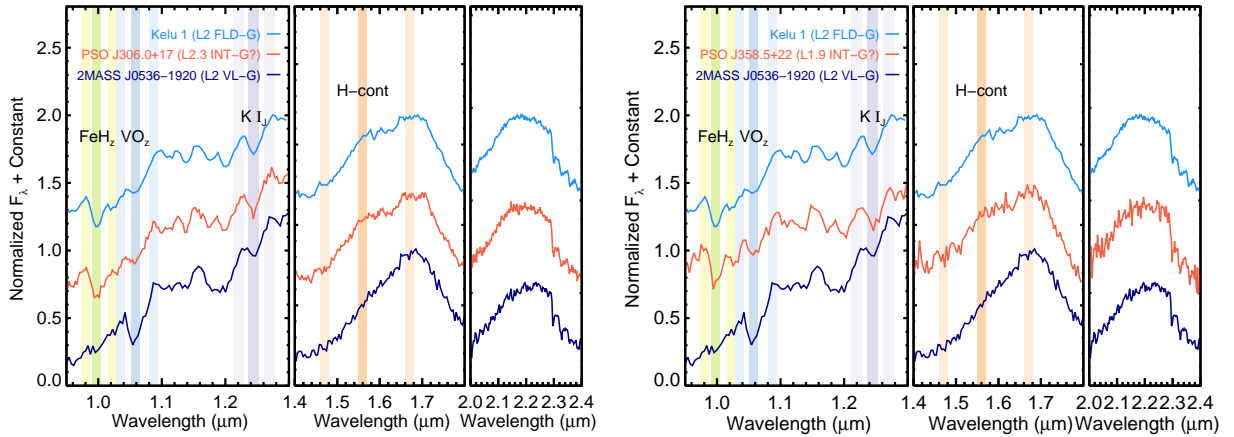


FIG. 14.— NIR low-resolution ($R \sim 130$) spectra from IRTF/SpeX of our candidates with overall gravity classifications of INT-G? compared with a FLD-G (*light blue*) and a young, very low gravity (*dark blue*) dwarf of similar spectral type (within half a spectral type). All comparison spectra have been chosen as described in Figure 5 and smoothed to $R \sim 130$. Gravity-sensitive features from Allers & Liu (2013) are labeled and the wavelength ranges used to calculate the gravity indices are highlighted for FeH_2 (yellow-green), VO_2 (blue), KI_J (purple), and H-cont (orange).

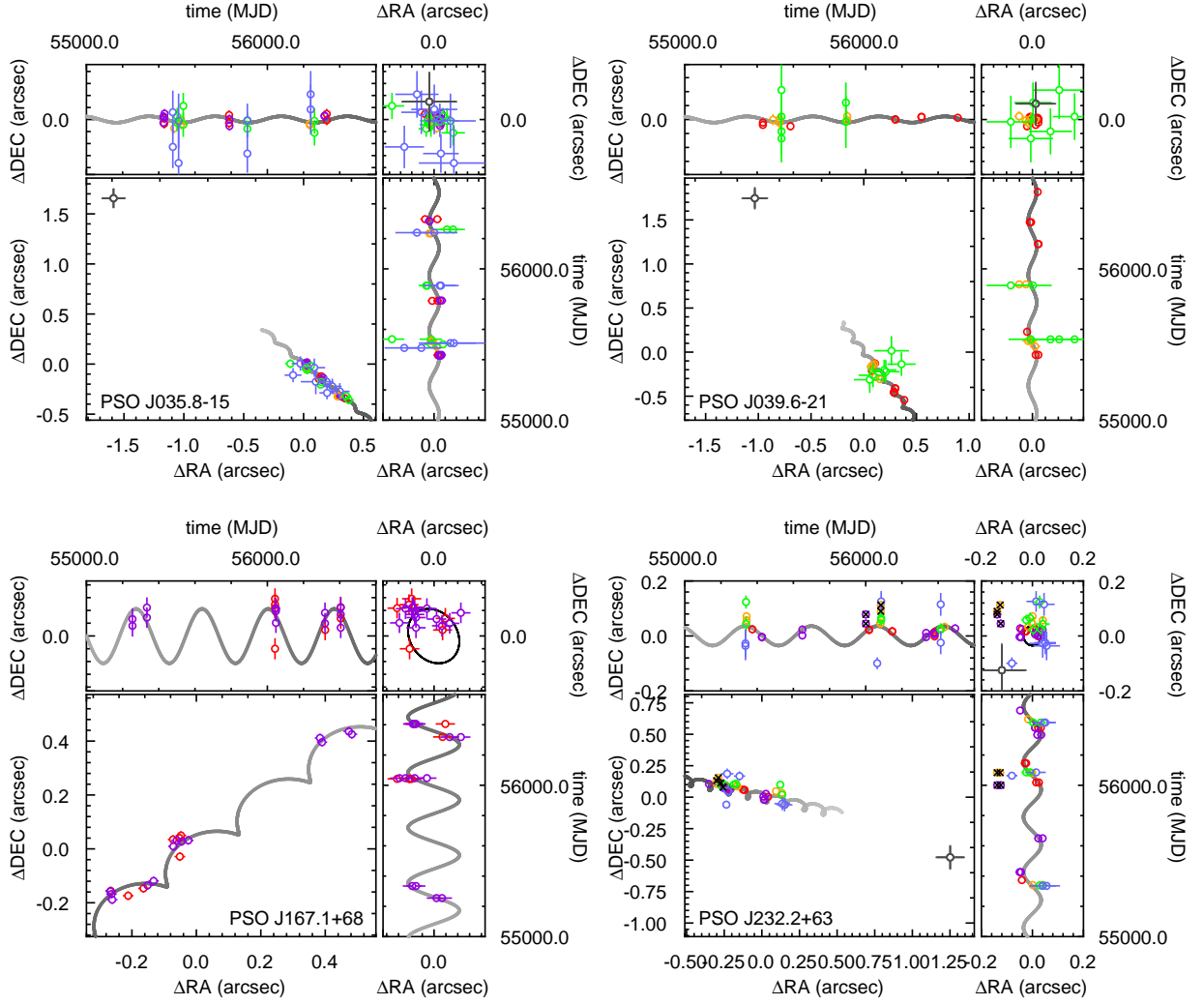


FIG. 15.— PS1 parallax motion and the motion in both R.A. and decl. for PSO J035.8-15 (top left), PSO J039.6-21 (top right), PSO J167.1+68 (bottom left), and PSO J232.2-63 (bottom right). The different color symbols correspond to the filter used to determine the astrometric position for g_{P1} (blue), r_{P1} (green), i_{P1} (orange), z_{P1} (purple), y_{P1} (red), and 2MASS (gray). The x marks denote points rejected as outliers during the astrometric fit. The thick gray line denotes the best fit where the object is moving from the light-dark gray over time.

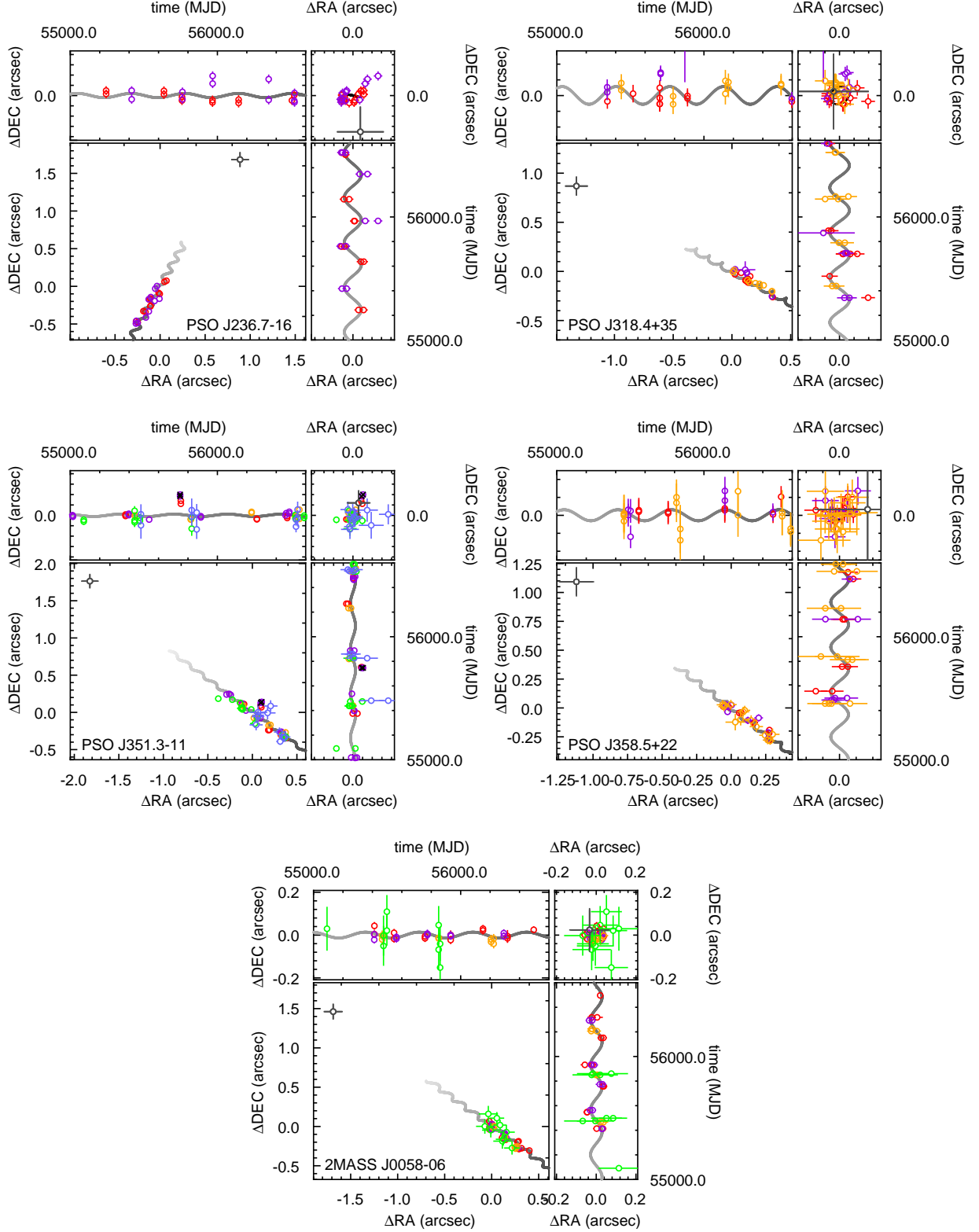


FIG. 16. — PS1 parallax motion and the motion in both R.A. and decl. for PSO J236.8-16 (top left), PSO J318.4+35 (top right), PSO J351.3-11 (middle left), PSO J358.5+22 (middle right) and the previously-identified candidate member, 2MASS J0058-06 (bottom left). The colors and symbols are the same as in Figure 15

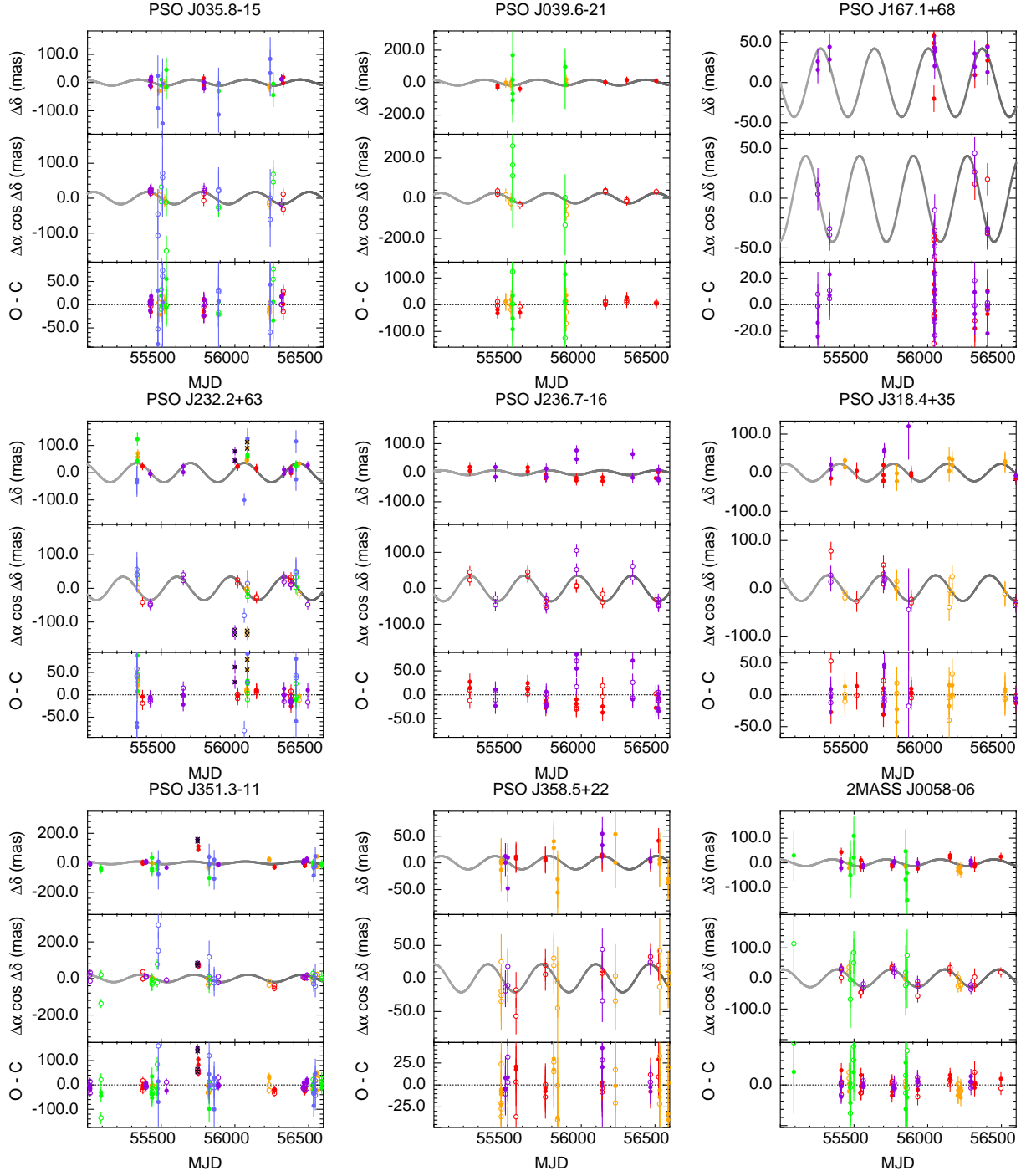


FIG. 17.— PS1 R.A. and decl. motion with the best fit overplotted in gray in the top two panels of each plot with the residuals in the bottom panel. In order from top left to bottom right, our objects are: PSO J035.8–15, PSO J039.6–21, PSO J167.1+68, PSO J236.8–16, PSO J318.4+35, PSO J351.3–11, PSO J358.5+22, and 2MASS J0058–06. The colors and symbols are the same as in Figure 15 except that *open circles* and *filled circles* correspond to R.A. and decl. positions, respectively.

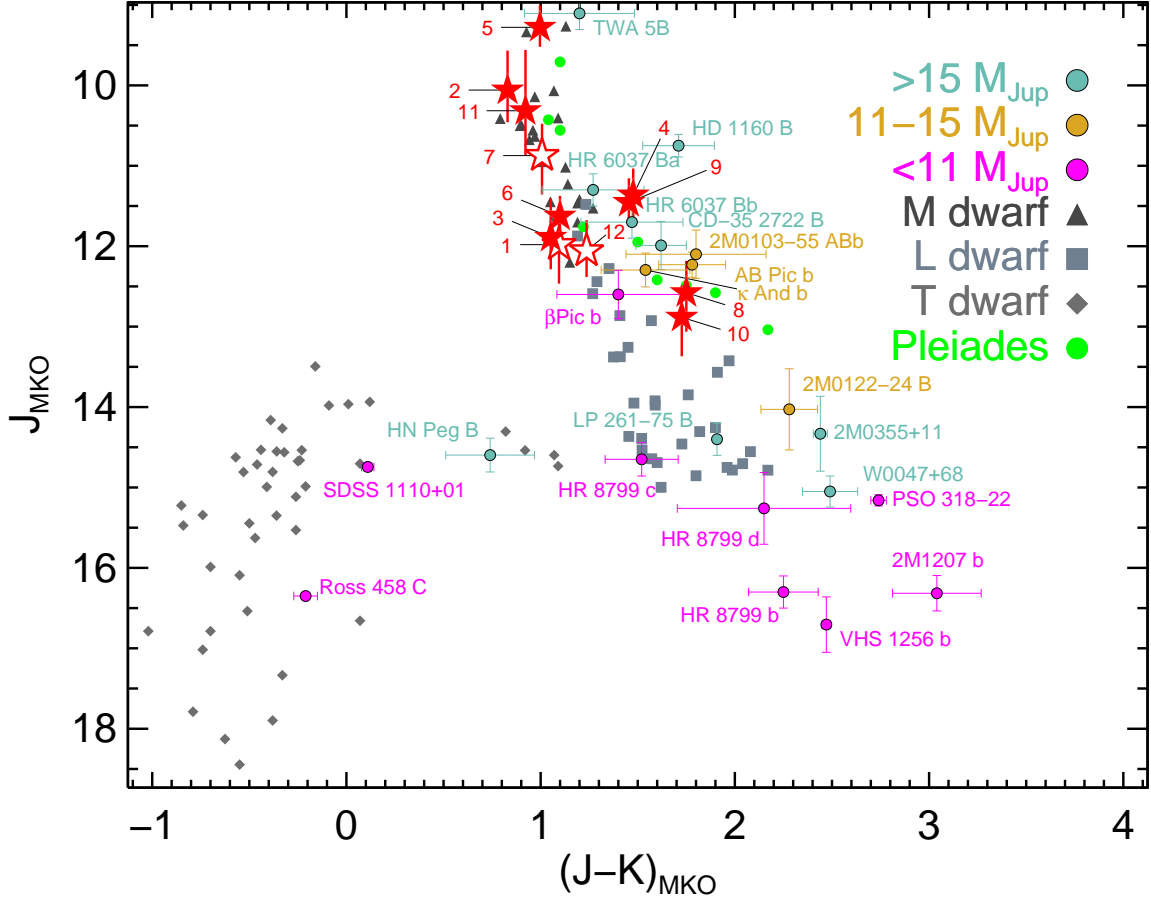


FIG. 18.— NIR $J-K$ color and absolute J magnitude of our candidate AB Dor Moving Group substellar members (*red stars*), field dwarfs (*gray symbols*), and known young brown dwarfs and planetary-mass objects (*colored circles*). Our objects are numbered the same as in Figure 5: (1) PSO J004.7+41, (2) PSO J035.8–15, (3) PSO J039.6–21, (4) PSO J167.1+68, (5) PSO J232.2+63, (6) PSO J236.8–16, (7) PSO J292.9–06, (8) PSO J306.0+16, (9) PSO J318.4+35, (10) PSO J334.2+28, (11) PSO J351.3–11, (12) PSO J358.5+22. We use the compilation of known objects from Dupuy & Liu (2012) for photometry and parallaxes of the field objects and for CD-35 2722 B, 2MASS J0355+11, and 2M1207 b. Photometric data is taken from the literature for TWA 5 B (Weinberger et al. 2013), HD 1060 B (Nielsen et al. 2012), HR 6037 Bab (Nielsen et al. 2013), 2MASS J0103–55 ABb (Delorme et al. 2013), AB Pic b (Biller et al. 2013), κ And b (Carson et al. 2013; Bonnefoy et al. 2014), β Pic b (Bonnefoy et al. 2013), 2MASS J0122–24 B LP 261–75 B (Reid & Walkowicz 2006; Bowler et al. 2013), (Bowler et al. 2013), WISEP J0047+68 (Gizis et al. 2015), PSO J318.5–22 (Liu et al. 2013b), HN Peg B (Luhman et al. 2007), SDSS J1110+01 (Gagné et al. 2015a), Ross 458 C (Burningham et al. 2011), VHS 1256 b (Gauza et al. 2015), and the HR 8799 planets (Marois et al. 2008). All photometry for previously known objects are on the MKO system. We synthesized MKO photometry for our candidates from the NIR spectra. Known Pleiades members (*green circles*) trace out the isochrones for an age of ≈ 125 Myr (Lodieu et al. 2007; Bihain et al. 2010). The AB Dor Moving Group is ≈ 125 Myr old. For our candidate without a parallax, we use photometric distances calculated using the relations from Dupuy & Liu (2012) and assume a photometric distance uncertainty of 20% (Section 5.2).

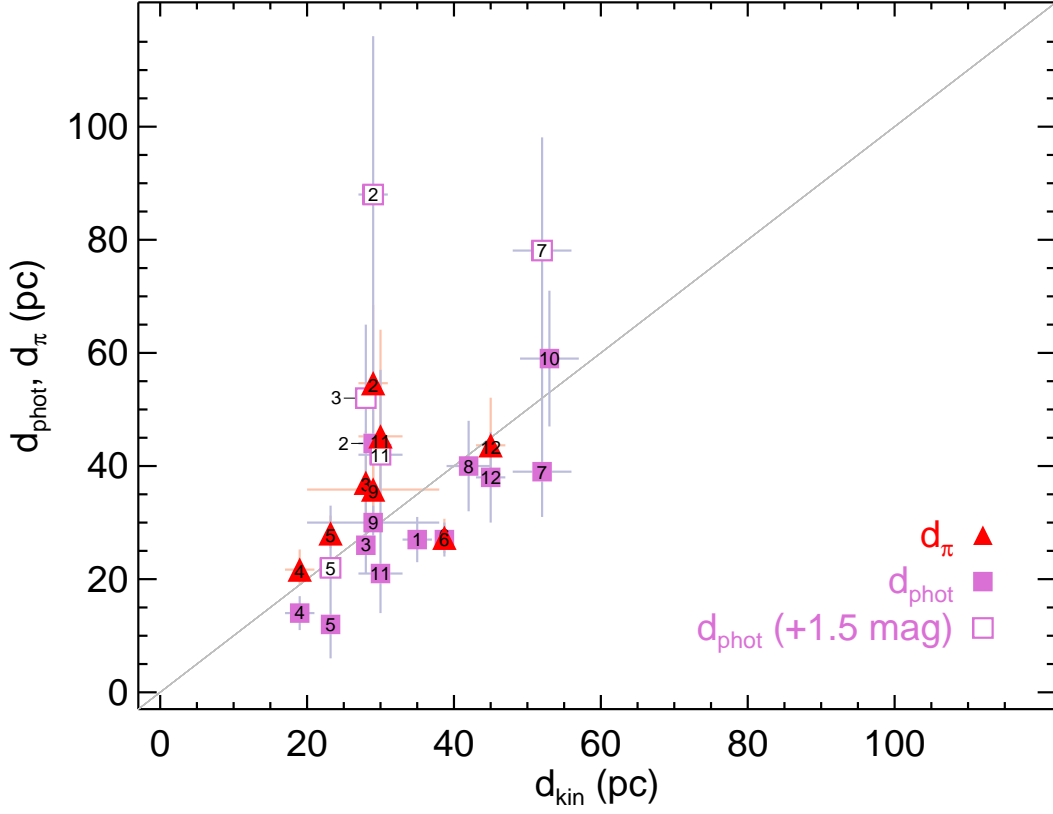


FIG. 19.— The kinematic distances (d_{kin}) of our candidate AB Dor Moving Group members compared with their photometric distances (d_{phot}) in *purple squares* and parallaxic distances (d_{π}) as *red triangles*. The *open purple squares* are the d_{phot} calculated assuming the object is overluminous compared with the field sequence by 1.5 mag which reflects the systematic uncertainty in the photometric distances for young late-M dwarfs. Our objects are numbered as in Figure 5: (1) PSO J004.7+41, (2) PSO J035.8–15, (3) PSO J039.6–21, (4) PSO J167.1+68, (5) PSO J232.2+63, (6) PSO J236.8–16, (7) PSO J292.9–06, (8) PSO J306.0+16, (9) PSO J318.4+35, (10) PSO J334.2+28, (11) PSO J351.3–11, (12) PSO J358.5+22. Eight of our objects (except PSO J004.7+41, PSO J292.9–06, PSO J306.0+16, PSO J318.4+35, and PSO J334.2+28) have parallaxic distances from PS1. Seven of our objects have parallaxes which are consistent with their d_{kin} , the distance they would have if they were AB Dor members.

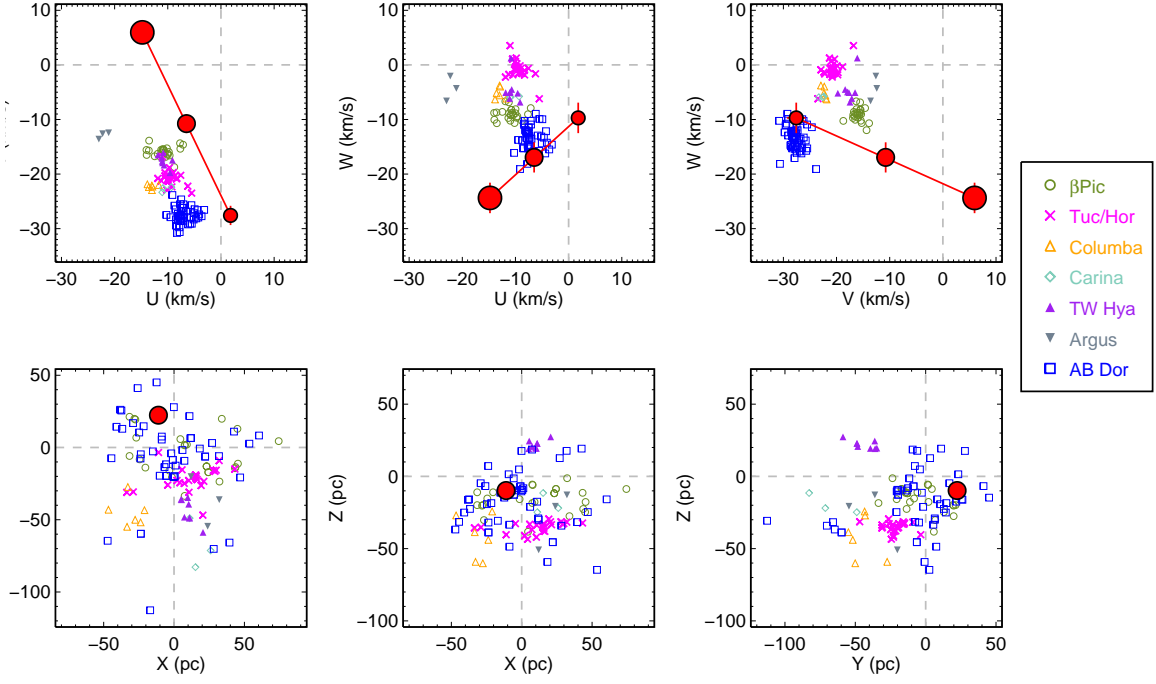


FIG. 20.— The heliocentric space velocity (UVW) and positions (XYZ) of PSO J004.7+41 compared with the kinematics and positions of YMG members from Torres et al. (2008) with membership probabilities of at least 75%. We have used RVs and parallaxes from the literature for objects which had no measured values in Torres et al. (2008). The *red lines* show the UVW range for an RV between -20 and 20 km/s, reasonable for young objects (i.e. the RV range for young objects in Torres et al. 2008). The error bars are due to uncertainties in photometric distance and proper motion.

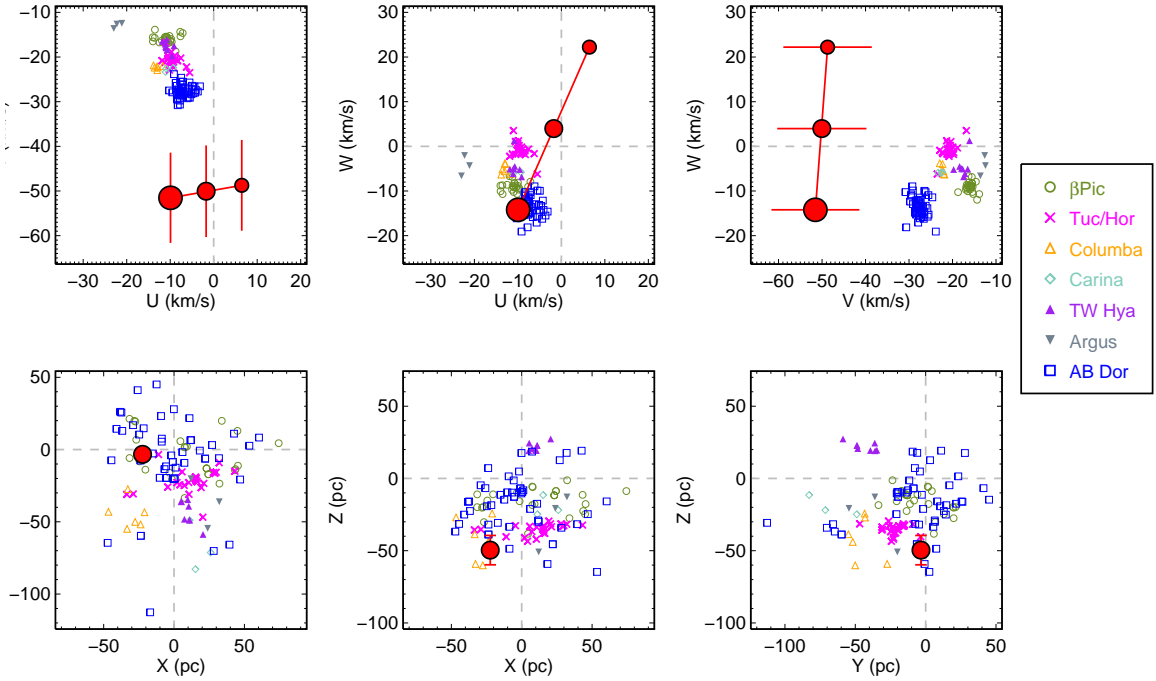


FIG. 21.— The heliocentric space velocity (UVW) and positions (XYZ) of PSO J035.8-15 compared with the kinematics and positions of known YMG members from Torres et al. (2008) as in Figure 20. The *red lines* show the UVW range for an RV between -20 and 20 km/s, reasonable for young objects (i.e. the RV range for young objects in Torres et al. 2008). The error bars are due to uncertainties in photometric distance and proper motion.

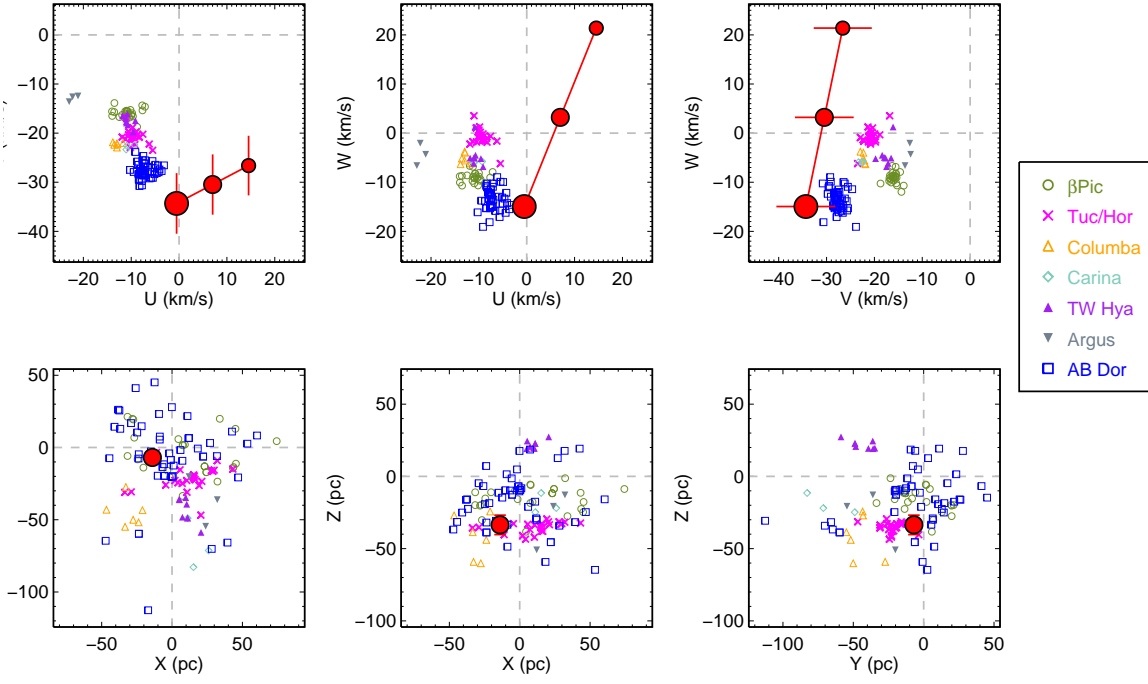


FIG. 22.— The heliocentric space velocity (UVW) and positions (XYZ) of PSO J039.6-21 compared with the kinematics and positions of known YMG members from Torres et al. (2008) as in Figure 20. The *red lines* show the UVW range for an RV between -20 and 20 km/s, reasonable for young objects (i.e. the RV range for young objects in Torres et al. 2008). The error bars are due to uncertainties in parallax and proper motion.

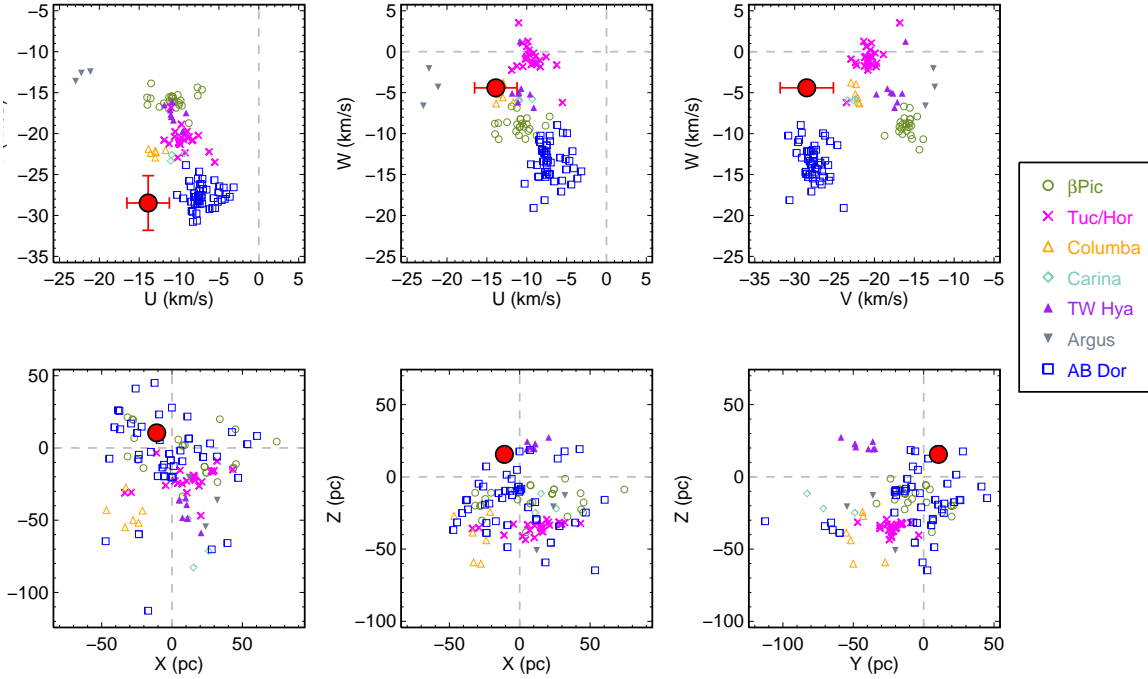


FIG. 23.— The heliocentric space velocity (UVW) and positions (XYZ) of PSO J167.1+68 compared with the kinematics and positions of known YMG members from Torres et al. (2008) as in Figure 20. The error bars are due to uncertainties in parallax, radial velocity, and proper motion.

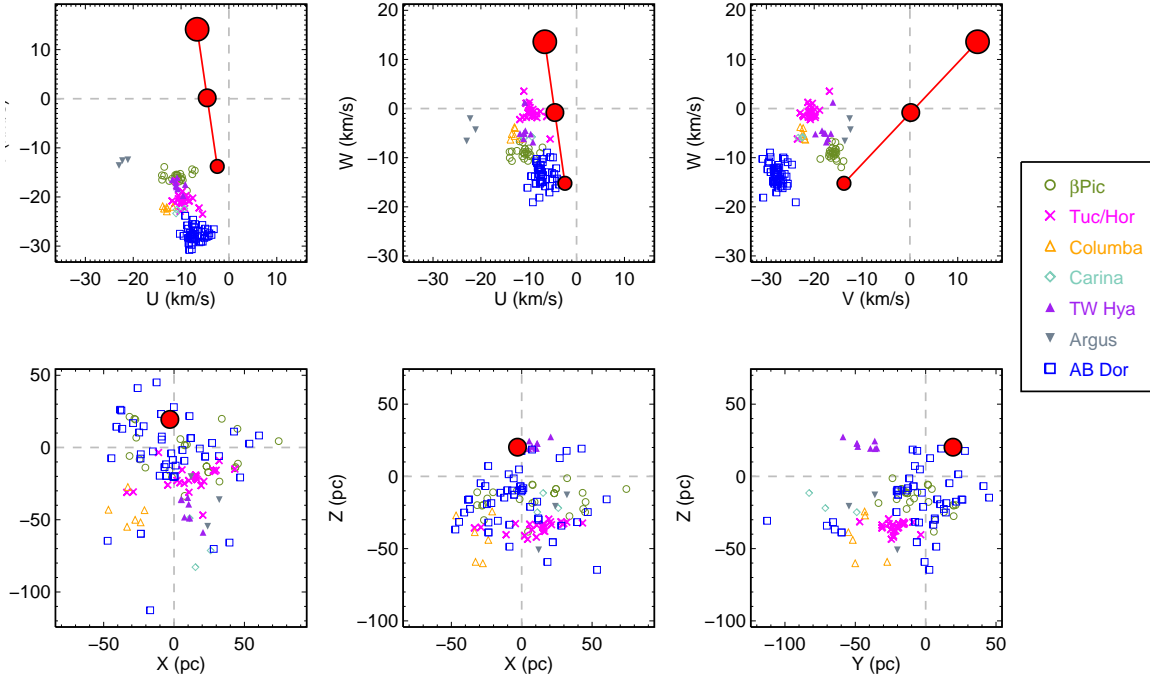


FIG. 24.— The heliocentric space velocity (UVW) and positions (XYZ) of PSO J232.2+63 compared with the kinematics and positions of known YMG members from Torres et al. (2008) as in Figure 20. The *red lines* show the UVW range for an RV between -20 and 20 km/s, reasonable for young objects (i.e. the RV range for young objects in Torres et al. 2008). The error bars are due to uncertainties in parallax and proper motion.

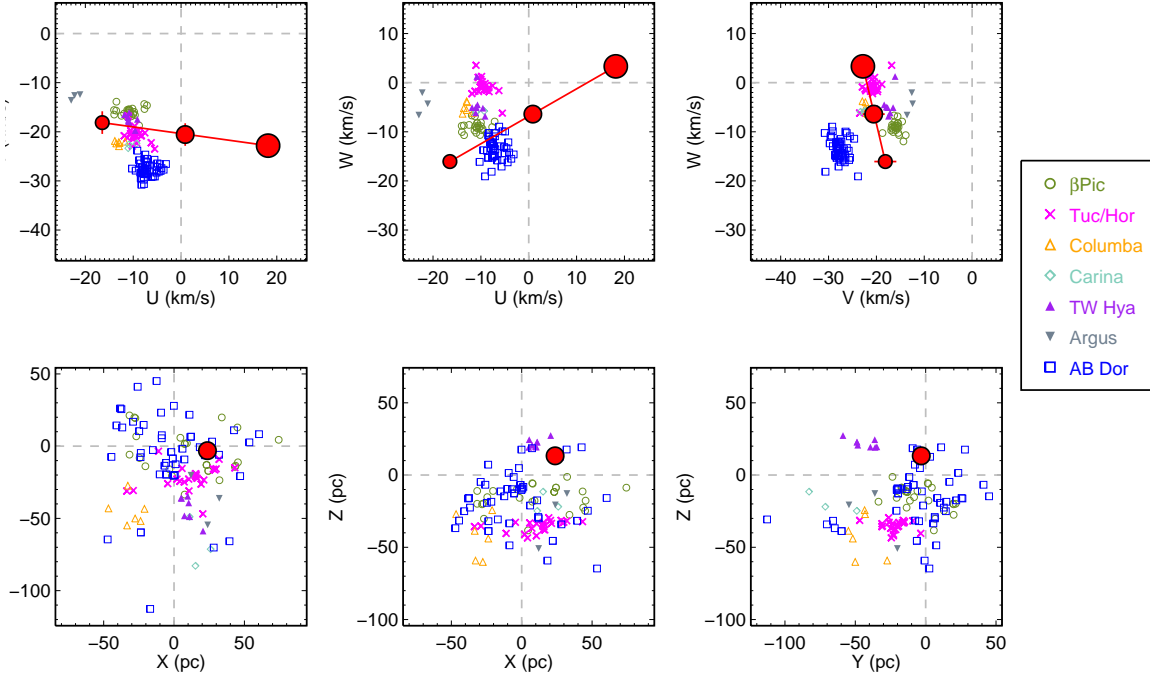


FIG. 25.— The heliocentric space velocity (UVW) and positions (XYZ) of PSO J236.8-16 compared with the kinematics and positions of known YMG members from Torres et al. (2008) as in Figure 20. The *red lines* show the UVW range for an RV between -20 and 20 km/s, reasonable for young objects (i.e. the RV range for young objects in Torres et al. 2008). The error bars are due to uncertainties in parallax and proper motion.

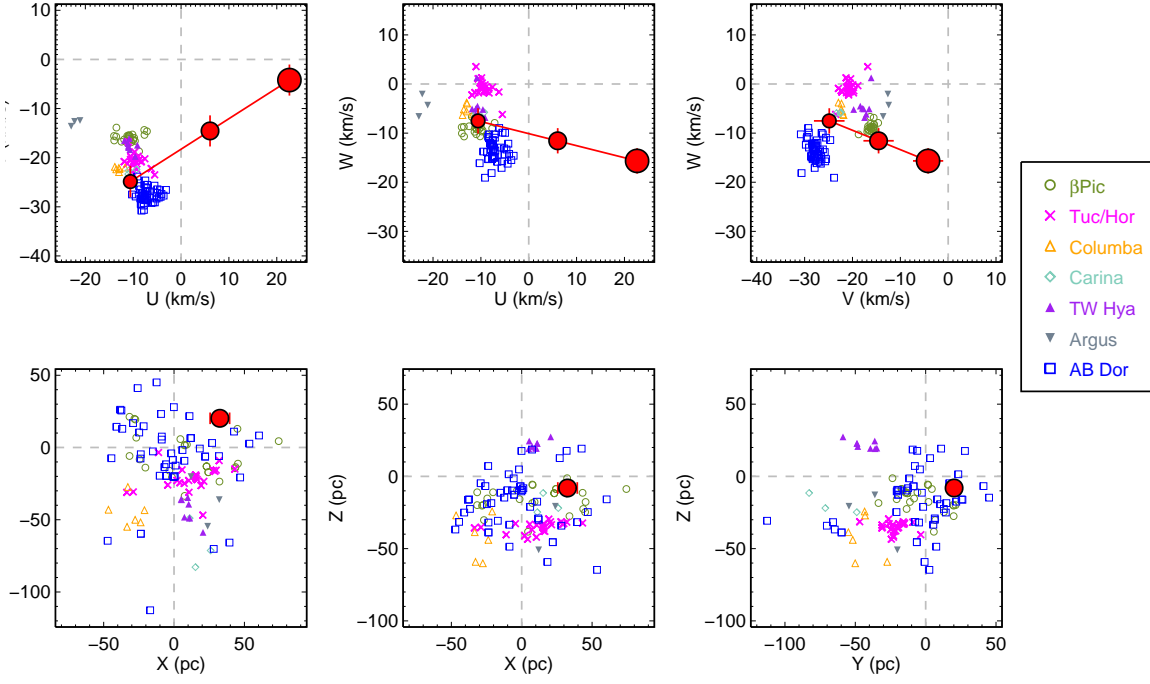


FIG. 26.— The heliocentric space velocity (UVW) and positions (XYZ) of PSO J292.9-06 compared with the kinematics and positions of known YMG members from Torres et al. (2008) as in Figure 20. The *red lines* show the UVW range for an RV between -20 and 20 km/s, reasonable for young objects (i.e. the RV range for young objects in Torres et al. 2008). The error bars are due to uncertainties in photometric distance and proper motion.

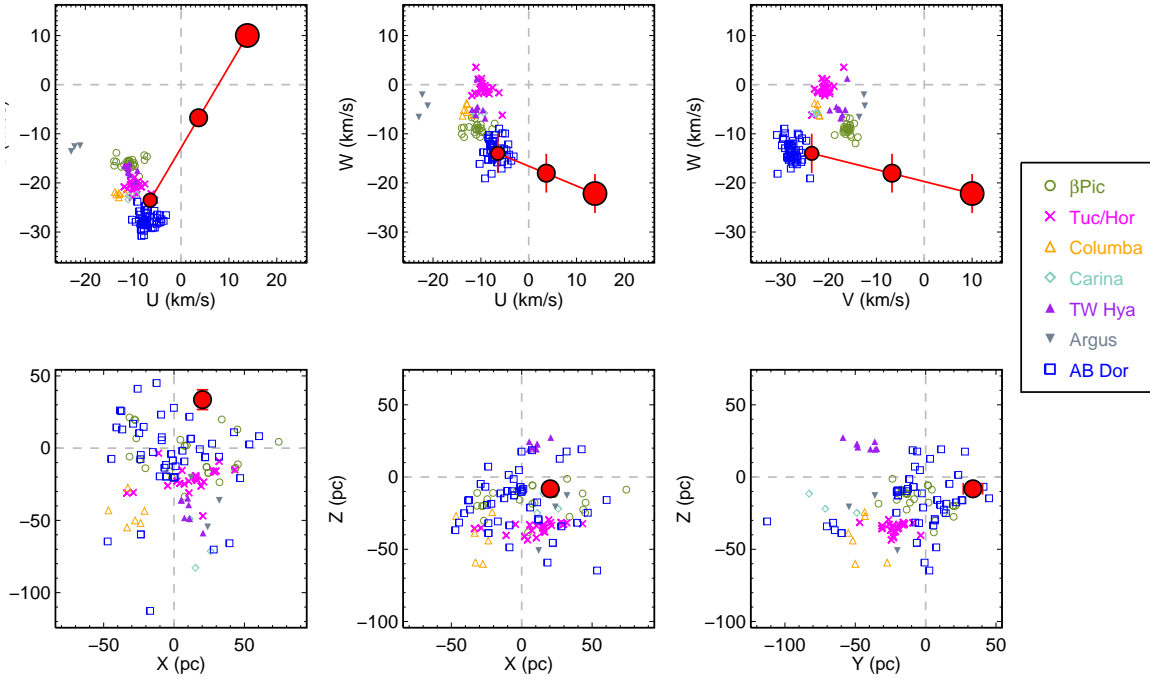


FIG. 27.— The heliocentric space velocity (UVW) and positions (XYZ) of PSO J306.0+16 compared with the kinematics and positions of known YMG members from Torres et al. (2008) as in Figure 20. The *red lines* show the UVW range for an RV between -20 and 20 km/s, reasonable for young objects (i.e. the RV range for young objects in Torres et al. 2008). The error bars are due to uncertainties in photometric distance and proper motion.

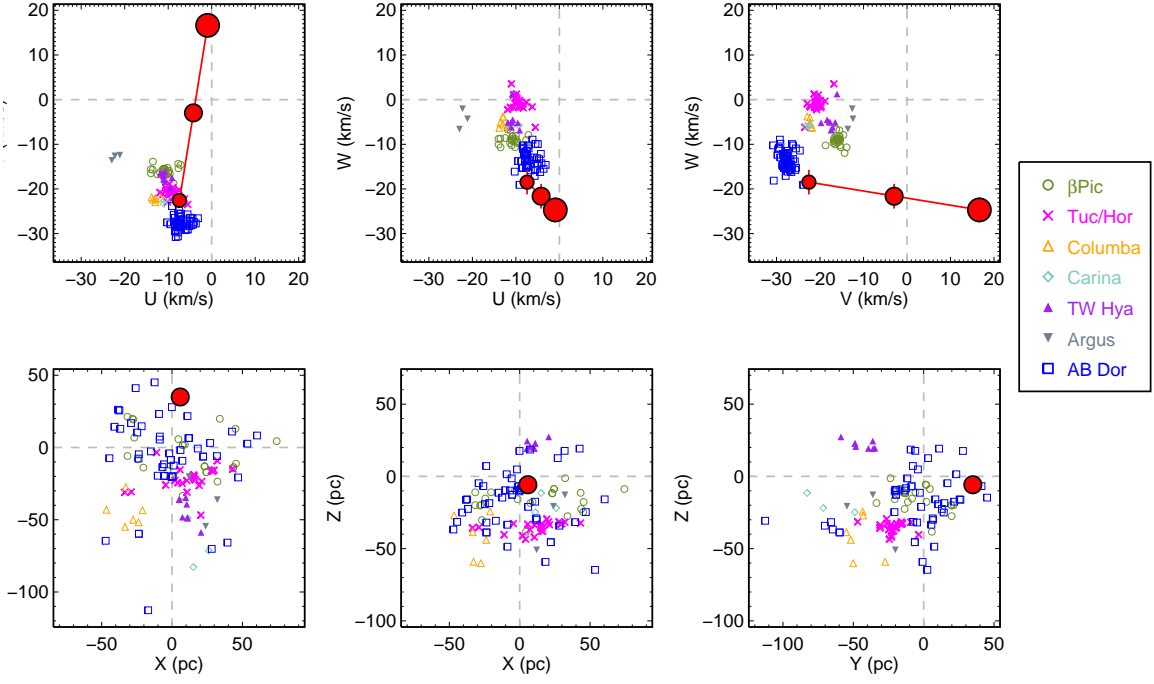


FIG. 28.— The heliocentric space velocity (UVW) and positions (XYZ) of PSO J318.4+35 compared with the kinematics and positions of known YMG members from Torres et al. (2008) as in Figure 20. The *red lines* show the UVW range for an RV between -20 and 20 km/s, reasonable for young objects (i.e. the RV range for young objects in Torres et al. 2008). The error bars are due to uncertainties in parallax and proper motion.

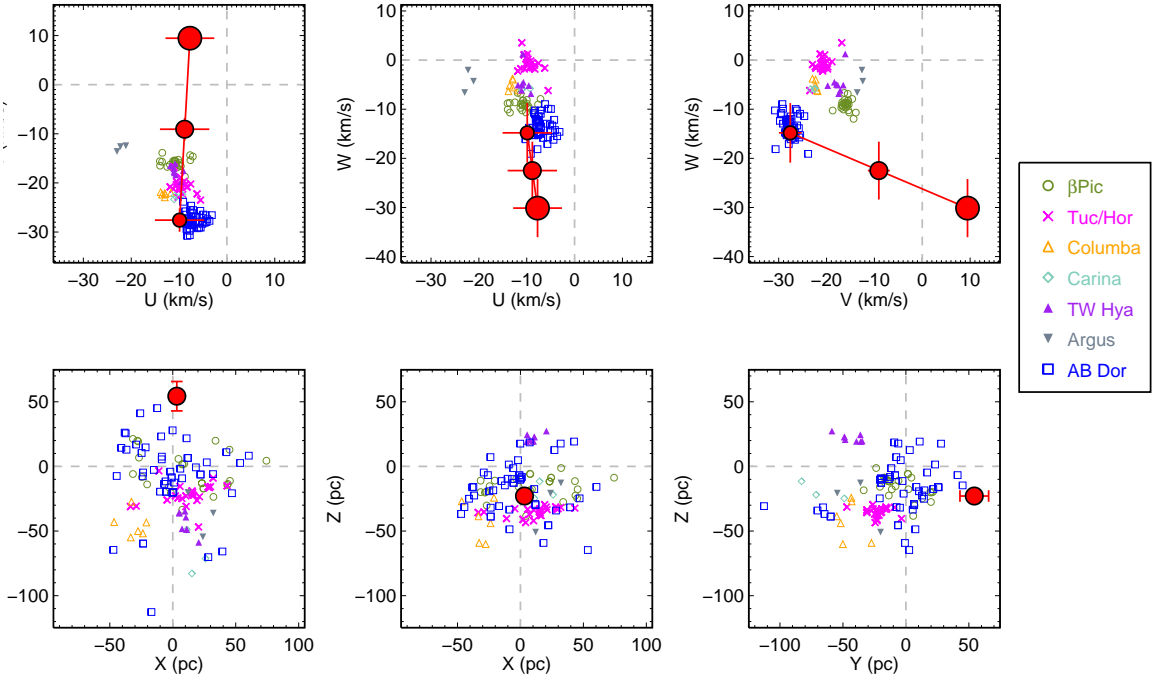


FIG. 29.— The heliocentric space velocity (UVW) and positions (XYZ) of PSO J334.2+28 compared with the kinematics and positions of known YMG members from Torres et al. (2008) as in Figure 20. The *red lines* show the UVW range for an RV between -20 and 20 km/s, reasonable for young objects (i.e. the RV range for young objects in Torres et al. 2008). The error bars are due to uncertainties in photometric distance and proper motion.

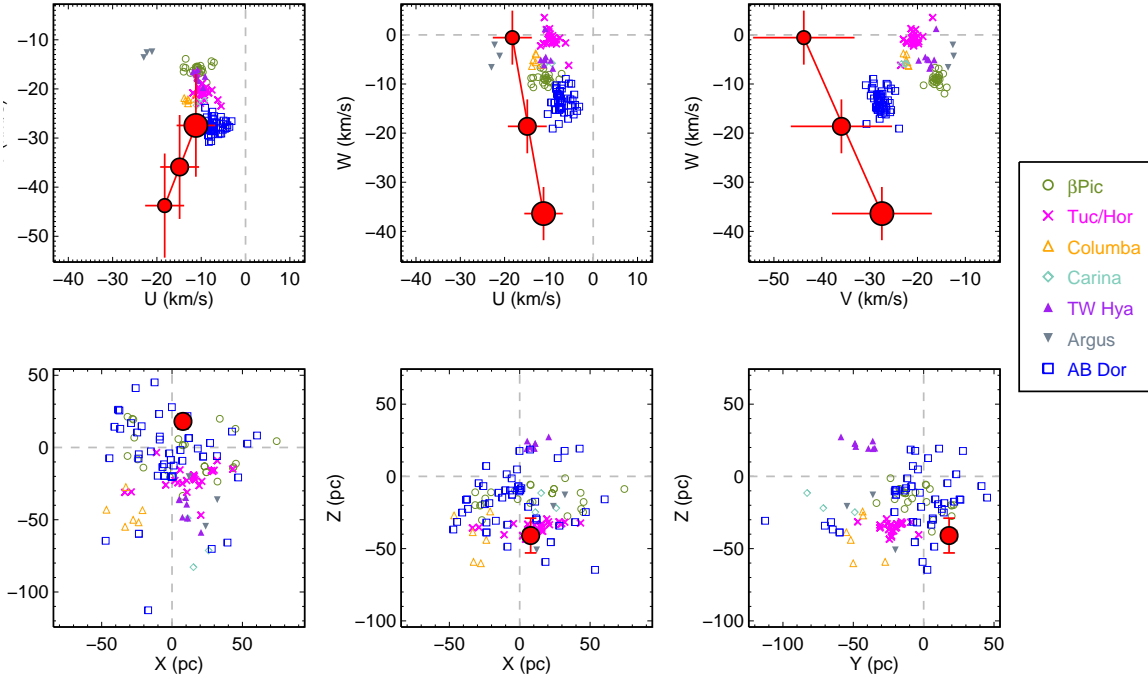


FIG. 30.— The heliocentric space velocity (UVW) and positions (XYZ) of PSO J351.3–11 compared with the kinematics and positions of known YMG members from Torres et al. (2008) as in Figure 20. The *red lines* show the UVW range for an RV between -20 and 20 km/s, reasonable for young objects (i.e. the RV range for young objects in Torres et al. 2008). The error bars are due to uncertainties in parallax and proper motion.

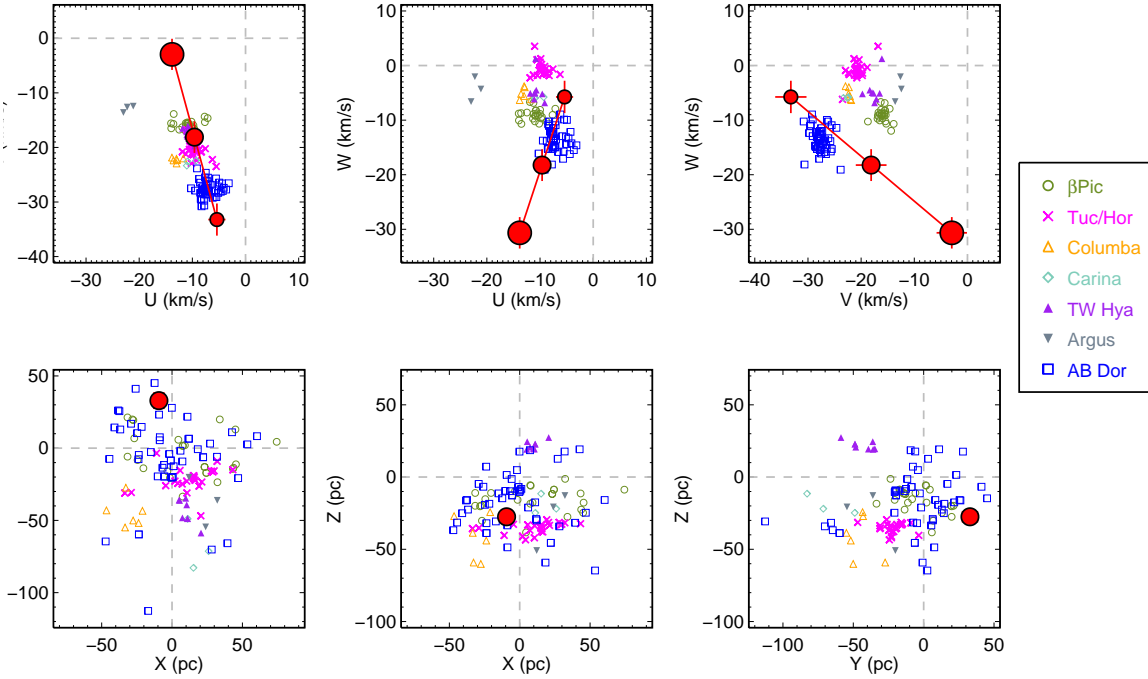


FIG. 31.— The heliocentric space velocity (UVW) and positions (XYZ) of PSO J358.5+22 compared with the kinematics and positions of known YMG members from Torres et al. (2008) as in Figure 20. The *red lines* show the UVW range for an RV between -20 and 20 km/s, reasonable for young objects (i.e. the RV range for young objects in Torres et al. 2008). The error bars are due to uncertainties in parallax and proper motion.

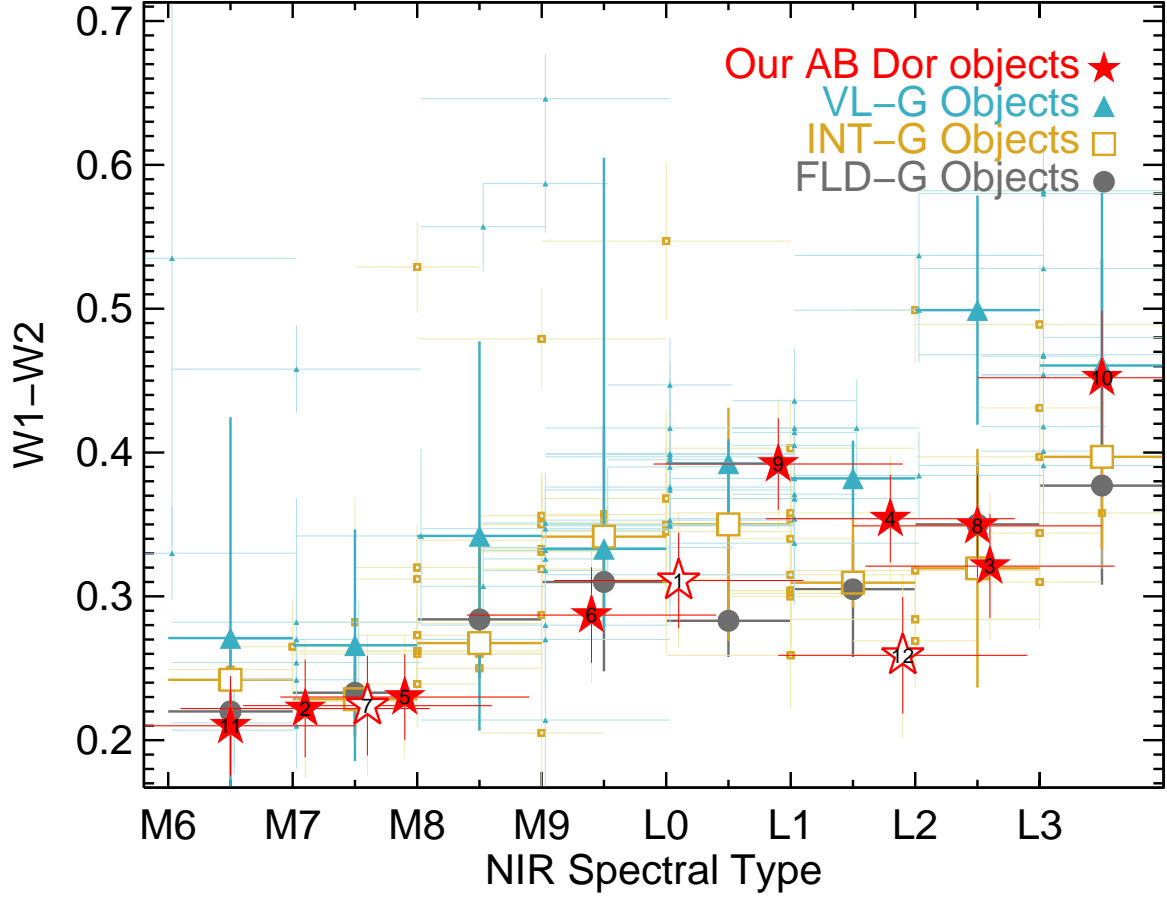


FIG. 32.— *WISE* $W1-W2$ color as a function of NIR spectral type for our candidate AB Dor Moving Group members. Those classified as INT-G are the *filled red stars* and those as INT-G? and FLD-G are the *empty red stars*. Our objects are numbered (as in Figure 5): (1) PSO J004.7+41, (2) PSO J035.8-15, (3) PSO J039.6-21, (4) PSO J167.1+68, (5) PSO J232.2+63, (6) PSO J236.8-16, (7) PSO J292.9-06, (8) PSO J306.0+16, (9) PSO J318.4+35, (10) PSO J334.2+28, (11) PSO J351.3-11, (12) PSO J358.5+22. The young field dwarfs with INT-G gravity classifications from Allers & Liu (2013) are the *small open yellow squares* and those with VL-G are the *small teal triangles*. We also include the Gagné et al. (2015c) INT-G (yellow) and VL-G (teal) substellar objects. The mean $W1-W2$ color for each spectral type bin and the 68th percentile confidence region are the *filled gray circles* for old field objects, *open yellow squares* for INT-G objects, and *teal triangles* for VL-G objects. The mean $W1-W2$ colors for each bin are plotted in the middle of the bin (e.g. for spectral type M6-M6.9, the mean color is plotted at M6.5). We note that the slightly blue $J-K$ colors of PSO J236.7-16 are likely due to blending from the earlier-type closeby companion (M5; Gagné et al. 2015c). We find that the VL-G dwarfs tend to have redder $W1-W2$ colors than the INT-G and then FLD-G dwarfs. However, the $W1-W2$ colors for INT-G dwarfs are consistent with their FLD-G counterparts within the uncertainties.

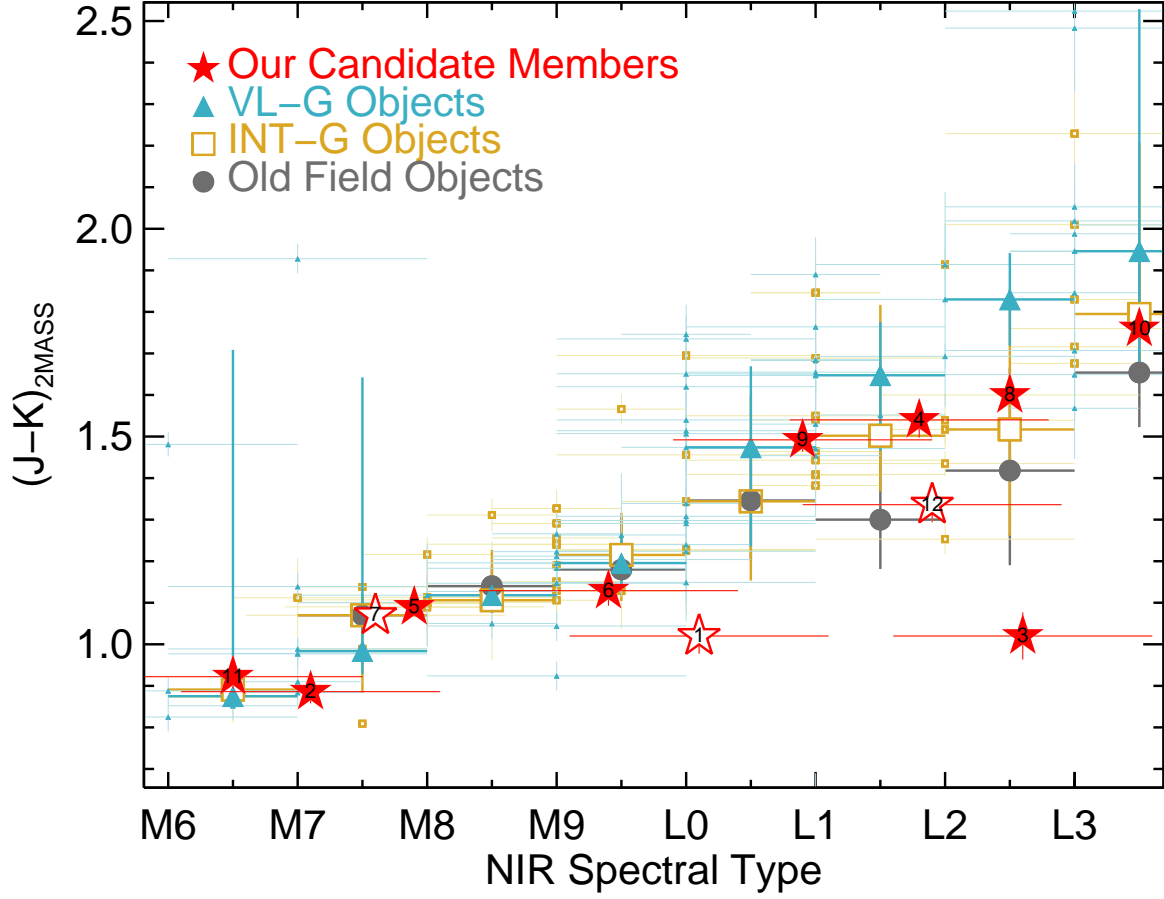


FIG. 33.— 2MASS $J-K$ color as a function of NIR spectral type for our candidate AB Dor Moving Group members. Those classified as INT-G are the *filled red stars* and those as INT-G? or FLD-G are the *empty red stars*. Our objects have the same numbers as in Figure 32. The young field dwarfs with INT-G gravity classifications from Allers & Liu (2013) are the *small open yellow squares* and those with VL-G are the *small teal triangles*. We also include the Gagné et al. (2015c) INT-G (yellow) and VL-G (teal) substellar objects. The mean $J-K$ color for each spectral type bin and the 68th percentile confidence region are the *filled gray circles* for old field objects, *open yellow squares* for INT-G objects, and *teal triangles* for VL-G objects. The mean $J-K$ colors for each bin are plotted in the middle of the bin (e.g. for spectral type M6–M6.9, the mean color is plotted at M6.5). We note that the slightly blue $J-K$ colors of PSO J236.7–16 are likely due to blending from the earlier-type closeby companion (M5; Gagné et al. 2015c). There is no significant difference between the mean $J-K$ colors for M6–M9 dwarfs with different gravities (VL-G, INT-G or FLD-G). However for L0–L3 dwarfs, the VL-G objects are redder than the FLD-G objects while the INT-G objects have colors redder than their FLD-G counterparts but not as extreme as their VL-G counterparts.

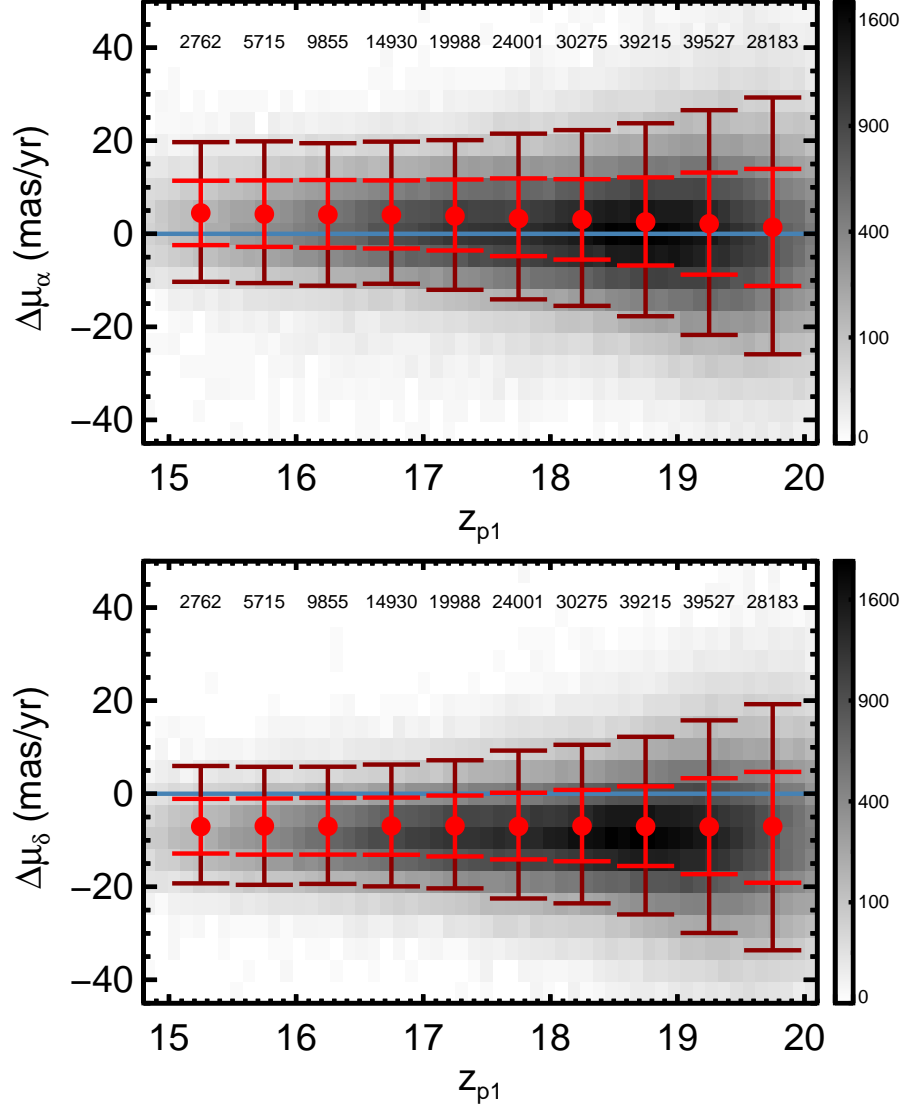


FIG. 34.— The deviation between the SDSS Stripe 82 and our PS1+2MASS proper motions in μ_α and μ_δ as a function of z_{p1} for all objects with PS1+2MASS proper motion uncertainties less than 20 mas yr^{-1} and at least 20 epochs (*gray-scale image*). In order to better show the distribution of our objects, we constructed a gray-scale image of the scatter plot of our data by binning by 0.2 mag in z_{p1} and 5 mas/yr in proper motion uncertainties. We scale the image by its squareroot for clarity. The median proper motion difference for each bin in z_{p1} magnitude are the *red dots* and the 68.5th and 95.4th confidence intervals are enclosed within the *red* and *brown* bars. The numbers at the top represent the number of objects in each magnitude bin. The proper motion difference between SDSS and PS1+2MASS does not change significantly as a function of z_{p1} . The median deviation in μ_α is $3 \pm 11 \text{ mas yr}^{-1}$ and in μ_δ is $-7 \pm 10 \text{ mas yr}^{-1}$.

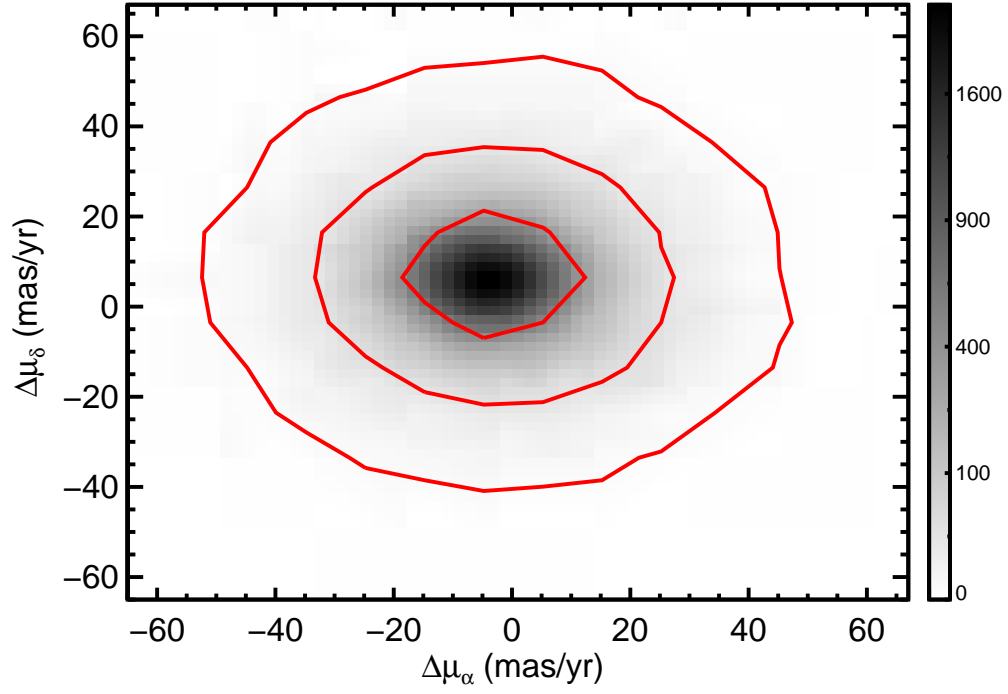


FIG. 35.— A gray-scale image of a scatter plot of the deviation between the SDSS Stripe 82 and our PS1+2MASS proper motions for all objects with PS1+2MASS proper motion uncertainties less than 20 mas yr^{-1} and at least 20 epochs. We constructed the image by binning the data into 2 mas/yr wide bins. Again, we scale the image by its square root for clarity. The x-axis is $\Delta\mu_\alpha$ ($\mu_{\alpha,PS1+2MASS} - \mu_{\alpha,SDSS}$) and the y-axis is $\Delta\mu_\delta$ ($\mu_{\delta,PS1+2MASS} - \mu_{\delta,SDSS}$). The red contour lines mark the 1σ , 2σ , and 3σ confidence intervals.

TABLE 1
OBSERVED PROPERTIES AND MEMBERSHIP

Property	PSO J004.7+41	PSO J035.8–15	PSO J039.6–21	PSO J167.1+68	PSO J232.2+63	PSO J236.8–16	PSO J292.9–06	PSO J306.0+16	PSO J318.4+35	PSO J334.2+28	PSO J351.3–11	PSO J358.5+22
$\mu_\alpha \cos \delta$ (mas/yr)	100.5±4.4	135.1±1.9	95.5±1.5	–221.9±3.1	–125.6±3.4	–70.1±1.5	21.0±2.9	63.5±4.3	109.0±1.9	76.8±26.7	148.8±2.3	97.0±2.1
μ_δ (mas/yr)	–130.3±1.1	–137.7±2.4	–150.4±4.3	–193.7±3.9	32.5±3.4	–148.9±3.7	–105.7±2.6	–83.0±6.2	–71.0±1.6	–52.6±11.0	–132.3±1.9	–88.3±1.9
$\mu_\alpha \cos \delta_{lit}^a$ (mas/yr)	94.2±5.6	147.8±8.8	102±7.3	–238±5.8	–119.7±3.6	–64.1±5.9	146.1±6.9	93.5±7.3
$\mu_{\delta, lit}^a$ (mas/yr)	–138±8.4	–148.8±9	–158.4±9.4	–197.7±8.4	44.5±6.9	–129.6±6.6	–144.0±6.9	–98.9±8.9
i_{p1} (mag)	18.09±0.01	16.98±0.04	19.12±0.01	17.733±0.005	15.40±0.01	18.42±0.015	17.48±0.01	20.258±0.015	18.91±0.01	21.56±0.08	16.816±0.006	19.74±0.02
z_{p1} (mag)	16.60±0.02	16.00±0.06	17.47±0.06	16.214±0.002	14.06±0.01	16.905±0.002	16.15±0.01	18.843±0.011	17.36±0.01	20.21±0.03	15.7±0.004	18.2±0.02
y_{p1} (mag)	15.80±0.01	15.24±0.06	16.55±0.01	15.211±0.002	13.30±0.01	15.931±0.003	15.43±0.01	17.872±0.0124	16.30±0.01	19.20±0.03	15.1±0.005	17.2±0.02
J^b (mag)	14.10±0.03	14.0±0.02	14.8±0.04	13.12±0.02	11.64±0.02	13.86±0.03	13.86±0.03	15.58±0.06	14.3±0.03	16.84±0.17	13.6±0.02	15.4±0.05
H^b (mag)	13.50±0.03	13.3±0.03	14.2±0.04	12.24±0.02	10.94±0.03	13.24±0.03	13.20±0.02	14.56±0.06	13.4±0.03	15.9±0.2	13.0±0.03	14.6±0.04
K^b (mag)	13.10±0.03	13.0±0.02	13.8±0.05	11.58±0.02	10.55±0.02	12.74±0.03	12.79±0.02	13.98±0.05	12.8±0.03	15.08±0.16	12.7±0.03	14.0±0.05
$W1$ (mag)	12.76±0.02	12.63±0.02	13.43±0.02	11.12±0.02	10.30±0.02	12.43±0.02	12.52±0.02	13.32±0.03	12.23±0.02	14.34±0.03	12.45±0.03	13.63±0.03
$W2$ (mag)	12.45±0.03	12.41±0.02	13.11±0.03	10.76±0.02	10.06±0.02	12.14±0.02	12.29±0.03	12.98±0.03	11.85±0.02	13.89±0.04	12.24±0.03	13.37±0.04
d_{phot}^c (pc)	27±4	44±14 (90±30)	26±5	14±3	12±6 (22±11)	26±6 (52±13)	39±8 (80±20)	40±8	29±9	59±12	21±7 (42±15)	38±8
d_π (pc)	...	54.6 $^{+14}_{-9.2}$	37 $^{+9}_{-6}$	22 $^{+4}_{-3}$	28 $^{+3}_{-3}$	27 $^{+3}_{-3}$	36 $^{+5}_{-4}$...	45 $^{+19}_{-10}$	43 $^{+8}_{-6}$
d_{stat}^d (pc)	34.6±2.4	28.9±1.4	26.1±1.6	16.9±1.2	22.5±2.8	37.4±1.8	49.4±2.8	40.2±4.0	28.9±3.0	45.8±5.4	33.3±1.6	46.6±2.8
d_{kin} (pc)	35 $^{+2}_{-3}$	29 $^{+2}_{-2}$	28 $^{+0.7}_{-0.7}$	19 $^{+2}_{-2}$	23.2 $^{+0.6}_{-0.6}$	38.7 $^{+0.9}_{-0.9}$	52.4 $^{+3}_{-3}$	42 $^{+3}_{-3}$	30 $^{+3}_{-3}$	53 $^{+4}_{-3}$	32.9 $^{+2}_{-1.5}$	45 $^{+2}_{-2}$
θ (degrees)	12 $^{+3}_{-3}$	2.0 $^{+3}_{-3}$	14 $^{+3}_{-3}$	4 $^{+4}_{-4}$	1.0 $^{+1.1}_{-0.7}$	1.2 $^{+1.3}_{-0.9}$	3.7 $^{+2}_{-2}$	4 $^{+4}_{-3}$	3 $^{+3}_{-2}$	6 $^{+3}_{-3}$	6 $^{+2}_{-2}$	3 $^{+3}_{-2}$
U_{best}^e (km/s)	[–0.3±1.3]	[–8.3±1.0]	[0.2±1.6]	–13.8±2.7 ^f	[–13.3±5.2]	[–7.8±1.3]	[–7.8±2.3]	[–6.5±5.0]	[–7.4±2.4]	[–9.3±6.7]	[–14.2±4.4]	[–7.3±1.6]
V_{best}^e (km/s)	[–23.2±2.1]	[–50.9±10.0]	[–34.0±6.2]	–28.5±3.4 ^f	[–24.5±5.5]	[–19.4±2.3]	[–23.9±3.4]	[–23.9±8.2]	[–22.0±13.8]	[–24.7±4.2]	[–34.4±10.6]	[–25.8±3.1]
W_{best}^e (km/s)	[–11.6±2.8]	[–10.6±1.9]	[–13.2±1.3]	–4.4±0.5 ^f	[–2.6±5.0]	[–11.3±1.0]	[–8.5±2.6]	[–14.3±4.4]	[–18.5±3.5]	[–16.0±7.0]	[–21.8±6.0]	[–11.5±3.0]
$\Delta(v)_{UVW}^e$ (km/s)	[8.6±1.7]	[23.6±9.9]	[10.0±4.1]	11.2±1.6 ^f	[12.4±5.1]	[8.7±2.3]	[6.6±3.0]	[4.5±8.3]	[7.4±9.2]	[4.4±5.5]	[12.1±8.3]	[2.5±3.0]
d_{XYZ}^e (pc)	[28.5±3.5]	37.9±9.2	20.1±6.1	35.4±2.0 ^f	50.9±8.5	41.2±2.1	[46.9±6.2]	[46.8±6.2]	42.4±4.2	[60.0±11.2]	13.8±2.2	39.5±5.2
P_{ABDor}	19.19%	49.06%	93.25%	0.23%	36.92	0.25%	6.77% (0%)	42.76%	88.1%	0.63%	50.37%	79.04%

^a The literature proper motion is taken from Gagné et al. (2015b).

^b J , H , and K are 2MASS magnitudes.

^c Properties in parenthesis are calculated assuming the object is overluminous compared with the field sequence by 1.5 mag. This reflects the systematic uncertainty in the photometric distances for our late-M dwarf candidates

^d The AB Dor Moving Group statistical distances are determined using the BANYAN II webtool.

^e The U_{best} , V_{best} and W_{best} positions are determined by the RV (between –20 to +20 km/s) that minimizes the distance between the UVW positions of our candidates and the mean UVW positions of the known AB Dor Moving Group Members with membership probabilities of at least 75% from Torres et al. (2008). The distances, $\Delta(v)_{UVW}$ and d_{XYZ} , are the distances between the XYZ and the best fit UVW position of our candidates and the mean positions of the known group members. As for all objects, except PSO J167.1+68^f, the values for U_{best} , V_{best} , W_{best} , Δv_{UVW} , and d_{XYZ} (for objects without parallaxes) are not true measurements, we have enclosed them in brackets.

^f As PSO J167.1+68 has an RV from Blake et al. (2010), we use this RV measurement to determine the UVW positions and the $\Delta(v)_{UVW}$. Thus, the values are not enclosed in brackets.

TABLE 2
SPECTROSCOPIC OBSERVATIONS

Name	R.A. (PS1) (J2000)	Decl. (PS1) (J2000)	Date (UT)	T_{exp} (s)	A0V Standard	Setup	Telescope	Mean S/N (J,H,K)
PSO J004.7+41	00:19:07.65	+41:01:23.30	2014 Jan 17	1680	HD 23594	prism	IRTF	57,61,68
PSO J035.8-15	02:23:28.40	-15:11:37.64	2013 Nov 23	960	HD 20911	SXD	IRTF	48,56,53
PSO J039.6-21	02:38:32.47	-21:46:28.78	2013 Sep 22	600	HD 31506	prism	IRTF	33,30,30
PSO J167.1+68	11:08:30.25	+68:30:14.39	2015 Jun 24	956	HD 89239	SXD	IRTF	65,86,102
PSO J232.2+63	15:29:09.96	+63:12:54.50	2013 Aug 09	180	HD 172728	SXD	IRTF	167,171,184
PSO J236.8-16	15:47:05.52	-16:26:32.20	2015 Jan 28	87.6	HD 133569	prism	IRTF	59,53,40
PSO J292.9-06	19:31:44.93	-06:20:48.91	2015 Sep 25	59.8	HD 190454	prism	IRTF	160,134,124
PSO J306.0+16	20:24:03.05	+16:47:49.09	2015 Jul 15	717.3	HD 192538	prism	IRTF	75,75,80
PSO J318.4+35	21:13:41.83	+35:07:39.95	2013 Sep 22	180	HD 209932	prism	IRTF	100,95,85
PSO J334.2+28	22:17:02.98	+28:56:37.98	2015 Jul 01	3000	HIP 111538	SXD	<i>Gemini</i>	30,44,41
PSO J351.3-11	23:25:22.42	-11:21:05.18	2013 Dec 11	1440	HD 3604	SXD	IRTF	35,32,29
PSO J358.5+22	23:54:12.66	+22:08:21.70	2013 Nov 23	720	HD 1561	prism	IRTF	46,33,28

TABLE 3
SPECTRAL TYPE

Name	J SpT ^a	K SpT ^a	H ₂ O	H ₂ O-D	H ₂ O-1	H ₂ O-2	Final SpT
PSO J004.7+41	M9±1	M9±1	L0.1 ^{+0.4} _{-0.4}	... ^b	L1.3 ^{+1.1} _{-1.1}	L0.4 ^{+0.5} _{-0.5}	L0.1±1.0
PSO J035.8-15	M7±1	M7±1	M6.9 ^{+0.4} _{-0.4}	... ^b	M8.6 ^{+1.1} _{-1.0}	M7.2 ^{+0.5} _{-0.5}	M7.1±1.0
PSO J039.6-21	L1±1	L3±1	L3.9 ^{+0.9} _{-1.0}	L2.0 ^{+0.9} _{-1.0}	L4.8 ^{+1.0} _{-1.1}	L0.9 ^{+1.0} _{-0.9}	L2.6±1.0
PSO J167.1+68	L2±1	L2±1	L2.1 ^{+0.4} _{-0.3}	L1.1 ^{+0.8} _{-0.7}	L2.5 ^{+1.1} _{-1.0}	L1.6 ^{+0.4} _{-0.5}	L1.8±1.0
PSO J232.2+63	M7±1	M7±1	M7.8 ^{+0.3} _{-0.4}	...	M8.6 ^{+1.1} _{-1.1}	M7.8 ^{+0.4} _{-0.5}	M7.8±1.0
PSO J236.8-16	M9±1	L0±1	L0.1 ^{+0.6} _{-0.6}	L1.1 ^{+0.9} _{-0.9}	M9.8 ^{+1.1} _{-1.0}	M7.8 ^{+0.6} _{-0.6}	M9.4±1.0
PSO J292.9-06	M8±1	M8±1	M7.2 ^{+0.4} _{-0.4}	...	M8.7 ^{+1.0} _{-1.1}	M7.7 ^{+0.6} _{-0.5}	M7.6±1.0
PSO J306.0+16	L3.5±1	L2.5±1	L2.0 ^{+0.4} _{-0.4}	L3.0 ^{+0.8} _{-0.8}	L2.1 ^{+1.1} _{-1.1}	L2.1 ^{+0.6} _{-0.5}	L2.3±1
PSO J318.4+35	L2±1	L1±1	L0.8 ^{+0.5} _{-0.4}	L2.0 ^{+0.7} _{-0.7}	L2.1 ^{+1.1} _{-1.0}	L0.1 ^{+0.5} _{-0.5}	L0.9±1.0
PSO J334.2+28	L4.5±1	L3±1	L3.8 ^{+0.3} _{-0.4}	L2.6 ^{+0.7} _{-0.7}	L3.4 ^{+1.0} _{-1.1}	...	L3.5±1
PSO J351.3-11	M6±1	M7±1	M6.8 ^{+0.4} _{-0.4}	... ^b	M6.6 ^{+1.1} _{-1.1}	M6.2 ^{+0.5} _{-0.5}	M6.5±1.0
PSO J358.5+22	L1±1	L3±1	L1.2 ^{+0.9} _{-1.0}	L1.8 ^{+1.0} _{-1.0}	L2.6 ^{+1.3} _{-1.2}	L2.1 ^{+0.6} _{-0.8}	L1.9±1.0

^a This spectral type is determined by visual classification.

^b The H₂O-D index is undefined for this spectral type.

TABLE 4
GRAVITY INDICES AND CLASSIFICATION

Name	FeH ₂	FeH _J	VO ₂	KI _J	H-cont	Index Scores ^a	NaI	KI [1.169]	KI [1.177]	KI [1.253]	EW Index Scores ^a	Final Gravity Scores ^a	Overall Gravity Value ^b	Overall Gravity Class
PSO J004.7+41	1.26 ^{+0.01} _{-0.01}	1.17 ^{+0.01} _{-0.01}	1.082 ^{+0.006} _{-0.006}	1.099 ^{+0.003} _{-0.004}	0.943 ^{+0.003} _{-0.003}	01001 (01001)	14 ⁺¹ ₋₁	7.2 ^{+0.4} _{-0.5}	9.7 ^{+0.4} _{-0.4}	7.6 ^{+0.4} _{-0.3}	0000 (0000)	1001 (100?)	0.5 ^{+0.0} _{-0.0}	FLD-G ^c
PSO J035.8-15	1.079 ^{+0.008} _{-0.008}	1.06 ^{+0.01} _{-0.01}	1.020 ^{+0.005} _{-0.006}	1.040 ^{+0.003} _{-0.003}	0.991 ^{+0.003} _{-0.004}	11n12 (11n12)	12 ⁺¹ ₋₁	2.2 ^{+0.6} _{-0.6}	5.1 ^{+0.4} _{-0.5}	2.2 ^{+0.3} _{-0.4}	0101 (0101)	1n12 (1n12)	1.0 ^{+1.0} _{-0.0}	INT-G
PSO J039.6-21	1.17 ^{+0.02} _{-0.02}	1.05 ^{+0.02} _{-0.02}	1.06 ^{+0.01} _{-0.01}	1.068 ^{+0.008} _{-0.009}	0.91 ^{+0.01} _{-0.02}	1n021 (1n02?)	1021 (102?)	1.0 ^{+0.0} _{-0.5}	INT-G
PSO J167.1+68	1.214 ^{+0.008} _{-0.009}	1.120 ^{+0.009} _{-0.008}	1.245 ^{+0.005} _{-0.005}	1.100 ^{+0.003} _{-0.003}	0.942 ^{+0.002} _{-0.002}	11211 (11211)	8.9 ^{+0.5} _{-0.5}	5.6 ^{+0.3} _{-0.3}	7.0 ^{+0.3} _{-0.3}	4.3 ^{+0.2} _{-0.2}	1111 (1111)	1211 (1211)	1.0 ^{+0.0} _{-0.0}	INT-G
PSO J232.2+63	1.129 ^{+0.002} _{-0.002}	1.114 ^{+0.003} _{-0.003}	1.057 ^{+0.0018} _{-0.0016}	0.960 ^{+0.001} _{-0.001}	1.065 ^{+0.001} _{-0.001}	11n10 (11n10)	9.8 ^{+0.3} _{-0.3}	2.8 ^{+0.15} _{-0.15}	5.0 ^{+0.13} _{-0.13}	2.6 ^{+0.12} _{-0.12}	1112 (1112)	1n10 (1n10)	1.0 ^{+0.0} _{-0.0}	INT-G
PSO J236.8-16	1.156 ^{+0.017} _{-0.016}	...	1.078 ^{+0.013} _{-0.013}	1.077 ^{+0.011} _{-0.011}	0.943 ^{+0.008} _{-0.008}	1nn11 (1nn11)	1n11 (1n?)	1.0 ^{+0.0} _{-0.0}	INT-G
PSO J292.9-06	1.104 ^{+0.005} _{-0.004}	1.013 ^{+0.008} _{-0.008}	1.042 ^{+0.004} _{-0.004}	0.984 ^{+0.004} _{-0.004}	1.068 ^{+0.004} _{-0.004}	1nn01 (1nn0?)	1n01 (1n0?)	1.0 ^{+0.0} _{-1.0}	INT-G
PSO J306.0+16	1.324 ^{+0.02} _{-0.019}	...	1.116 ^{+0.011} _{-0.010}	0.900 ^{+0.006} _{-0.006}	1.125 ^{+0.009} _{-0.008}	0n110 (0n110)	0101 (010?)	0.5 ^{+0.5} _{-0.0}	INT-G?
PSO J318.4+35	1.16 ^{+0.02} _{-0.02}	...	1.18 ^{+0.01} _{-0.01}	1.10 ^{+0.006} _{-0.006}	0.934 ^{+0.006} _{-0.005}	1n111 (1n111)	1111 (1111)	1.0 ^{+0.0} _{-0.0}	INT-G
PSO J334.2+28	...	1.21 ^{+0.07} _{-0.06}	1.10 ^{+0.02} _{-0.02}	0.926 ^{+0.008} _{-0.007}	1.106 ^{+0.009} _{-0.009}	n1111 (n1111)	10.9±0.9	-1.5±4.5	7.5±2.5	6.6±0.7	1211 (021?)	1111 (111?)	1.0 ^{+0.0} _{-0.0}	INT-G
PSO J351.3-11	1.05 ^{+0.01} _{-0.01}	1.06 ^{+0.02} _{-0.01}	1.033 ^{+0.009} _{-0.008}	1.043 ^{+0.004} _{-0.004}	0.968 ^{+0.006} _{-0.006}	21n10 (21n10)	8 ⁺² ₋₂	0.6 ^{+0.8} _{-0.8}	3.0 ^{+0.7} _{-0.7}	2.0 ^{+0.6} _{-0.6}	1212 (1212)	2n20 (2n20)	1.0 ^{+1.0} _{-0.0}	INT-G
PSO J358.5+22	1.36 ^{+0.07} _{-0.05}	...	1.13 ^{+0.03} _{-0.02}	1.13 ^{+0.010} _{-0.014}	0.920 ^{+0.010} _{-0.015}	0n111 (0n1?)	0111 (01?)	0.5 ^{+0.5} _{-0.0}	INT-G?

^a Scores in parenthesis are the scores determined with the Allers & Liu (2013) classification scheme. Objects with index values corresponding to INT-G but are within 1 σ of the FLD-G value are classified with a score of ?.

^b The overall gravity classification value and the 68% confidence limits calculated using our modified version of the Allers & Liu (2013) classification scheme (Section 5).

^c Although classified as FLD-G, the spectral indices show hints of INT-G.

TABLE 5
SUBSTELLAR MEMBERS OF THE AB DOR MOVING GROUP

Name	SpT	Gravity (NIR ^c)	$\mu_{\alpha\cos\delta}, \mu_{\delta}$ (mas yr ⁻¹)	π (mas)	d_{phot} ^a (pc)	RV (km/s)	BANYAN II Web kinematics		BANYAN II kinematics+SED		Ref ^b
							P_{ABDor} ^{a,d}	P_{others} ^{a,d}	P_{ABDor} ^{a,e}	P_{others} ^{a,e}	
Bona Fide Members ^f											
CD-35 2722B	L3	INT-G	-4.6±1.9, -59.8±1.6	47±3	...	31.4±1.0	1,2
2MASS 14252798-3650229	L4	INT-G	-268±15, -47.3±19	111±12	...	5.37 ±0.256	3,4,5
2MASS 03552337+1133437	L3	VL-G	218±5, -626±5,	109.6±1.3	...	11.92±0.22	6,7
WISEP J00470106+680352	L6	INT-G	381±12, -212±12	82±3	...	-20±1.4	8
SDSS J11101001+0116131	T5.5	low	-217.1±0.7, -280.9±0.6	52.1±12	...	7.5±3.8	97%	...	9,4
Strong Candidate Members ^g											
2MASS J00012171+1535355	L4	INT-G,[β]	129±4, -177±7	...	28±6	...	98%	...	97%	...	5,10
2MASS J00584253-0651239	L1	INT-G,[β]	138±4, -123±4	31.4±2.5	29±6	...	95%	...	64%	34% β Pic	5,12
GU Psc b ^h	T3.5	low	98±15, -92±15	...	47±9	-1.6±0.4	56%	11% β Pic	88%	12% β Pic	11
PSO J039.6352-21.7746	L2.6	INT-G	95.5±1.5, -150.4±4.3	27.0±5.4	26±5	...	93%	12
2MASS J03164512-2848521	L1	INT-G,[β]	98±4, -99±7	...	33±7	...	97%	...	97%	...	5
2MASS J03264225-2102057 ⁱ	L5	FLD-G [β/γ]	93±6, -135±6	...	26±5	...	98%	...	99%	...	5,10
PSO J318.4243+35.1277	L0.9	INT-G	109.0±1.9, -71.5±1.6	27.9±3.6	29±9	...	88%	12
2MASS J22064498-4217208	L3	VL-G,[γ]	132.6±4.8, -187.7±9.3	...	36±7	...	92%	...	99%	...	5,10
2MASS J22443167+2043433 ^j	L6.5	low	242.6±7.3, -219.6±7.1	...	24±8	...	95%	3% β Pic	99.6%	10	...
PSO J358.5527+22.1393	L1.9	INT-G?	97.0±2.1, -88.3±1.9	22.9±3.7	38±8	...	79%	12
Possible Candidate Members ^k											
2MASS J00192626+4614078	M8	INT-G,[β]	125±4, -75±4	...	18±5 (36±10)	...	<0.1% (60%)	67% (9%) β Pic	53%	...	5
2MASS J00425923+1142104	M9	INT-G,[β]	92.7±10.0, -75±9	...	40±8 (81±16)	...	1% (<0.1%)	75% (<0.1%) β Pic	13%	6% β Pic	5
2MASS J06322402-5010349	L3	[[β]]	-96.3±4.2, 9.1±6.7	...	28±6	...	0.2%	...	30%	...	5
2MASS J06420559+4101599	L/T	pec	-4.8±4.9, -370.5±8.5	...	1	49%	10	...
2MASS J08034469+0827000	M6	INT-G,[β]	-72±3, -201±5	...	20±4 (40±8)	...	17% (7%)	69% (<0.1%) CAR	91%	...	5
PSO J232.2915+63.2151	M7.8	INT-G,[β]	-125.6±3.4, 32.5±3.4	35.5±4.2	11±3	...	37%	...	25%	...	5,12
PSO J292.9372-06.3469	M7.6	INT-G	21±3, -106±3	...	39±8 (80±20)	...	7% (0%)	3% β Pic	12
PSO J306.0126+16.7969	L2.3	INT-G?	64±4, -83±6	...	40±8	...	43%	12
2MASS J20391314-1126531	M7	INT-G,[β]	54±3, -100±4	...	45±9 (92±20)	...	17% (<0.1%)	5% (<0.1%) β Pic	2%	...	5
2MASS J21572060+8340575	M9	[[γ]]	116.2±1.3, 46±9	...	29±6 (58±18)	...	53% (<0.1%)	...	31%	...	5
PSO J334.2624+28.9438	L3.5	INT-G	77±27, -53±11	...	59±12	...	0.6%	12
PSO J351.3434-11.3514	M6.5	INT-G	148.8±2.3, -132.3±1.9	22.1±6.5	44±10	...	50%	12
2MASS J23255604-0259508	L1	INT-G,[γ]	85±6, -106±4	...	63±13	...	3%	...	73%	...	5,10
2MASS J23360735-3541489	M9	VL-G,[β]	70±8, -80.7±10.0	...	39±8 (79±16)	...	0.2% (<0.1%)	97% (<0.1%) THA	60%	39% THA	5
2MASS J23433470-3646021	L3-L6	VL-G,[γ]	97±6, -109.4±10.1	...	40±16	...	52%	30% THA	46%	38% β Pic, 16% THA	5
2MASS J23520507-1100435	M8	INT-G,[β]	100±4, -121±4	...	20±7 (42±15)	...	0.1% (82%)	95% (5%) β Pic	91%	...	5,10
2MASS J23532556-1844402A	M6.5	VL-G,[γ]	90±3, -78±3	...	15±3 (30±6)	...	<0.1% (<0.1%)	<0.1% (90%) β Pic	20%	46% THA, 34% β Pic	5
Probable Young Field Interlopers ^m											
PSO J004.7818+41.0231	L0.1	FLD-G	101±4, -133±1	...	27±4	...	19%	47% β Pic	12
PSO J035.8683-15.1937 ⁿ	M7.1	INT-G	135.1±1.9, -137.7±2.4	18.3±3.7	44±14	...	49%	12
PSO J167.1260+68.5039	L1.8	INT-G,[γ]	-221.9±3.1, -193.7±3.9	46.1±6.5	14±3	-9.8±0.1	0.2%	6% CAR	5,12
PSO J236.7729-16.4422	M9.4	INT-G,[β]	-70.1±1.5, -148.9±3.7	36.6±4.1	26±6	...	0.3%	...	11%	...	5,12

TABLE 5 — *Continued*

Name	SpT	Gravity (NIR ^c)	$\mu_{\alpha \cos \delta}, \mu_{\delta}$ (mas yr ⁻¹)	π (mas)	d_{phot} ^a (pc)	RV (km/s)	BANYAN II Web kinematics		BANYAN II kinematics+SED		Ref ^b
							P_{ABDor} ^{a,d}	P_{others} ^{a,d}	P_{ABDor} ^{a,e}	P_{others} ^{a,e}	

^a Properties in parenthesis are calculated assuming the object is overluminous compared with the field sequence by 1.5 mag. This reflects the systematic uncertainty in the photometric distances for our late-M dwarf candidates (Section 5.2).

^b Table references: 1–Wahhaj et al. (2011), 2–Shkolnik et al. (2012), 3–Blake et al. (2010), 4–Dupuy & Liu (2012), 5–Gagné et al. (2015c), 6–Liu et al. (2013a), 7–Faherty et al. (2013), 8–Gizis et al. (2015), 9–Gagné et al. (2015a), 10–Gagné et al. (2014), 11–Naud et al. (2014), 12–this paper

^c The NIR gravity classification system used is from Allers & Liu (2013). Gravity classifications in single brackets are visual classifications using NIR spectra by Gagné et al. (2015c). For objects without NIR spectra, we note the visual gravity classifications from optical spectra by Gagné et al. (2015c) in double brackets.

^d Probability based on BANYAN II web tool which only uses the kinematic information to calculate membership probability. Membership for other significant groups is included.

^e Probability from BANYAN II using kinematic and photometric information from Gagné et al. (2015c) and Gagné et al. (2015b). The membership probability is the probability of being a young moving group member (with the most likely group being the AB Dor Moving Group), not necessarily of only the AB Dor Moving Group.

^f *Bona Fide* members have parallaxes, radial velocities, and spectroscopically confirmed low gravity.

^g Objects with membership probability as determined by the BANYAN II webtool of at least 75% and spectroscopically confirmed low gravity.

^h GU Psc b is a widely accepted strong candidate to the AB Dor Moving Group.

ⁱ 2MASS J03264225–2102057 has discrepant NIR gravity classifications of β/γ (visual) and FLD-G (Allers & Liu (2013) indices) from Gagné et al. (2015c). Thus because there are visual signs of youth and the membership probability is high, we still consider it to be a strong candidate member.

^j CFHT parallax for this object (Liu et al., submitted) also suggests that it is a strong candidate member.

^k Objects with membership probability as determined by the BANYAN II webtool of 15–75% or *UVWXYZ* positions consistent with AB Dor Moving Group membership.

^l We did not compute a photometric distance because the object is very peculiar, thus any photometric distance would likely be inaccurate.

^m We consider objects with BANYAN II membership probabilities <15% and *UVWXYZ* positions inconsistent with AB Dor Moving Group membership to be likely field interlopers.

ⁿ We consider PSO J035.8–15 as a likely field interloper because its *UVWXYZ* positions are inconsistent with membership (Section 5.6)

TABLE 6
SYNTHESIZED PHOTOMETRY^a

Name	J_{MKO} (mag)	H_{MKO} (mag)	K_{MKO} (mag)
PSO J004.7+41	14.150±0.009	13.539±0.007	13.056±0.007
PSO J035.8-15	13.75±0.01	13.32±0.01	12.92±0.01
PSO J039.6-21	14.73±0.04	14.24±0.05	13.68±0.05
PSO J167.1+68	13.044±0.009	12.295±0.006	11.57±0.005
PSO J232+63	11.534±0.003	10.992±0.003	10.538±0.003
PSO J236.8-16	13.81±0.02	13.237±0.014	12.708±0.017
PSO J292-06	13.837±0.011	13.296±0.009	12.830±0.009
PSO J306+16	15.57±0.03	14.657±0.020	13.823±0.016
PSO J318.4+35	14.23±0.02	13.47±0.02	12.77±0.02
PSO J334+28	16.737±0.008	15.821±0.005	15.010±0.003
PSO J351.3-11	13.59 ±0.01	13.09±0.01	12.67±0.01
PSO J358.5+22	15.26±0.04	14.62±0.04	14.02±0.04

^a MKO magnitudes are synthesized from our NIR spectra (Section 5).

TABLE 7
PHYSICAL PROPERTIES^{ab}

Name	M_{bol} (mag)	Mass (M_{Jup})	T_{eff} (K)
Our AB Dor Moving Group Candidates			
PSO J004.7+41	14.1 ± 0.4	$[40^{+11}_{-13}]$	$[1950^{+200}_{-200}]$
PSO J035.8-15	12.1 ± 0.7	80^{+40}_{-30}	2700^{+300}_{-400}
PSO J039.6-21	14.1 ± 0.4	37^{+30}_{-5}	1950^{+190}_{-150}
PSO J167.1+68	13.3 ± 0.2	52^{+14}_{-16}	2300^{+150}_{-190}
PSO J232.2+63	11.3 ± 0.2	130^{+20}_{-40}	3050^{+150}_{-180}
PSO J236.8-16	13.7 ± 0.3	44^{+12}_{-15}	2090^{+160}_{-180}
PSO J292.9-06	$[12.9 \pm 0.4 (11.4 \pm 0.5)]$	$[55^{+11}_{-9} (110^{+30}_{-30})]$	$[2450^{+180}_{-200} (3000^{+120}_{-170})]$
PSO J306.0+16	$[14.3 \pm 0.5]$	$[34^{+5}_{-6}]$	$[1850^{+170}_{-190}]$
PSO J318.4+35	13.4 ± 0.2	45^{+5}_{-5}	2220^{+110}_{-110}
PSO J334.2+28	$[14.6 \pm 0.5]$	$[31^{+8}_{-5}]$	$[1740^{+180}_{-180}]$
PSO J351.3-11	12.3 ± 1.4	70^{+50}_{-30}	2700^{+400}_{-700}
PSO J358.5+22	14.1 ± 0.4	36^{+5}_{-6}	1930^{+140}_{-170}
Bona Fide Members			
CD-35 2722B	13.7 ± 0.3	40^{+4}_{-4}	2090^{+80}_{-80}
WISEP J00470106+680352	15.7 ± 0.2	20^{+3}_{-7}	1340^{+40}_{-40}
2MASS J03552337+1133437	15.4 ± 0.2	23^{+2}_{-5}	1430^{+40}_{-40}
2MASS J14252798-3650229	15.4 ± 0.4	22^{+3}_{-8}	1420^{+80}_{-100}
SDSS J11101001+0116131 ^c	17.30 ± 0.05	$10-12$	940 ± 20
Previously Identified Candidates			
2MASS J00011217+1535355	$[14.9 \pm 0.5]$	$[28^{+5}_{-4}]$	$[1630^{+160}_{-150}]$
2MASS J00192626+4614078	$[13.2 \pm 0.6 (11.7 \pm 0.6)]$	$[49^{+12}_{-11} (90^{+30}_{-30})]$	$[2300^{+200}_{-300} (2890^{+190}_{-200})]$
2MASS J00425923+1142104	$[13.7 \pm 0.5 (12.2 \pm 0.3)]$	$[41^{+7}_{-7} (72^{+13}_{-11})]$	$[2090^{+180}_{-200} (2720^{+110}_{-150})]$
2MASS J00584253-0651239	13.9 ± 0.5	39^{+7}_{-7}	2040^{+180}_{-200}
Gu Psc b	$[16.9 \pm 0.3]$	$[11.9^{+2}_{-1.5}]$	$[1060^{+100}_{-110}]$
2MASS J03164512-2848521	$[13.9 \pm 0.5]$	$[38^{+9}_{-7}]$	$[2010^{+180}_{-200}]$
2MASS J03264225-2102057	$[14.9 \pm 0.5]$	$[28^{+4}_{-4}]$	$[1610^{+150}_{-190}]$
2MASS J06322402-5010349	$[14.5 \pm 0.5]$	$[31^{+5}_{-5}]$	$[1750^{+180}_{-180}]$
2MASS J06420559+4101599 ^d	...	$[11-12]$...
2MASS J08034469+0827000	$[12.4 \pm 0.5 (10.8 \pm 0.5)]$	$[67^{+15}_{-13} (150^{+30}_{-30})]$	$[2650^{+160}_{-200} (3160^{+70}_{-110})]$
2MASS J15291017+6312539	$[13.2 \pm 0.6 (11.7 \pm 0.6)]$	$[50^{+12}_{-11} (100^{+30}_{-30})]$	$[2300^{+200}_{-300} (2910^{+180}_{-200})]$
2MASS J20391314-1126531	$[12.4 \pm 0.6 (10.9 \pm 0.5)]$	$[67^{+17}_{-15} (150^{+30}_{-30})]$	$[2660^{+160}_{-200} (3150^{+80}_{-120})]$
2MASS J21572060+8340575	$[13.5 \pm 0.5 (12.0 \pm 0.3)]$	$[44^{+7}_{-7} (81^{+15}_{-13})]$	$[2190^{+150}_{-200} (2800^{+100}_{-120})]$
2MASS J22064498-4217208	$[14.4 \pm 0.5]$	$[32^{+6}_{-4}]$	$[1810^{+180}_{-190}]$
2MASS J22443167+2043433	$[22.0 \pm 0.5]$	$[22^{+4}_{-6}]$	$[1380^{+130}_{-150}]$
2MASS J23255604-0259508	$[13.7 \pm 0.5]$	$[41^{+8}_{-7}]$	$[2110^{+180}_{-200}]$
2MASS J23360735-3541489	$[13.6 \pm 0.5 (12.1 \pm 0.3)]$	$[42^{+8}_{-6} (78^{+14}_{-12})]$	$[2140^{+180}_{-180} (2770^{+90}_{-120})]$
2MASS J23433470-3646021	$[14.1 \pm 0.9]$	$[37^{+9}_{-8}]$	$[1950^{+280}_{-310}]$
2MASS J23520507-1100435	$[13.3 \pm 0.6 (11.8 \pm 0.6)]$	$[47^{+12}_{-12} (90^{+30}_{-30})]$	$[2280^{+240}_{-310} (2880^{+190}_{-200})]$
2MASS J23532556-1844402	$[12.4 \pm 0.5 (10.8 \pm 0.5)]$	$[68^{+16}_{-14} (150^{+30}_{-40})]$	$[2660^{+160}_{-200} (3170^{+60}_{-160})]$

^a Properties in parenthesis are calculated assuming the object is overluminous compared with the field sequence by 1.5 mag. This reflects the systematic uncertainty in the photometric distances for our late-M dwarf candidates.

^b Properties in brackets are calculated using photometric distances for objects where no parallax was available.

^c Properties from Gagné et al. (2015a)

^d Because of the spectral peculiarities, this object is classified only as an L/T dwarf and does not have a precise spectral type, thus we do not estimate the M_{bol} , mass, or T_{eff} . The mass range estimate is taken from Gagné et al. (2014).